UNIVERSITY OF CALIFORNIA
RIVERSIDE

Novel Phases of Quantum Matter; a Case Study of Weyl Semimetals and Transition Metal Dichalcogenides

A Dissertation submitted in partial satisfaction
of the requirements for the degree of

Doctor of Philosophy

in

Physics

by

Robert Donald Dawson

September 2024

Dissertation Committee:

Dr. Vivek Aji, Chairperson
Dr. Shan-Wen Tsai
Dr. Kirill Shtengel

The Dissertation of Robert Donald Dawson is approved:

Committee Chairperson

University of California, Riverside

Acknowledgments

I would like to thank my advisor Vivek Aji for his guidance on each of these projects, the entire UCR graduate instructor faculty who helped me develop my skills in mathematical physics, and to my colleague Yifan Liu for his help with the Phonon project. I would also like to thank Dr. Steven Lewis, Dr. Craig Wiegert, and Dr. Andrei Galiautdinov for inspiring me to pursure graduate study at UCR.

Chapters 1.1 (Noninteracting Fermi gas) and 1.2 (Periodic Potential and Band Structure) contain excerpts from Ashcroft and Mermin's *Solid State Physics*. Specifically, it contains some of their work from chapters 2 and 8.

Chapter 1.4 (Band Structure and Topology) contains work from Bernevig and Hughes' *Topological Insulators and Topological Superconductors*. Specifically, it contains a reproduction of the derivation of the Berry Phase, with minor adjustments for brevity. It also covers chapters 3.6 (Chern number as an obstruction to Stokes' Theorem over the Whole BZ) and 4.5 (Vanishing of Hall Conductance for T-invariant Half-Integer Spin Particles) of the same work.

Portions of Chapter 2 are reprints of material as it appears in *Phys. Rev. B* 109, **094 517** (2024). R. Dawson and V. Aji. The dissertation author and the Ph.D. committee chair were the principal investigators and co-authors of this paper.

Appendix A.2 and A.2.1 contain work from Haug and Koch's *Quantum Theory of the Optical and Electronic Properties of Semiconductors*. These sections reproduce their solutions to the Wannier equation in two dimensions.

In loving memory of my grandmother, Jean Dawson.

ABSTRACT OF THE DISSERTATION

Novel Phases of Quantum Matter; a Case Study of Weyl Semimetals and Transition Metal Dichalcogenides

by

Robert Donald Dawson

Doctor of Philosophy, Graduate Program in Physics
University of California, Riverside, September 2024
Dr. Vivek Aji, Chairperson

In quantum materials, the interactions between the bulk lattice, free electrons, and lattice vibrations give rise to interesting phases of matter. In recent years, new materials have been discovered that have nontrivial topological physics, allowing them to host topologically protected surface states. Much work has been done in exploring whether or not such materials can be rendered superconducting via the proximity effect. In this work, I will explore interesting phases of two topological materials: Weyl semimetals and transition metal dichalcogenides. In the first section, I explore the properties of proximity induced superconductivity within these materials. Using a numerical technique known as the spectral method, I determine what, if any, types of superconductivity can be induced within these materials, and whether or not the superconducting state retains their topological properties. Ultimately, I show that, in the absence of a non-trivial tunneling interaction at the interface, no interesting superconducting properties can be induced. In the second section, I will explore the optical absorption properties of semiconducting materials in the presence of electron-phonon interactions, which typically give rise to phonon side-bands in optical

spectra. I demonstrate how, with an appropriate transformation, an expression for the optical spectra to arbitrary phonon side-band order can be calculated for a general interacting system. To demonstrate its validity, I fit the model to the measured optical absorption spectrum of a device consisting of layered transition metal dichalcogenides.

Contents

List of Figures

Chapter 1

Introduction

Discovering, enabling and understanding new states of matter and phenomena are the fundamental objectives in condensed matter physics. This is theoretically challenging due to the interplay of a large number of degrees of freedom, inter-particle interactions, and quantum correlations. Over the last two decades the discovery of topologically nontrivial materials and phases have opened new frontiers while also adding to the complexity. The focus of this thesis is on two such materials namely Weyl semimetals and transition metal dichalogenides. I explore the nature of superconducting states induced by proximity in both systems and vibronic excitations in the latter. Beginning with the noninteracting system and adding in interactions, this chapter provides the background, motivation, and roadmap for the thesis.

1.1 Noninteracting Fermi Gas

We begin with a consideration of a collection of indistinguishable, noninteracting fermions in three dimensions. Independently, each fermion must satisfy the Schrödinger equation:

$$-\frac{\hbar^2}{2m}\nabla^2\Psi(\mathbf{r}) = \varepsilon\Psi(\mathbf{r}) \tag{1.1}$$

Due to the symmetry of the gas, we may invoke periodic boundary conditions over some effective length scales:

$$\Psi(\mathbf{r} + \mathbf{R}_i) = \Psi(\mathbf{r}) \tag{1.2}$$

$$\mathbf{R}_i = L_i\hat{i},\ i\epsilon\{x, y, z\} \tag{1.3}$$

Which yields the wave function and corresponding energy state of a free particle:

$$\Psi_{\mathbf{k}}(\mathbf{r}) = \frac{1}{\sqrt{V}}e^{i\mathbf{k}\cdot\mathbf{r}} \tag{1.4}$$

$$\varepsilon_{\mathbf{k}} = \frac{\hbar^2\mathbf{k}^2}{2m} \tag{1.5}$$

Where $V = L_xL_yL_z$. According to our boundary conditions, the wave vector $\mathbf{k}$ must satisfy:

$$k_i = \frac{2\pi n_i}{L_i} \tag{1.6}$$

With n_i an integer.

In the ground state of the many body system, N fermions must occupy the N lowest energy states with no two electrons sharing the same state due to the Pauli exclusion principle. At zero temperature, this yields an expression for the highest occupied momentum state k_F in terms of the electron density $n = N/V$ [1]:

$$n = \frac{k_F^3}{3\pi^2} \tag{1.7}$$

The highest occupied energy state, the *Fermi Energy*, is:

$$\mathcal{E}_F = \frac{\hbar^2 k_F^2}{2m} \tag{1.8}$$

And at finite temperature, the average number of fermions with energy $\varepsilon_{\mathbf{k}}$ is given by the Fermi function:

$$f(\varepsilon_{\mathbf{k}}) = \left[e^{(\varepsilon_{\mathbf{k}} - \mu)/k_B T} + 1 \right]^{-1} \tag{1.9}$$

Where $\mathcal{E}_F = \mu$ is the chemical potential at zero temperature.

1.2 Periodic Potential and Band Structure

While the above model serves as a good baseline for understanding the kinetic properties of free electrons, it is insufficient for modeling electrons confined to a material's ionic crystal lattices. The above model neglects not only the electron-electron interactions (discussed in the next section), but also the effects of the periodic coulomb potential created

by the lattice ions. To understand these effects, we follow Chapters 8 and 9 of Ashcroft and Mermin [1], beginning with the second derivation of Bloch's Theorem. We first assume a periodic lattice potential:

$$U(\mathbf{r}+\mathbf{R}) = U(\mathbf{r}) \tag{1.10}$$

Where $\mathbf{R}$ is a Bravais lattice vector. Its plane wave expansion must also be periodic in the lattice, and is thus an expansion of the reciprocal lattice vectors $\mathbf{K}$:

$$U(\mathbf{r}) = \sum_{\mathbf{K}} U_{\mathbf{K}} e^{i\mathbf{K}\cdot\mathbf{r}} \tag{1.11}$$

Finally, expanding the electronic wave function as a plane wave:

$$\Psi(\mathbf{r}) = \sum_{\mathbf{k}} \Psi_{\mathbf{k}} e^{i\mathbf{k}\cdot\mathbf{r}} \tag{1.12}$$

We obtain the eigenvalue equation [1]:

$$\left[\frac{\hbar^2}{2m}(\mathbf{k}-\mathbf{K})^2 - \varepsilon\right]\Psi_{\mathbf{k}-\mathbf{K}} + \sum_{\mathbf{K}'} U_{\mathbf{K}'-\mathbf{K}}\Psi_{\mathbf{k}-\mathbf{K}'} = 0 \tag{1.13}$$

Note that, by definition, Eq.(1.13) must be invariant under translation by a reciprocal lattice vector $\mathbf{k} \to \mathbf{k}+\mathbf{K}$. Thus, not only are the electronic wave functions periodic in momentum space, but the energy levels are as well:

$$\Psi_{n,\mathbf{k}+\mathbf{K}}(\mathbf{r}) = \Psi_{n,\mathbf{k}}(\mathbf{r}) \tag{1.14}$$

$$\varepsilon_{n,\mathbf{k}+\mathbf{K}} = \varepsilon_{n,\mathbf{k}} \tag{1.15}$$

This has an interesting consequence for the energy levels when the potential is relatively small compared to the free kinetic energy. Near the reciprocal lattice vectors, the energy resembles that of a free electron, creating a periodic collection of quadratic energy levels. However, there is a collection of momenta where these levels cross. At these points, the lattice potential acts as a perturbation of the free system, splitting the levels into periodic energy bands. The periodic nature of the energy bands means it is sufficient to determine the band structure within the *First Brillouin Zone*, as seen in Fig.1.1, which is known as the reduced zone scheme.

1.3 Interacting Systems: Superconductivity

While the above theory is sufficient for describing some of the basic electronic properties of materials, it is still missing many underlying interactions of the many-body problem. Furthermore, in the early twentieth century, while studying the conductive properties of materials at low temperatures, dutch physicist Heike Kmerlingh Onnes discovered that some metals had zero electrical resistance below some critical temperature T_c. At the time, there was no microscopic theory to explain why the electrical resistance spontaneously vanished. This remained the case until 1957, when Bardeen, Cooper, and Schrieffer

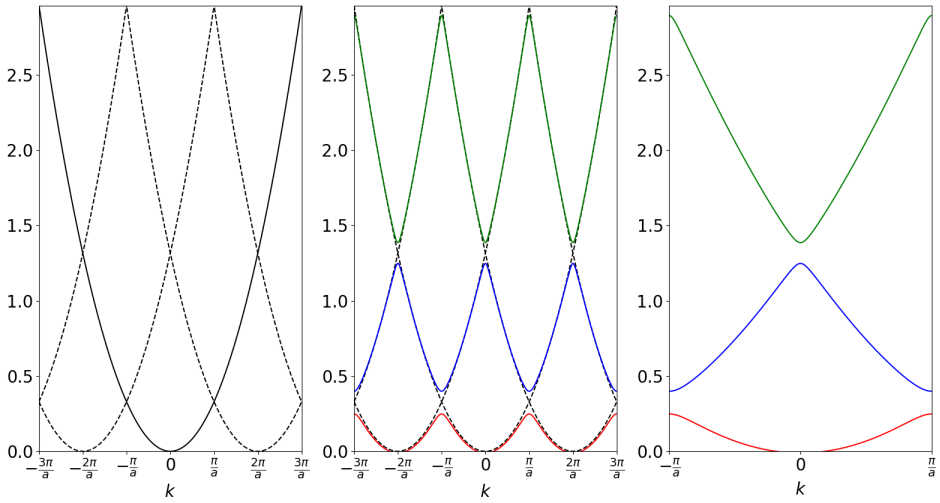

Figure 1.1: Construction of the reduced zone scheme for the lowest three energy bands of a crystal. (Left) A free electron gas with translational invariance, (Middle) the same system under the influence of a weak, periodic potential, and (Right) the band structure in the First Brillouin Zone.

put forth the BCS theory of superconductivity, which attributed the phenomenon to an attractive electron-electron interaction mediated by lattice vibrations (phonons).

Up until this point, we have written in our systems in *first quantization*, in which we solve the quantum mechanical eigenvalue problem for the appropriate single-particle wave functions and energies. However, in the interacting N-body problem, we would then be tasked with finding the N-body wave function which, for fermions, would be found from the Slater determinant. For a macroscopic system, this approach is highly non-trivial, and instead we will approach the problem through *second quantization*. In this framework, the system's physics is modeled through field operators $\Psi_n^\dagger(\mathbf{r})$ ($\Psi_n(\mathbf{r})$) which create (annihilate) a particle at position $\mathbf{r}$ with quantum number(s) n. To satisfy the bosonic/fermionic statistics, these operators obey the commutation relations:

$$[\Psi_n, \Psi_m^\dagger]_\eta = \delta_{n,m} \tag{1.16}$$

$$[\Psi_n, \Psi_m]_\eta = [\Psi_n^\dagger, \Psi_m^\dagger]_\eta = 0 \tag{1.17}$$

Where $\eta = 1$ ($\eta = -1$) for bosons (fermions) denotes the commutator (anti-commutator). Furthermore, we define the quantum state in terms of the number of particles occupying each available state, i.e. for a system with N states, $|\Psi\rangle \equiv |n_1, n_2, \ldots, n_N\rangle$. With a proper choice of normalization factors, it is easy to show that such a configuration is an eigenstate of the number operator $N_i \equiv \Psi_i^\dagger \Psi_i$ with eigenvalue n_i. Therefore, in this language, the non-interacting Hamiltonian:

$$H_0 = \sum_{n,\mathbf{k}} \varepsilon_{n,\mathbf{k}} \Psi_{n,\mathbf{k}}^\dagger \Psi_{n,\mathbf{k}} \tag{1.18}$$

is diagonal, and we write the electron-electron Coulomb interaction as:

$$H_{el-el} = \sum_{n,m} \sum_{\mathbf{k},\mathbf{k}',\mathbf{q}} V_{\mathbf{q}}^{n,m} \Psi_{n,\mathbf{k}+\mathbf{q}}^\dagger \Psi_{m,\mathbf{k}'-\mathbf{q}}^\dagger \Psi_{m,\mathbf{k}'} \Psi_{n,\mathbf{k}} \tag{1.19}$$

At this point, our theory is composed of three pieces: 1) An electron gas with free kinetic energy, 2) a periodic, ionic lattice potential that binds the electron gas, giving rise to a periodic band structure, and 3) a repulsive electron-electron interaction acting as a perturbation to the already solved system. If we were to proceed from here, we would follow the steps of Hartree and Fock, replacing the repulsive two-particle interaction with an effective

screening potential [1]. However, Bardeen et. al. realized that there was one additional missing piece: vibrations of the crystal lattice.

In our original model, we treated the ions of the lattice as a static distribution. In reality, local ions in the lattice are free to oscillate about their equilibrium position. In the presence of a local electric field (i.e. from a passing electron, or some other source), the ion is displaced from equilibrium, and its repulsive interaction with the other ions propagates the displacement through the rest of the lattice as a wave known as the phonon. Bardeen et. al. argued that, localized distortions would create an effective attractive interaction between electrons that overpowers the coulomb repulsion [2]. Below a critical temperature, this interaction leads to a new global minimum in the system's free energy described by a collection of paired electrons that have Bose-condensed into a collective ground state. It is these *Cooper pairs* move through the lattice without resistance.

The current focus is on exploring *unconventional* superconductivity. Broadly speaking, this includes any type of superconductivity that is not explained by the BCS theory (for instance, cuprates with significantly higher critical temperatures compared to their BCS counterparts). For our purposes, we will focus on the principle of *topological superconductivity*, in which the superconducting states can manifest as topologically protected edge states. Additionally, my work will make use of the proximity effect, wherein a traditionally non-superconducting material can be rendered superconducting due to proximity to a superconductor.

1.4 Band Structure and Topology

To understand what "topologically nontrivial" means, we introduce the concept of the Berry phase. Here I follow the procedure outlined in Bernevig and Hughes [3], and derive the Berry phase from an adiabatic evolution of a quantum system in a parameter space $\mathbf{k}$. I then demonstrate how this phase gives rise to edge states, and the role of symmetry in determining what type of topological invariants are allowed in a system.

1.4.1 Berry Phase

In systems with translational invariance (such as a crystal lattice), we can model the system in momentum space $\mathbf{k}$ in terms of the Bloch wave functions $|\Psi_n(\mathbf{k})\rangle$:

$$H(\mathbf{k})\,|\Psi_n(\mathbf{k})\rangle = E_n(\mathbf{k})\,|\Psi_n(\mathbf{k})\rangle \tag{1.20}$$

Where $H(\mathbf{k})$ describes the Hamiltonian in momentum space. We will explore the behavior of this system under an adiabatic perturbation following a path C in momentum space, parameterized by $\mathbf{k}(t)$. The adiabatic theorem requires that the initial state remain an eigenstate of the system [3–6]; assuming we can choose a smooth gauge for the wave function by writing it as $|\Psi(\mathbf{k}(t))\rangle = e^{-i\theta(t)}\,|\Psi_n(\mathbf{k}(t))\rangle$, with $\theta(t)$, the Schrödinger equation gives us:

$$i\hbar\frac{d}{dt}\,|\Psi(\mathbf{k}(t))\rangle = H(\mathbf{k}(t))\,|\Psi(\mathbf{k}(t))\rangle \tag{1.21}$$

Thus:

$$e^{-i\theta(t)}E_n(\mathbf{k}(t))\left|\Psi_n(\mathbf{k}(t))\right\rangle = e^{-i\theta(t)}\hbar\left(\frac{d\theta}{dt}\right)\left|\Psi_n(\mathbf{k}(t))\right\rangle + e^{-i\theta(t)}i\hbar\frac{d}{dt}\left|\Psi_n(\mathbf{k}(t))\right\rangle \tag{1.22}$$

Removing the common phase factor and applying a normalized inner product, we obtain:

$$\hbar\left(\frac{d\theta}{dt}\right) = E_n(\mathbf{k}(t)) - i\hbar\left\langle\Psi_n(\mathbf{k}(t))\right|\frac{d}{dt}\left|\Psi_n(\mathbf{k}(t))\right\rangle \tag{1.23}$$

Which yields the phase:

$$\theta(t) = \frac{1}{\hbar}\int_0^t dt' E_n(\mathbf{k}(t')) - i\int_0^t dt'\left\langle\Psi_n(\mathbf{k}(t'))\right|\frac{d}{dt'}\left|\Psi_n(\mathbf{k}(t'))\right\rangle \tag{1.24}$$

The first term in Eq.(1.24) is the usual dynamical phase; the negative of the second term is the *Berry Phase* [3]:

$$\begin{aligned}\gamma_n &= i\int_0^t dt'\left\langle\Psi_n(\mathbf{k}(t'))\right|\frac{d}{dt'}\left|\Psi_n(\mathbf{k}(t'))\right\rangle \\ &= i\int_C d\mathbf{k}\cdot\left\langle\Psi_n(\mathbf{k})\right|\partial_{\mathbf{k}}\left|\Psi_n(\mathbf{k})\right\rangle\end{aligned} \tag{1.25}$$

Defining the Berry connection:

$$\mathbf{A}_n(\mathbf{k}) = \left\langle\Psi_n(\mathbf{k})\right|\partial_{\mathbf{k}}\left|\Psi_n(\mathbf{k})\right\rangle \tag{1.26}$$

And noting that it is purely imaginary:

$$\begin{aligned} 1 &= \langle \Psi_n(\mathbf{k}) | \Psi_n(\mathbf{k}) \rangle \\ \implies 0 &= \partial_{\mathbf{k}} \langle \Psi_n(\mathbf{k}) | \Psi_n(\mathbf{k}) \rangle = \langle \Psi_n(\mathbf{k}) | \partial_{\mathbf{k}} | \Psi_n(\mathbf{k}) \rangle + \langle \Psi_n(\mathbf{k}) | \partial_{\mathbf{k}} | \Psi_n(\mathbf{k}) \rangle^* \\ \implies \langle \Psi_n(\mathbf{k}) | \partial_{\mathbf{k}} | \Psi_n(\mathbf{k}) \rangle &= - \langle \Psi_n(\mathbf{k}) | \partial_{\mathbf{k}} | \Psi_n(\mathbf{k}) \rangle^* \end{aligned} \tag{1.27}$$

We can write the Berry Phase as:

$$\gamma_n = -Im \int_C d\mathbf{k} \cdot \mathbf{A}_n(\mathbf{k}) \tag{1.28}$$

1.4.2 Topological Invariants and Edge States

Suppose now the curve C is closed in momentum space (i.e. $\mathbf{k}(0) = \mathbf{k}(T)$ for a period T). We will assume $\mathbf{k}$ is two dimensional, (i.e. $\mathbf{k} = (k_x, k_y)$), and consider a filled band. If $\mathbf{A}_n(\mathbf{k})$ is smooth everywhere along C, we may apply Stokes' Theorem:

$$\begin{aligned} \gamma_n &= -Im \int d\mathbf{S} \cdot (\partial_{\mathbf{k}} \times \mathbf{A}_n(\mathbf{k})) \\ &= Im \int d\mathbf{S} \cdot \mathbf{F}_n(\mathbf{k}) \end{aligned} \tag{1.29}$$

Where S is the surface bound by C, in this case the Brillouin zone, and $\mathbf{F}_n(\mathbf{k}) = -\partial_{\mathbf{k}} \times \mathbf{A}_n(\mathbf{k})$ is the *Berry Curvature* and is gauge invariant. However, in two dimensions, the Brillouin zone is a torus with no natural boundary, and thus Eq.(1.28) (and Eq.(1.29)) must vanish. Therefore, for materials with nontrivial Berry phase, the Berry connection must be singular at some point(s) $\{\mathbf{k}_0\}$ in the Brillouin zone, obstructing the application of Stokes' theorem.

To correct for this, we apply a gauge transformation $|\Psi_n(\mathbf{k})\rangle \to e^{-i\phi_n(\mathbf{k})}|\Psi_n(\mathbf{k})\rangle$ within a region R of each singularity such that $A_n(\mathbf{k})$ is non-singular within R [3, 4]. The Berry connection becomes:

$$\mathbf{A}_n^R(\mathbf{k}) = \mathbf{A}_n(\mathbf{k}) - i\partial_{\mathbf{k}}\phi_n(\mathbf{k}) \tag{1.30}$$

The Berry connection is now piece-wise smooth everywhere, and we may apply Stokes' theorem. Since the only boundary is the (inverse) of region R, we have:

$$\begin{aligned}\gamma_n &= -Im \oint_{\partial R} d\mathbf{k} \cdot (\mathbf{A}_n^R(\mathbf{k}) - \mathbf{A}_n(\mathbf{k})) \\ &= \oint_{\partial R} d\mathbf{k} \cdot \partial_{\mathbf{k}}\phi_n(\mathbf{k})\end{aligned} \tag{1.31}$$

Finally, we note that for a closed path, we must have $|\Psi_n(\mathbf{k}(T))\rangle = |\Psi_n(\mathbf{k}(0))\rangle$, thus:

$$\begin{aligned}e^{i\phi_n(\mathbf{k}(T))} &= e^{i\phi_n(\mathbf{k}(0))} \\ \implies \phi_n(\mathbf{k}(T)) - \phi_n(\mathbf{k}(0)) &= 2\pi n\end{aligned} \tag{1.32}$$

Which allows us to write the Berry phase as:

$$\gamma_n = 2\pi C h_1^{(n)} \tag{1.33}$$

Where we have defined the band Chern number:

$$Ch_1^{(n)} = \frac{1}{2\pi} \oint_{\partial R} d\mathbf{k} \cdot \partial_{\mathbf{k}} \phi_n(\mathbf{k}) = \frac{1}{2\pi i} \int_{BZ} \mathbf{dS} \cdot \mathbf{F}_n(\mathbf{k}) \tag{1.34}$$

which is an integer. For a multi-band system, the full Chern number of the bulk system is given by the sum of the Chern number of each filled band.

The fact that the Berry phase is quantized in units of 2π leads to an interesting conflict with the adiabatic theorem. In the context of two gapped systems (i.e. no states with zero energy), the adiabatic theorem would suggest that each system can be smoothly evolved into the other (more explicitly, the ground states of one gapped system can be adiabatically evolved into the ground states of the other). However, a smooth transformation would be incapable of changing the Chern number (it's an integer). Thus, at the interface between two gapped systems with different Chern numbers, the gap must close, giving rise to *topologically protected edge states*. This is known as the Bulk Boundary Correspondence [3, 7], and is the reason why bulk insulators with nontrivial Chern number have conducting edge states.

1.4.3 Role of Symmetry

The topological invariant described by Eq.(1.34) characterizes the Hall Conductance, but other invariants, such as the $\mathbb{Z}_2$ invariant, exist. In general, there is a collection of topological invariants, and which class of invariants a material belongs to will depend on the inherent symmetries of the problem. For instance, in the presence of time reversal symmetry (TRS) ($[H, \mathcal{T}] = 0$, with $\mathcal{T}$ the time reversal operator and $\mathcal{T}^2 = -1$), we find:

$$H\left|\Psi\right\rangle = E\left|\Psi\right\rangle$$

$$\implies H(T\left|\Psi\right\rangle) = TH\left|\Psi\right\rangle = E(T\left|\Psi\right\rangle) \tag{1.35}$$

Thus, a state $|\Psi\rangle$ and its time-reversal partner have the same energy. When $\mathcal{T}^2 = -1$ (which is the case for half-integer spin particles) [3], these state are orthogonal:

$$\begin{aligned}\langle\Psi|\mathcal{T}\Psi\rangle &= \langle\mathcal{T}(\mathcal{T}\Psi)|\mathcal{T}\Psi\rangle \\ &= \left\langle\mathcal{T}^2\Psi\right|\left.\mathcal{T}\Psi\right\rangle \\ &= -\langle\Psi|\mathcal{T}\Psi\rangle\end{aligned} \tag{1.36}$$

Thus $\langle\Psi|\mathcal{T}\Psi\rangle = 0$, and the energy states come in time reversal, orthogonal pairs known as *Kramers' Pairs*. Recalling that, under time reversal, momentum transforms as $\mathcal{T}\mathbf{k}\mathcal{T}^{-1} = -\mathbf{k}$, we can investigate the Berry connection of a state $|\Psi^n_{\mathbf{k}}\rangle$ and compare it with its time reversal partner $\left|\Psi^{\bar{n}}_{-\mathbf{k}}\right\rangle$:

$$\left\langle\Psi^{\bar{n}}_{-\mathbf{k}}\right|\partial_{\mathbf{k}}\left|\Psi^{\bar{n}}_{-\mathbf{k}}\right\rangle = \langle\Psi^n_{\mathbf{k}}|\,T^{-1}\partial_{\mathbf{k}}T\,|\Psi^n_{\mathbf{k}}\rangle = -\langle\Psi^n_{\mathbf{k}}|\,\partial_{\mathbf{k}}\,|\Psi^n_{\mathbf{k}}\rangle \tag{1.37}$$

Thus, we must have:

$$\begin{aligned}Ch^{(\bar{n})} &= \frac{1}{2\pi i}\int_{BZ}\mathbf{dS}\cdot\mathbf{F}_{\bar{n}}(\mathbf{k}) = \frac{1}{2\pi i}\int_{BZ}\mathbf{dS}\cdot(\partial_{\mathbf{k}}\times A_{\bar{n}}(\mathbf{k})) \\ &= -\frac{1}{2\pi i}\int_{BZ}\mathbf{dS}\cdot(\partial_{\mathbf{k}}\times A_n(-\mathbf{k})) = -Ch^{(n)}\end{aligned} \tag{1.38}$$

This result holds even when obstructions of Stokes' theorem require a local gauge transformation:

$$|\Psi_n(\mathbf{k})\rangle \to e^{-i\phi_n(\mathbf{k})}|\Psi_n(\mathbf{k})\rangle \implies |\Psi_{\bar{n}}(-\mathbf{k})\rangle \to e^{i\phi_n(-\mathbf{k})}|\Psi_{\bar{n}}(-\mathbf{k})\rangle$$
$$\implies A_{\bar{n}}(-\mathbf{k}) \to A_{\bar{n}}(-\mathbf{k}) + i\partial_{\mathbf{k}}\phi_n(-\mathbf{k}) \tag{1.39}$$

Summation over all bands gives the Chern number of the bulk system, which is zero. However, we may now define a new topological invariant called the $\mathbb{Z}_2$ invariant:

$$\mathbb{Z}_2^{(n)} = \Big[\tfrac{1}{2}\Big(Ch^{(n)} - Ch^{(\bar{n})}\Big)\Big] mod(2) \tag{1.40}$$

which is simply the parity of the Chern invariant, and is valid when n and $\bar{n}$ are good quantum numbers for the system (for instance, in a spin-diagonal system). Such an invariant is nontrivial for odd parity Chern invariants, which is typically true of systems that break inversion symmetry (IS).

1.4.4 Spin Orbit Coupling

Consider a three dimensional lattice of bare ions and non-interacting electrons. In the tight binding model, the kinetic motion of electrons through the lattice is expressed through a "hopping interaction" that moves electrons from one ion to its nearest neighbor:

$$H = -t\sum_{i,j,s}(\Psi^\dagger_{\mathbf{r}_i+\mathbf{R}_j,s}\Psi_{\mathbf{r}_i,s} + \Psi^\dagger_{\mathbf{r}_i-\mathbf{R}_j,s}\Psi_{\mathbf{r}_i,s}) + h.c. \tag{1.41}$$

where $\Psi^{\dagger}_{\mathbf{r}_i,s}$ ($\Psi_{\mathbf{r}_i,s}$) creates (annihilates) an electron on lattice site $\mathbf{r}_i$ with spin s, and the lattice is defined by the lattice vectors $\mathbf{R}_j \equiv a\hat{j}$ for $j\epsilon\{x, y, z\}$. In terms of the electronic momentum, the Hamiltonian is:

$$\begin{aligned} H_s &= -2t \sum_{s,\mathbf{k},j} cos(\mathbf{k} \cdot \mathbf{R}_j) \Psi^{\dagger}_{\mathbf{k},s} \Psi_{\mathbf{k},s} \\ &\approx \sum_{s,\mathbf{k}} (ta^2\mathbf{k}^2 - 2t) \Psi^{\dagger}_{\mathbf{k},s} \Psi_{\mathbf{k},s} \end{aligned} \tag{1.42}$$

where the last line is the approximate energy near $\mathbf{k} = 0$. This model for the cubic lattice depicts electronic kinetic energy analogous to the free electron (a spin degenerate, quadratic function of the electron's momentum); however, the materials we're interested in have a more unique band structure. Consider the band structures in Fig.(1.2). The system on the left has broken time reversal symmetry generated by interaction of the form $B_0 S_z$, and potentially has nontrivial Chern topology. The system on the right has broken inversion symmetry, leading to an interaction of the form $\mathbf{k} \cdot \mathbf{S}$ (spin-orbit coupling), and potentially has nontrivial $\mathbb{Z}_2$ topology.

1.4.5 Weyl Semimetals

WSM's are characterized by energy bands of linear dispersion intersecting at a collection of momenta points known as Weyl nodes [4, 8–10]. They can be classified by whether they break time reversal symmetry (TRS) or inversion symmetry (IS); to demonstrate their topological properties, we will focus our attention on those with broken TRS.

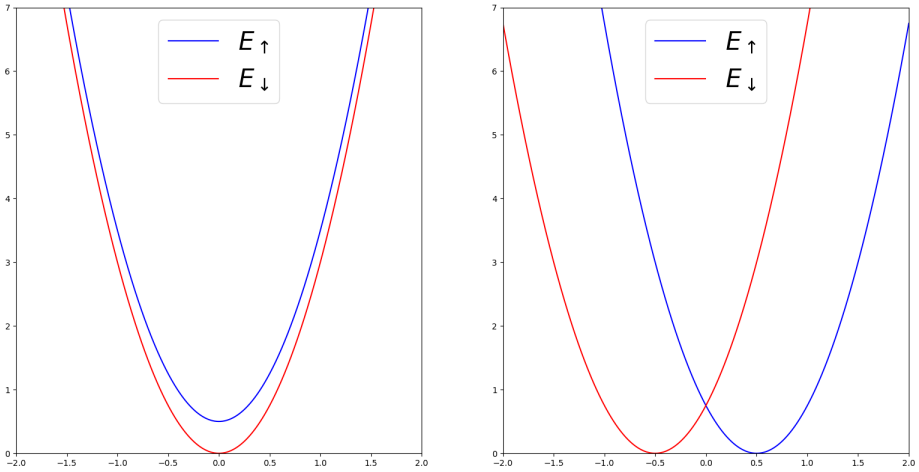

Figure 1.2: Quadratic band structure with (Left) an interaction that breaks time-reversal symmetry and (Right) a spin-orbit coupling interaction that breaks inversion symmetry.

The general low energy Hamiltonian has the form [9, 10]:

$$\mathbf{H_k} = v\sigma_x(\mathbf{s}\cdot\mathbf{k}) + m\sigma_z + bs_z + b'\sigma_z s_x \tag{1.43}$$

where σ_i and s_i are Pauli matrices in the pseudo-spin orbital and spin degrees of freedom. In the case of $m = b = b' = 0$, the system can instead be written in the block-diagonal form [9]:

$$H_\pm = \pm v\mathbf{s}\cdot\mathbf{k} \tag{1.44}$$

where $\pm$ corresponds to the chirality of the system. The Berry curvature and Chern number are then [9]:

$$\mathbf{F}_{\pm}(\mathbf{k}) = \pm\frac{\hat{e}_k}{2k^2} \tag{1.45}$$

$$C_1^{\pm} = \pm 1 \tag{1.46}$$

In other words, the Weyl points at $\mathbf{k} = 0$ act as "magnetic" monopoles of the Berry flux. We may break TRS by taking $b \neq 0$, and obtain a similar expression, but with Weyl nodes at $\mathbf{k}_{\pm} = (0, 0, \pm k_0)$ [9]. The monopoles of opposite chirality are now separated along k_z, and we may treat each instantaneous k_z layer between them as an effective 2-D system in (k_x, k_y). These layers must each have nonzero Berry flux, and thus have a topologically protected edge state crossing the chemical potential [9, 10]. However, the opposite is true of layers not located between the two monopoles, as they have net zero Berry flux. This results in a pair of topologically protected edge states connecting the Fermi surfaces centered on the monopoles known as *Fermi Arcs* [9, 10]. It has been shown that these surface states can also occur in WSM's that preserve TRS, but break IS [11].

Despite not having a gapped energy spectrum, WSM's still contain robust topological properties, making them an interesting candidate for studies of proximity induced topological superconductivity. Furthermore, for WSM's that break TRS, Cooper pairs with net zero momentum must form a spin triplet pairing [4]. In such a situation, it is possible to form electron-hole excitations that are their own anti-particle, i.e. a Majorana Fermion [4]. On the other hand, WSM's that preserve TRS but break IS are more likely to be susceptible to the proximity effect of an S-wave superconductor, since the superconductor's Cooper pairs are formed from the system's Kramers' pairs. Such a WSM can be described

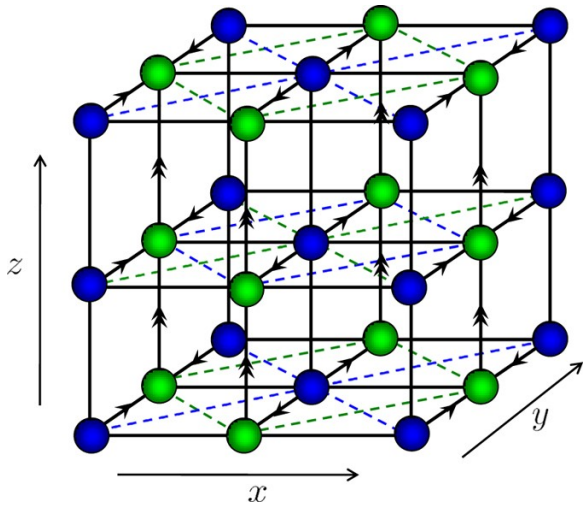

Figure 1.3: Schematic of the cubic structure of a WSM with broken inversion symmetry. The system has two sub-lattices: 1) Green and 2) Blue (Hou et. al., 2016).

by a cubic lattice with an underlying sub-lattice, as shown in Fig.(1.3) [12]. The low energy band structure of such a system is plotted along $k_y = k_z = 0$ in Fig.(1.4).

1.4.6 Transition Metal Dichalcogenides

Monolayer transition metal dichalcogenides (TMDC's) are a class of materials described by a hexagonal (honeycomb) lattice with an underlying sub-lattice, similar to Graphene (see Fig. 1.5) [13, 14]. However, unlike Graphene, they possess a strong Ising spin-orbit coupling (SOC). Their effective low energy Hamiltonian is given by [15–17]:

$$H_\nu(\mathbf{k}) = at(\nu k_x \sigma_x + k_y \sigma_y) + \tfrac{E_G}{2}\sigma_z - \tfrac{\nu}{2} E_{soc}(\sigma_z - 1) S_z \tag{1.47}$$

where $\nu = \pm 1$ gives the valley (sub-lattice) degree of freedom of the reciprocal lattice, and σ_i are the Pauli matrices in the orbital $|1\rangle_\nu = \left|d_{x^2-y^2}\right\rangle + i\nu \left|d_{xy}\right\rangle$, $|2\rangle = \left|d_{z^2}\right\rangle$ subspace.

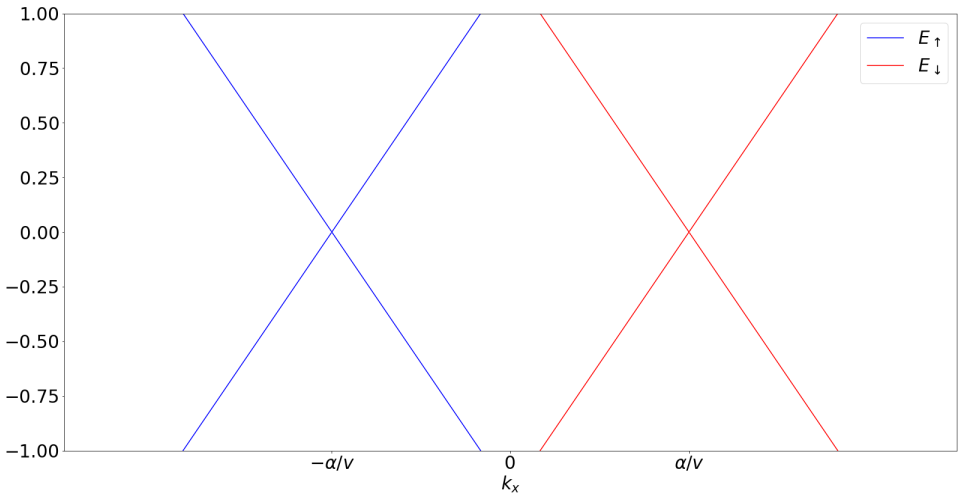

Figure 1.4: Band structure of a WSM with broken inversion symmetry, cut along $k_y = k_z = 0$. Spin up states are plotted in blue and spin down states are plotted in red.

The parameters a, t, and E_G give the lattice constant, hopping parameter, and band gap, respectively. The band structure of the two valleys have opposite spin physics, as shown in Fig. (1.6)[15].

The valley wave functions have an intrinsic phase winding that yields a valley dependent Berry Curvature [15]:

$$\Omega^n_{\nu s}(k) = -n\nu\Big[2(at)^2(E_G - \nu s E_{soc})\Big]\Big[(2atk)^2 + (E_G - \nu s E_{soc})^2\Big]^{-3/2} \tag{1.48}$$

where $n = \pm 1$ denotes the conduction/valence band. While the presence of TRS yields a net zero Chern invariant (integration of Eq.(1.48) over the full Brillouin zone gives opposite Chern numbers for the two valleys), the topological invariant $\mathbb{Z}_2 = \frac{1}{2}(Ch^\uparrow - Ch^\downarrow) mod 2$ is nontrivial.

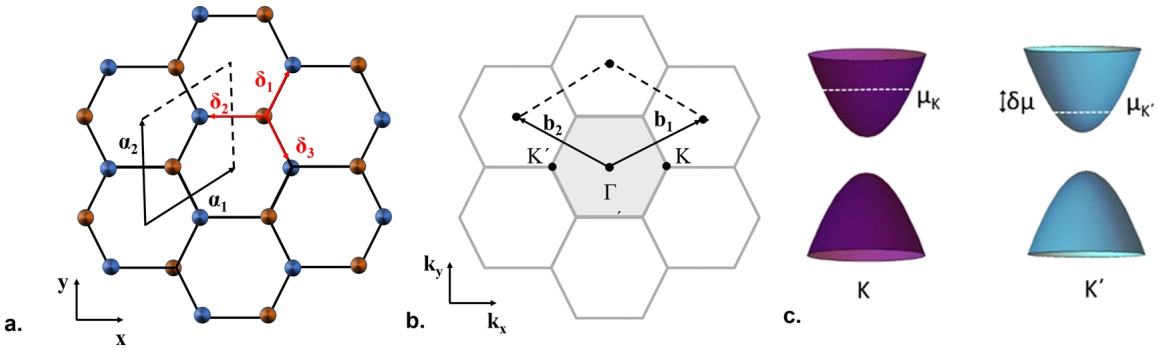

Figure 1.5: Hexagonal lattice structure of a TMDC. The system has two sub-lattices (depicted in blue and red). (b) First Brillouin zone of the hexagonal lattice, showing the two valleys K and K'. (c) Sketch of the conduction and valence bands of the two valleys. (Mouchliadis et. al., 2021).

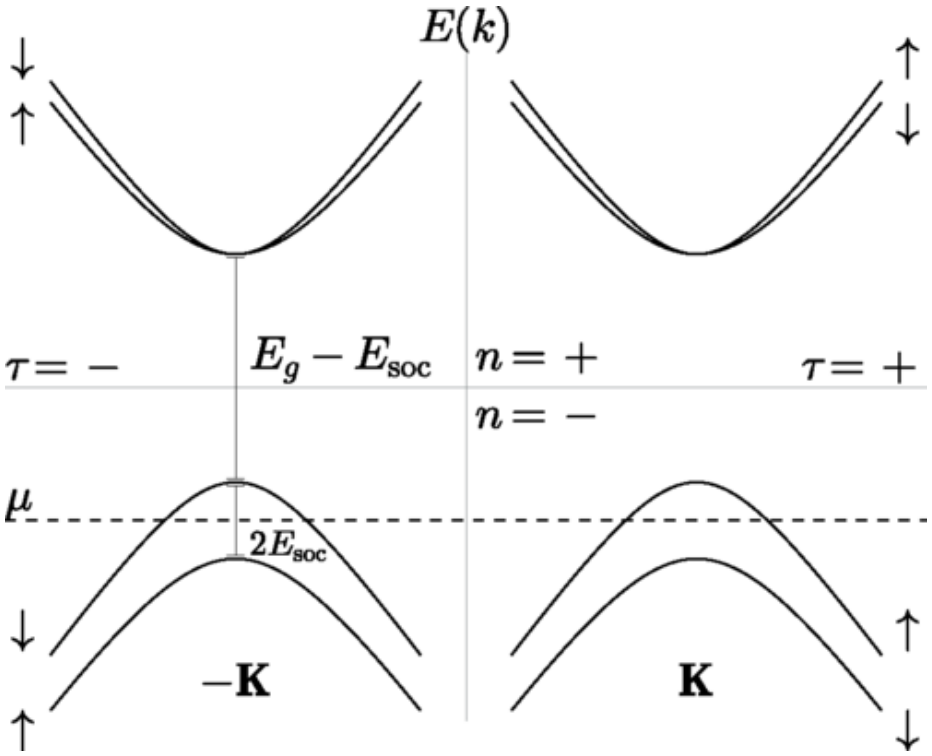

Figure 1.6: Conduction and valence bands of a TMDC for both valleys, cut along $k_y = 0$. The two valleys have opposite spin physics, breaking the system's inversion symmetry (Sosenko et. al., 2017).

1.5 Organization of the thesis

This work is organized as follows. In Chapter 1, we explore the effects of proximity induced superconductivity on Weyl semimetals with broken inversion symmetry and Transition Metal Dichalcogenides. We begin with a review of BCS theory and how it explains the proximity effect. We then demonstrate how, by expanding the electronic wave function in a Fourier basis, we can self consistently calculate the electron-electron correlation function throughout a device coupling a BCS superconductor to a normal material. Finally, we apply this technique to the chosen materials, and analyze what correlations, if any, can be induced by proximity.

In Chapter 2, we turn our attention to the optical properties of a stacked Transition Metal Dichalcogenide structure. A recent experiment has managed to utilize the principles of laser spectroscopy and photo-current to measure the inter-layer exciton binding energies of such a device. The data shows numerous peaks in the absorption spectra near the expected exciton energies. These phonon side-bands have traditionally appeared in photo-luminescent spectra, thus we aim to explain their existence in the context of photo-current absorption. In this chapter, we will derive various features of the *Interacting Polaron Model*. We obtain a general expression for the optical absorption coefficient and demonstrate how fitting it to experimental data can be used to obtain a better estimate of the exciton binding energy.

Chapter 2

Proximitized Superconductivity

2.1 Introduction

In 1957, Bardeen, Cooper, and Schrieffer proposed a microscopic description of superconductivity, wherein electrons experience a net attractive interaction due to coupling with lattice vibrations (phonons) [2]. In the superconducting phase, these electrons form Cooper pairs, and the super current can be described by correlations between electrons with opposite momentum and spin. Later, Pierre de Gennes would show that this theory allows for an interesting phenomenon near the interface of a BCS superconductor and a normal material called the Proximity Effect [18, 19]. In this section, we will review the BCS theory of superconductivity and how it allows normal materials to become superconducting near an interface with a superconductor.

2.1.1 BCS Theory of Superconductivity

Bardeen-Cooper-Schrieffer (BCS) superconductivity attributes the superconducting phenomenon of certain metals to an attractive interaction between two electrons:

$$H = \sum_{\mathbf{k},s} \xi_{\mathbf{k}} \Psi^{\dagger}_{\mathbf{k},s} \Psi_{\mathbf{k},s} + \sum_{\mathbf{k},\mathbf{k}'} V_{\mathbf{k},\mathbf{k}'} \Psi^{\dagger}_{\mathbf{k},\uparrow} \Psi^{\dagger}_{-\mathbf{k},\downarrow} \Psi_{-\mathbf{k}',\downarrow} \Psi_{\mathbf{k}',\uparrow} \tag{2.1}$$

where the spin degenerate, non-interacting band structure is defined to be $\xi_{\mathbf{k}} \equiv \varepsilon_{\mathbf{k}} - \mu$, with μ the chemical potential, and we have also assumed the presence of time reversal symmetry such that $\xi_{\mathbf{k},s} = \xi_{-\mathbf{k},\bar{s}}$. In the superconducting state, the interaction causes two electrons with opposite momentum and spin to become correlated. We apply the standard mean field analysis by assuming negligible fluctuations about an average correlation [20–23]:

$$b_{\mathbf{k}} \equiv \langle \Psi_{-\mathbf{k},\downarrow} \Psi_{\mathbf{k},\uparrow} \rangle \tag{2.2}$$

Defining $\delta_{\mathbf{k}} \equiv \Psi_{-\mathbf{k},\downarrow} \Psi_{\mathbf{k},\uparrow} - b_{\mathbf{k}}$ and expanding Eq.(2.1), we obtain:

$$\begin{aligned} \Psi^{\dagger}_{\mathbf{k},\uparrow} \Psi^{\dagger}_{-\mathbf{k},\downarrow} \Psi_{-\mathbf{k}',\downarrow} \Psi_{\mathbf{k}',\uparrow} &= (b^{*}_{\mathbf{k}} + \delta^{*}_{\mathbf{k}})(b_{\mathbf{k}'} + \delta_{\mathbf{k}'}) \\ &\approx b^{*}_{\mathbf{k}} b_{\mathbf{k}'} + b_{\mathbf{k}'} \Psi^{\dagger}_{\mathbf{k},\uparrow} \Psi^{\dagger}_{-\mathbf{k},\downarrow} + b^{*}_{\mathbf{k}} \Psi_{-\mathbf{k}',\downarrow} \Psi_{\mathbf{k}',\uparrow} - 2 b^{*}_{\mathbf{k}} b_{\mathbf{k}'} \end{aligned} \tag{2.3}$$

where we have discarded the small fluctuation $\delta^{*}_{\mathbf{k}} \delta_{\mathbf{k}'}$. We define the gap function:

$$\Delta_{\mathbf{k}} \equiv - \sum_{\mathbf{k}'} V_{\mathbf{k},\mathbf{k}'} \left\langle \Psi_{-\mathbf{k}',\downarrow} \Psi_{\mathbf{k}',\uparrow} \right\rangle \tag{2.4}$$

and obtain the BCS Hamiltonian:

$$H_{BCS} = \sum_{\mathbf{k},s} \xi_{\mathbf{k}} \Psi^{\dagger}_{\mathbf{k},s} \Psi_{\mathbf{k},s} - \sum_{\mathbf{k}} (\Delta_{\mathbf{k}} \Psi^{\dagger}_{\mathbf{k},\uparrow} \Psi^{\dagger}_{-\mathbf{k},\downarrow} + \Delta^{*}_{\mathbf{k}} \Psi_{-\mathbf{k},\downarrow} \Psi_{\mathbf{k},\uparrow}) + \sum_{\mathbf{k}} \Delta_{\mathbf{k}} b^{*}_{\mathbf{k}} \tag{2.5}$$

The interaction strength $V_{\mathbf{k},\mathbf{k}'}$ originates from electronic interactions with lattice vibrations (phonons). The interaction scatters an electron and its time reversal (Kramer's) pair from the Fermi surface via virtual phonon scattering when the energy difference of the involved states is less than the phonon energy [2]. Thus, the interaction strength is defined to be $V_{\mathbf{k},\mathbf{k}'} \equiv V_0$ for electronic states with energy $|\xi_{\mathbf{k},s}|, |\xi_{\mathbf{k}',s}| < \hbar\omega_D$, where ω_D is the Debye frequency.

It will prove useful to write Eq.(2.5) in the bogoliubov-de gennes (BdG) form:

$$H_{BCS} = \frac{1}{2} \sum_{\mathbf{k}} \mathbf{\Psi}^{\dagger}_{\mathbf{k}} \mathcal{H}_{\mathbf{k}} \mathbf{\Psi}_{\mathbf{k}} + E_0 \tag{2.6}$$

where, in the Nambu basis:

$$\mathbf{\Psi}_{\mathbf{k}} \equiv [\Psi_{\mathbf{k},\uparrow}, \Psi^{\dagger}_{-\mathbf{k},\downarrow}, \Psi_{\mathbf{k},\downarrow}, \Psi^{\dagger}_{-\mathbf{k},\uparrow}]^{T} \tag{2.7}$$

the BdG Hamiltonian $\mathcal{H}_{\mathbf{k}}$ and constant energy are given by:

$$\mathcal{H}_{\mathbf{k}} = \xi_{\mathbf{k}} S_0 \tau_z - \Delta_{\mathbf{k}} (iS_y) \tau_+ + \Delta^{*}_{\mathbf{k}} (iS_y) \tau_- \tag{2.8}$$

$$E_0 = \sum_{\mathbf{k}} (\xi_{\mathbf{k}} + \Delta_{\mathbf{k}} b^{*}_{\mathbf{k}}) \tag{2.9}$$

S_i and τ_i are the Pauli matrices in the spin and particle/hole subspace, respectively, with $\tau_\pm = \frac{1}{2}(\tau_x \pm i\tau_y)$. We identify a unitary transformation that diagonalizes $\mathcal{H}_{BdG}$:

$$U_{\mathbf{k}}^\dagger \mathcal{H}_{\mathbf{k}} U_{\mathbf{k}} = \mathcal{D}_{\mathbf{k}} \tag{2.10}$$

The columns of $U_{\mathbf{k}}$ are the eigenvectors of $\mathcal{H}_{\mathbf{k}}$. We define a Bogoliubov transformation $\mathbf{\Psi}_{\mathbf{k},s} \equiv U_{\mathbf{k},s}\gamma_{\mathbf{k},s}$:

$$\begin{pmatrix} \Psi_{\mathbf{k},s} \\ \\ \Psi^\dagger_{-\mathbf{k},\bar{s}} \end{pmatrix} = \begin{pmatrix} u^*_{\mathbf{k},s} & v_{\mathbf{k},s} \\ \\ -v^*_{\mathbf{k},\bar{s}} & u_{\mathbf{k},\bar{s}} \end{pmatrix} \begin{pmatrix} \gamma_{\mathbf{k},s} \\ \\ \gamma^\dagger_{-\mathbf{k},\bar{s}} \end{pmatrix} \tag{2.11}$$

with $|u_{\mathbf{k},s}|^2 + |v_{\mathbf{k},s}|^2 = 1$ and $\bar{s} = -s$, such that:

$$H = \frac{1}{2}\sum_{\mathbf{k}} \gamma^\dagger_{\mathbf{k}} \mathcal{D}_{\mathbf{k}} \gamma_{\mathbf{k}} \tag{2.12}$$

where $\gamma_{\mathbf{k}} = [\gamma_{\mathbf{k},\uparrow}, \gamma_{\mathbf{k},\downarrow}]^T$, and the quasi-particle energy dispersion is given by $E_{\mathbf{k},s} = \sqrt{\xi^2_{\mathbf{k}} + |\Delta_{\mathbf{k}}|^2}$. The electron/hole weights satisfy:

$$2\xi_{\mathbf{k}} v_{\mathbf{k}} u_{\mathbf{k}} - \Delta_{\mathbf{k}} u^2_{\mathbf{k}} + \Delta^*_{\mathbf{k}} v^2_{\mathbf{k}} = 0 \tag{2.13}$$

Thus:

$$\frac{v_{\mathbf{k}}}{u_{\mathbf{k}}} = \frac{\pm\sqrt{\xi^2_{\mathbf{k}} + |\Delta_{\mathbf{k}}|^2} - \xi_{\mathbf{k}}}{\Delta^*_{\mathbf{k}}} \tag{2.14}$$

The sign in the numerator is assigned to the quasi-particle/quasi-hole wave functions. Under

the normalization condition $|u_{\mathbf{k}}^2|+|v_{\mathbf{k}}|^2 = 1$, and gauge fixing the phase of the gap function $\Delta_{\mathbf{k}} = |\Delta_{\mathbf{k}}|e^{i\phi_{\mathbf{k}}}$ to the hole weight, we find:

$$u_{\mathbf{k}} = \frac{1}{\sqrt{2}}\left(1 + \frac{\xi_{\mathbf{k}}}{\sqrt{\xi_{\mathbf{k}}^2 + |\Delta_{\mathbf{k}}|^2}}\right)^{1/2} \tag{2.15}$$

$$v_{\mathbf{k}} = \frac{e^{i\phi_{\mathbf{k}}}}{\sqrt{2}}\left(1 - \frac{\xi_{\mathbf{k}}}{\sqrt{\xi_{\mathbf{k}}^2 + |\Delta_{\mathbf{k}}|^2}}\right)^{1/2} \tag{2.16}$$

With this transformation, the Hamiltonian in Eq.(2.6) becomes:

$$H_{BCS} = \sum_{\mathbf{k},s} E_{\mathbf{k}}\gamma_{\mathbf{k},s}^\dagger\gamma_{\mathbf{k},s} + \sum_{\mathbf{k}}(\xi_{\mathbf{k}} - E_{\mathbf{k}} + \Delta_{\mathbf{k}}b_{\mathbf{k}}^*) \tag{2.17}$$

where the constant term gives the ground state energy.

We find that, due to the presence of time reversal symmetry, the quasi-particle/hole weights are symmetric under a $\mathbf{k} \to -\mathbf{k}, s \to \bar{s}$ transformation. Dropping the redundant subscripts, we find a self consistent equation for the gap function:

$$\begin{aligned}\Delta_{\mathbf{k}} &= -\sum_{\mathbf{k}'} V_{\mathbf{k},\mathbf{k}'}\left\langle(u_{\mathbf{k}'}^*\gamma_{-\mathbf{k}',\downarrow} - v_{\mathbf{k}'}\gamma_{\mathbf{k}',\uparrow}^\dagger)(u_{\mathbf{k}'}^*\gamma_{\mathbf{k}',\uparrow} + v_{\mathbf{k}'}\gamma_{-\mathbf{k}',\downarrow}^\dagger)\right\rangle \\ &= -\sum_{\mathbf{k}'} V_{\mathbf{k},\mathbf{k}'}u_{\mathbf{k}'}^*v_{\mathbf{k}'}\left(\left\langle\gamma_{-\mathbf{k}',\downarrow}\gamma_{-\mathbf{k}',\downarrow}^\dagger\right\rangle - \left\langle\gamma_{\mathbf{k}',\uparrow}^\dagger\gamma_{\mathbf{k}',\uparrow}\right\rangle\right)\end{aligned} \tag{2.18}$$

Note that this bogoliubov transformation has preserved our commutation relations:

$$\begin{aligned}\{\gamma_{\mathbf{k},s}, \gamma_{\mathbf{k}',s'}^\dagger\} &= u_{\mathbf{k}}u_{\mathbf{k}'}^*\{\Psi_{\mathbf{k},s}, \Psi_{\mathbf{k}',s'}^\dagger\} - v_{\mathbf{k}}v_{\mathbf{k}'}^*\{\Psi_{\mathbf{k},s}^\dagger, \Psi_{\mathbf{k},s}\} \\ &= \delta_{\mathbf{k},\mathbf{k}'}\delta_{s,s'}(|u_{\mathbf{k}}|^2 + |v_{\mathbf{k}}|^2) = \delta_{\mathbf{k},\mathbf{k}'}\delta_{s,s'}\end{aligned} \tag{2.19}$$

Thus the the quasi-particle operators obey fermionic statistics:

$$\left\langle \gamma_{-\mathbf{k}',\downarrow}\gamma^{\dagger}_{-\mathbf{k}',\downarrow} \right\rangle - \left\langle \gamma^{\dagger}_{\mathbf{k}',\uparrow}\gamma_{\mathbf{k}',\uparrow} \right\rangle = -tanh\left(\frac{E_{\mathbf{k}'}}{2k_BT}\right) \tag{2.20}$$

We also have:

$$u^{*}_{\mathbf{k}'}v_{\mathbf{k}'} = |u'_k|^2\frac{v_{\mathbf{k}'}}{u_{\mathbf{k}'}} = \frac{1}{2}\frac{E^2_{\mathbf{k}'} - \xi^2_{\mathbf{k}'}}{\Delta^{*}_{\mathbf{k}'}E_{\mathbf{k}'}} = \frac{\Delta_{\mathbf{k}'}}{2E_{\mathbf{k}'}} \tag{2.21}$$

yielding the self consistent gap function:

$$\Delta_{\mathbf{k}} = \sum_{\mathbf{k}'}\frac{V_{\mathbf{k},\mathbf{k}'}\Delta_{\mathbf{k}'}}{2E_{\mathbf{k}'}}tanh\left(\frac{E_{\mathbf{k}'}}{2k_BT}\right) \tag{2.22}$$

From here, one can derive the critical temperature at which the material becomes superconducting; however, our interests lie in what happens when the system's translational invariance is broken.

2.1.2 Proximity Effect

To illustrate the proximity effect, we consider a basic system: a rectangular box with a boundary at $z = L_B$ separating two regions along the z-axis, terminating at two endpoints $z = 0$ and $z = L$, as in Fig.(2.1). Both pieces will be given the same metallic base, with a superconducting interaction added to the left region only. The Hamiltonian for the non-interacting system is:

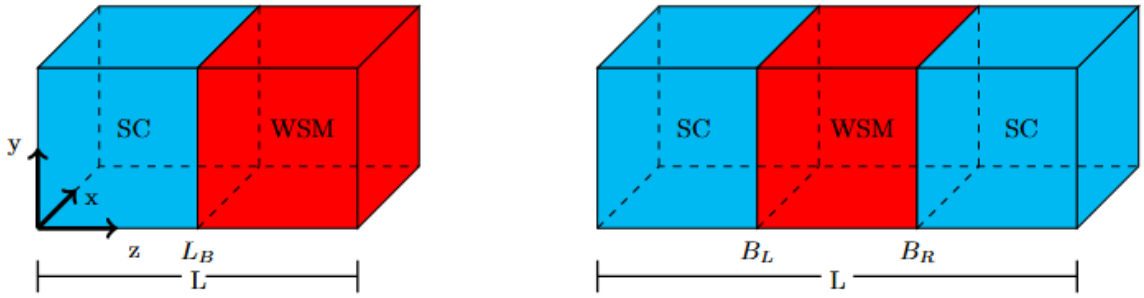

Figure 2.1: Sketch of (Left) a device consisting of an S-Wave superconductor (SC) in contact with a WSM (WSM) with the boundary located at L_B, and (Right) a Josephson Junction architecture with boundaries at B_L and B_R.

$$H_0 = \int \mathbf{dr} \sum_{ss'} \Psi_s^\dagger(\mathbf{r}) \left(\frac{-\hbar^2 \nabla^2}{2m} + E_0 - \mu \right) (S_0)_{ss'} \Psi_{s'}(\mathbf{r}) \tag{2.23}$$

and the superconducting Hamiltonian is given by:

$$H_{SC} = \int \mathbf{dr} \sum_{ss'} \Delta(z) (iS_y)_{ss'} \Psi_s^\dagger(\mathbf{r}) \Psi_{s'}^\dagger(\mathbf{r}) + h.c. \tag{2.24}$$

S_i are the Pauli matrices in the spin subspace, with S_0 being the identity. The semiconductor gap is given by $2E_0$, the chemical potential is μ, and the superconducting gap $2\Delta(z)$ is nonzero only for the superconductor. We now Fourier Transform along x and y:

$$\Psi_s(\mathbf{r}) = \frac{1}{(2\pi)^2} \int d\mathbf{k}_\perp \Psi_{\mathbf{k}_\perp, s}(z) e^{-i\mathbf{k}_\perp \cdot \mathbf{r}} \tag{2.25}$$

Defining $m_0 \equiv \hbar^2/2m$, we obtain:

$$H_0 = \int dz \int \mathbf{dr}_\perp \int \frac{\mathbf{dk}_\perp}{(2\pi)^2} \int \frac{\mathbf{dk'}_\perp}{(2\pi)^2} \sum_{ss'} \Psi^\dagger_{\mathbf{k}_\perp,s}(z) e^{i\mathbf{k}_\perp\cdot\mathbf{r}}(-m_0\nabla^2 + E_0 - \mu)(S_0)_{ss'} \Psi_{\mathbf{k'}_\perp,s'}(z) e^{-i\mathbf{k'}_\perp\cdot\mathbf{r}_\perp}$$

$$= \int dz \int \frac{\mathbf{dk}_\perp}{(2\pi)^2} \int \frac{\mathbf{dk'}_\perp}{(2\pi)^2} \sum_{ss'} (m_0({\mathbf{k'}_\perp}^2 - \partial_z^2) + E_0 - \mu)(S_0)_{ss'} e^{i(\mathbf{k}_\perp - \mathbf{k'}_\perp)\cdot\mathbf{r}} \Psi^\dagger_{\mathbf{k}_\perp,s}(z) \Psi_{\mathbf{k'}_\perp,s'}(z)$$
$$\times (2\pi^2)\delta^2(\mathbf{k}_\perp - \mathbf{k'}_\perp)$$

$$= \int dz \int \frac{\mathbf{dk}_\perp}{(2\pi)^2} \sum_{s,s'} (m_0({\mathbf{k}_\perp}^2 - \partial_z^2) + E_0 - \mu)(S_0)_{ss'} \Psi^\dagger_{\mathbf{k}_\perp,s}(z) \Psi_{\mathbf{k}_\perp,s'}(z) \tag{2.26}$$

and:

$$H_{SC} = \int dz \int d\mathbf{r}_\perp \int \frac{d\mathbf{k}_\perp}{(2\pi)^2} \int \frac{\mathbf{dk'}_\perp}{(2\pi)^2} \sum_{ss'} \Delta(z)(iS_y)_{ss'} e^{-i(\mathbf{k}_\perp + \mathbf{k'}_\perp)\cdot\mathbf{r}_\perp} \Psi^\dagger_{\mathbf{k}_\perp,s}(z) \Psi^\dagger_{\mathbf{k'}_\perp,s'}(z) + h.c.$$

$$= \int dz \int \frac{d\mathbf{k}_\perp}{(2\pi)^2} \int \frac{\mathbf{dk'}_\perp}{(2\pi)^2} \sum_{ss'} \Delta(z)(iS_y)_{ss'} (2\pi)^2 \delta^2(\mathbf{k}_\perp + \mathbf{k'}_\perp) \Psi^\dagger_{\mathbf{k}_\perp,s}(z) \Psi^\dagger_{\mathbf{k'}_\perp,s'}(z) + h.c.$$

$$= \int dz \int \frac{d\mathbf{k}_\perp}{(2\pi)^2} \sum_{ss'} \Delta(z)(iS_y)_{ss'} \Psi^\dagger_{\mathbf{k}_\perp,s}(z) \Psi^\dagger_{-\mathbf{k}_\perp,s'}(z) + h.c. \tag{2.27}$$

Finally, in the Nambu Basis $\mathbf{\Psi}_{\mathbf{k}_\perp} = [\Psi_{\mathbf{k}_\perp,\uparrow}(z), \Psi_{\mathbf{k}_\perp,\downarrow}(z), \Psi^\dagger_{-\mathbf{k}_\perp,\downarrow}(z), \Psi^\dagger_{-\mathbf{k}_\perp,\uparrow}(z)]^T$, the Hamiltonian is given by:

$$H = \frac{1}{2}\int dz \int \frac{\mathbf{dk}_\perp}{(2\pi)^2} \mathbf{\Psi}^\dagger{}_{\mathbf{k}_\perp} \mathcal{H}_{BdG}(\mathbf{k}_\perp, z) \mathbf{\Psi}_{\mathbf{k}_\perp} \tag{2.28}$$

The BdG Hamiltonian is given by:

$$\mathcal{H}_{BdG}(\mathbf{k}_\perp, z) = [m_0(\mathbf{k}_\perp^2 - \partial_z^2) + E_0 - \mu] S_0 \tau_z + \Delta(z)(iS_y)\tau_+ - \Delta^*(z)(iS_y)\tau_- \tag{2.29}$$

with the Pauli matrices τ_i acting in the particle/hole subspace and $\tau_\pm = (1/2)(\tau_x \pm i\tau_y)$.

Our goal now would be to solve the BdG equation:

$$\mathcal{H}_{BdG}(\mathbf{k}_\perp, z)\mathbf{\Psi}_{\mathbf{k}_\perp}(z) = E_{\mathbf{k}_\perp}\mathbf{\Psi}_{\mathbf{k}_\perp}(z) \tag{2.30}$$

which can be written as the following set of coupled differential equations:

$$[m_0(\mathbf{k}_\perp^2 - \partial_z^2) + E_0 - \mu]\Psi_{\mathbf{k}_\perp,\uparrow}(z) + \Delta(z)\Psi^\dagger_{-\mathbf{k}_\perp,\downarrow}(z) = E_{\mathbf{k}_\perp}\Psi_{\mathbf{k}_\perp,\uparrow}(z) \tag{2.31}$$

$$[m_0(\mathbf{k}_\perp^2 - \partial_z^2) + E_0 - \mu]\Psi_{\mathbf{k}_\perp,\downarrow}(z) - \Delta(z)\Psi^\dagger_{-\mathbf{k}_\perp,\uparrow}(z) = E_{\mathbf{k}_\perp}\Psi_{\mathbf{k}_\perp,\downarrow}(z) \tag{2.32}$$

$$[\mu - E_0 - m_0(\mathbf{k}_\perp^2 - \partial_z^2)]\Psi^\dagger_{-\mathbf{k}_\perp,\downarrow}(z) + \Delta^*(z)\Psi_{\mathbf{k}_\perp,\uparrow}(z) = E_{\mathbf{k}_\perp}\Psi^\dagger_{-\mathbf{k}_\perp,\downarrow}(z) \tag{2.33}$$

$$[\mu - E_0 - m_0(\mathbf{k}_\perp^2 - \partial_z^2)]\Psi^\dagger_{-\mathbf{k}_\perp,\uparrow}(z) - \Delta^*(z)\Psi_{\mathbf{k}_\perp,\downarrow}(z) = E_{\mathbf{k}_\perp}\Psi^\dagger_{-\mathbf{k}_\perp,\uparrow}(z) \tag{2.34}$$

Solving for the terms involving the partial derivative operators:

$$-\partial_z^2\mathbf{\Psi}_{\mathbf{k}_\perp}(z) + M^R_{\mathbf{k}_\perp}(z)\mathbf{\Psi}_{\mathbf{k}_\perp}(z) = E_{\mathbf{k}_\perp}\mathbf{\Psi}_{\mathbf{k}_\perp}(z) \tag{2.35}$$

where $M(z)$ captures the coupled behavior of the differential equations and, for simplicity, we have set $m_0 = 1$. We now consider a solution within a specific region R:

$$-\partial_z^2 \mathbf{\Psi}^R_{\mathbf{k}_\perp}(z) + M^R_{\mathbf{k}_\perp} \mathbf{\Psi}^R_{\mathbf{k}_\perp}(z) = E_{\mathbf{k}_\perp} \mathbf{\Psi}^R_{\mathbf{k}_\perp}(z) \tag{2.36}$$

with the assumption that $M(z)$ is constant (but not necessarily identical) within each region. We take the Ansatz:

$$\mathbf{\Psi}^R(\mathbf{k}_\perp, z) \equiv f^R(z) y^R_{\mathbf{k}_\perp} \tag{2.37}$$

$$M_R\, y^R_{\mathbf{k}_\perp} = \varepsilon^R_{\mathbf{k}_\perp} y^R_{\mathbf{k}_\perp} \tag{2.38}$$

yielding the differential equation:

$$-\partial_z^2 f^R(z) + \varepsilon^R_{\mathbf{k}_\perp} f^R(z) = E_{\mathbf{k}_\perp} f^R(z) \tag{2.39}$$

This is analogous to the usual square well potential, with the region dependent eigenvalue $\varepsilon^R_{\mathbf{k}_\perp}$ replacing the usual $V(z)$ potential.

In principle, Eq.(2.39) can be solved to find the exact form of the wave functions in each region. In the absence of a gap function, and assuming the two regions are identical, we would find the usual solution of the infinite square well. However, in the presence of the gap function, continuity of the electronic wave function across the interface requires that the electron-hole correlation of the host superconductor "leaks" into the normal region. This, in turn, requires the presence of a gap function to be induced in the normal region near

the SC-N interface. De Gennes showed that the gap function decays exponentially into the normal system:

$$\Delta(z) \propto e^{-k(z-L_B)} \tag{2.40}$$

and satisfies the interface boundary conditions:

$$\frac{\Delta(L_B)}{\nu(\varepsilon_F)V} = \frac{\Delta_S(L_B)}{\nu_S(\varepsilon_F)V_S} \tag{2.41}$$

$$\frac{\xi^2}{V}\frac{d\Delta}{dz}\bigg|_{L_B} = \frac{\xi_S^2}{V_S}\frac{d\Delta_S}{dz}\bigg|_{L_B} \tag{2.42}$$

Here ν (ν_S) is the density of states of the normal (superconductor) at the Fermi surface, V (V_S) is the strength of the pairing potentials, and ξ (ξ_S) is the coherence length of the cooper pair [18, 19]. This phenomenon, which renders a portion of the normal system superconducting, is known as *the proximity effect*.

2.2 Methods

The effects of proximitized superconductivity are typically explored in one of two methods: 1) An assumed intrinsic gap function is inserted into the material's BdG Hamiltonian and evaluated through mean field theory [15, 24–30], and 2) A tunneling model is constructed to connect the SC layers of a heterostructure to those of the material of interest, and the resultant gap function is calculated either through exact diagonalization or from the tunneling self energy [15–17, 25, 31–38]. Mean-field analysis reveals that WSM's and

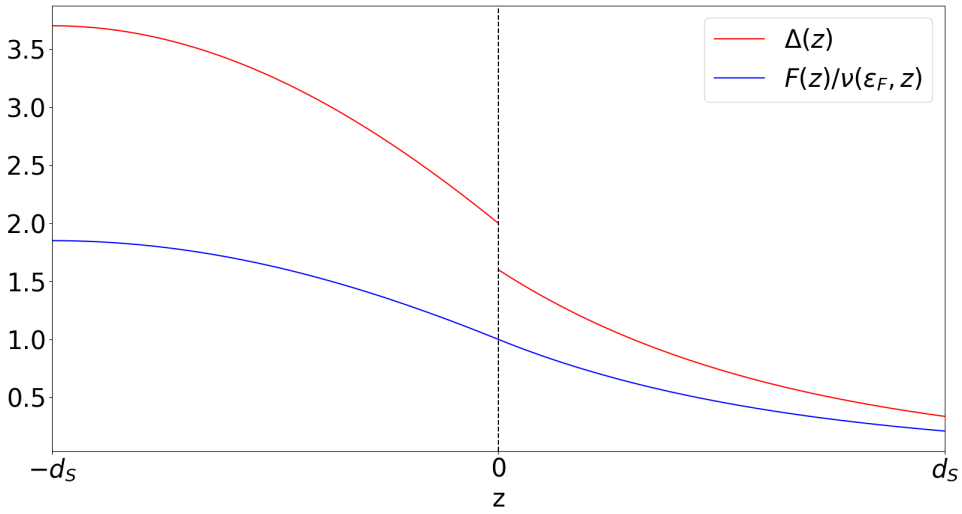

Figure 2.2: Sketch of (red) the gap function and (blue) the correlation function across an SC-N interface, with the boundary placed at $L_B = 0$. In general, the gap function is discontinuous across the interface, while the fraction of paired electrons $F/\nu(\varepsilon_F)$ is continuous. Both functions decay exponentially into the normal material.

TMDC's can support intra-valley/intra-nodal spin triplet pairings of the form $\langle \Psi_{\mathbf{k},s} \Psi_{\mathbf{k}+\delta_{\mathbf{k}},s} \rangle$. However, such analysis can only reveal the possible forms of the induced superconductivity, and cannot tell you which ones are realized experimentally. The same can be said for the tunneling approach, as the form of the induced superconductivity will depend on any assumptions made of the tunneling model. In this section, we will explore a method for obtaining a self-consistent calculation of the gap function while making a minimal assumption of the tunneling model: continuity of the electronic wave function and its derivative across the SC-N interface.

2.2.1 The Spectral Method

We now return to Eq.(2.39), writing it in the form:

$$\partial_z^2 f^R(z) = -\tilde{E}^R_{\mathbf{k}_\perp} f^R(z) \tag{2.43}$$

where $\tilde{E}_{\mathbf{k}_\perp}$ is the difference between the energy of the system and that of a piece-wise region. Assuming $\tilde{E}_{\mathbf{k}_\perp} > 0$, and applying the boundary conditions $f(0) = 0$ for the left region (or, equivalently, $f(L) = 0$ for the right), we have:

$$f^R(z) = Asin(k_R z) \tag{2.44}$$

In the region containing L, we must have:

$$k_R = \frac{n\pi}{L},\ n\epsilon\mathcal{N} \tag{2.45}$$

This suggests that the wave functions in the region containing L can be expanded in the form:

$$f(z) = \sqrt{\frac{2}{L}} \sum_n C_n sin(k_n z) \tag{2.46}$$

In fact, by invoking continuity of the wave function and its derivative at the interface, and the uniqueness theorem for linear differential equations, we see that Eq.(2.46) is the general solution for the full system.

In general, calculating the energies in Eqs.(2.31-2.34) is still nontrivial, as it requires knowledge of the Fourier coefficients C_n. However, now that we know we can expand the wave functions in a Fourier basis, we are free to re-cast the piece-wise Hamiltonian in the same basis [39]:

$$\langle n|\,\mathcal{H}_{BdG}(\mathbf{k}_\perp)\,|m\rangle = \frac{2}{L}\int_0^L dz\,\sin(k_n z)\mathcal{H}_{BdG}(\mathbf{k}_\perp, z)\,\sin(k_m z) \tag{2.47}$$

This approach, known as the spectral method, converts Eqs.(2.31-2.34) from a set of coupled differential equations into a numerical eigenvalue problem, allowing us to obtain the (now smooth) energy dispersion of the piece-wise system as well as the Fourier coefficients of the wave functions. The advantage of this approach is that we may now self-consistently calculate the gap function of the proximitized system without relying on a tunneling model to mix the two regions.

To illustrate the calculation, we return to our earlier expression for the gap function, now modified to account for its real space dependence. We assume zero temperature and an attractive interaction of the form $V_{\mathbf{k},\mathbf{k}'} = -V_0$ for non-interacting states within the Debye window. We obtain:

$$\Delta_{\mathbf{k}_\perp}(z) = V_0(z)\sum_{\mathbf{k}'_\perp}\left(\sum_{|\xi_{\alpha,\mathbf{k}'_\perp}|\leq\hbar\omega_D}\sum_m u^{*(n)}_{\alpha,\mathbf{k}'_\perp,\downarrow}v^{(m)}_{\alpha,-\mathbf{k}'_\perp,\uparrow}sin(kz)sin(k_m z)\right) \tag{2.48}$$

with α the eigenstate index of the Fourier system. The gap function now has the form:

$$\Delta_{\mathbf{k}_\perp}(z) = g(z)F(z) \tag{2.49}$$

$g(z)$ accounts for the strength of the interaction within the host superconductor and the pairing amplitude $F(z)$ is given by:

$$F(z) = \sum_{m} \sum_{\mathbf{k}'_{\perp}} C_{nm}(\mathbf{k}'_{\perp}) sin(k_n z) sin(k_m z) \tag{2.50}$$

with the Fourier coefficients:

$$C_{nm}(\mathbf{k}'_{\perp}) = \sum_{|\xi_{\alpha,\mathbf{k}'_{\perp}}| \leq \hbar\omega_D} u^{*(n)}_{\alpha,\mathbf{k}'_{\perp},\downarrow} v^{(m)}_{\alpha,-\mathbf{k}'_{\perp},\uparrow} \tag{2.51}$$

We are now equipped to solve for the pairing amplitude self consistently by: (1) Finding the wave functions of the proximitized Hamiltonian whose elements are given by Eq.(2.47), and (2) inserting the wave function coefficients into Eq.(A.2). This can, in principle, be done iteratively; however, the algorithm is computationally expensive, and our simulations have shown convergent solutions after just one iteration. We therefore limit our analysis to one loop simulations.

We conclude this section by exploring a limitation of the prescribed technique. Suppose we were to define two simple, metallic Hamiltonians:

$$\begin{aligned} H_L &= \int dz \Psi^{\dagger}(z) \Big[m_L P_z^2 \Big] \Psi(z) \\ H_R &= \int dz \Psi^{\dagger}(z) \Big[m_R P_z^2 \Big] \Psi(z) \end{aligned} \tag{2.52}$$

where m_L is considered nonzero in the region $0 < z < L_B$ and m_R is considered nonzero in the region $L_B < z < L$. This model describes a spinless particle in a box of length L such

that it has a different mass on either side of a boundary at L_B. If we were to attempt to expand this Hamiltonian in our Fourier Basis, we would find the following matrix elements:

$$\begin{aligned} H_{nm} &= -\frac{2m_L}{L}\int_0^{L_B} dz sin(kz)(-i\partial_z)^2 sin(k_m z) - \frac{2m_R}{L}\int_{L_B}^{L} dz sin(kz)(-i\partial_z)^2 sin(k_m z) \\ &= k_m^2\left[\frac{2m_L}{L}\int_0^{L_B} dz sin(kz) sin(k_m z) - \frac{2m_R}{L}\int_{L_B}^{L} dz sin(kz) sin(k_m z)\right] \\ &\propto k_m^2(m_R - m_L) \end{aligned} \tag{2.53}$$

This is not symmetric under an exchange of $n \leftrightarrow m$, and the expanded Hamiltonian is not Hermitian, leading to restrictions on the Bulk models used to generate differential equations similar to Eq.(2.35). When constructing the Bulk Hamiltonians, coefficients attached to momentum terms of the axis with broken translational invariance must be continuous throughout the device. They must either be constant (likely leading to a Fourier basis) or some continuous function that allows for a set of normalized, orthogonal basis functions to be chosen.

2.2.2 Metallic Simulations

To demonstrate that the numerical approach faithfully accounts for proximal superconductivity, we consider a metallic Hamiltonian (Eq.(2.23)). We study three cases.

- The parameters of the Hamiltonian are identical on both sides of the interface. This is the standard model of SC-N junction. In Fig.(2.3b), we recover the smooth evolution from the SC to the metal without any oscillatory behavior. For a clean superconductor the coherence length is 0.74ξ[18, 40] which is quantitatively consistent with the data.

- To introduce a mismatch at the interface we introduce a relative shift of the bands. The net effect is to introduce mismatch in velocity and density of states at the chemical potential. While an oscillatory behavior is beginning to emerge in Fig.(2.3d), a sharp drop off or an evanescent behavior is not observed.

- To test the effect of inversion breaking, we introduce Eq.(2.55) to the metallic side of the interface. A sharp change in symmetry across the interface leads to a sharper fall off and the emergence of oscillatory behavior (see Fig.(2.3f)).

  We estimate the decay length of each case by fitting to an exponential decay. For these simulations, the Cooper pair size ξ is approximately $0.01L$.

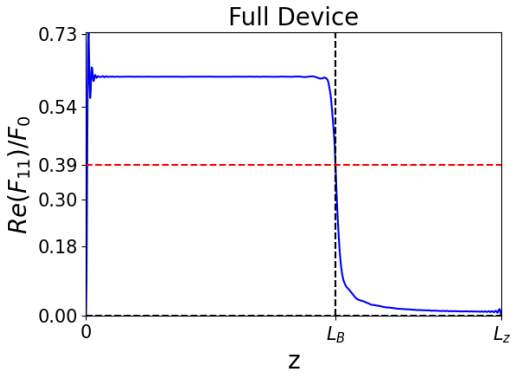

(a) $\alpha = 0, E_0 = 0.05$

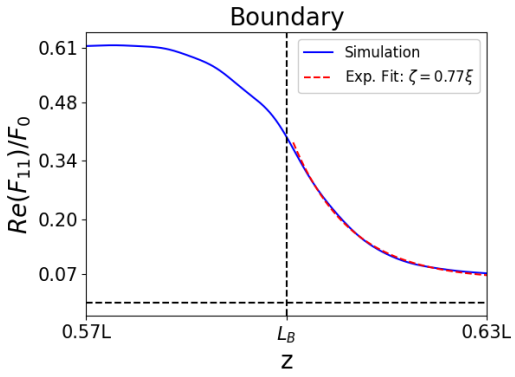

(b) $\alpha = 0, E_0 = 0.05$

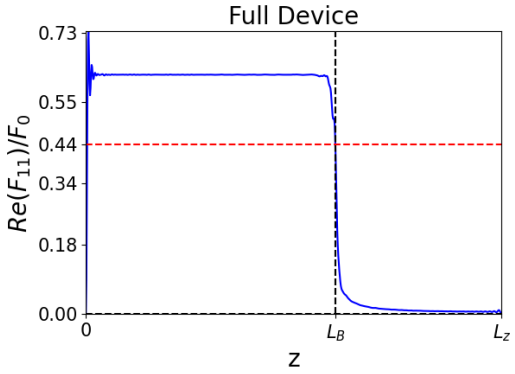

(c) $\alpha = 0, E_0 = 0.3$

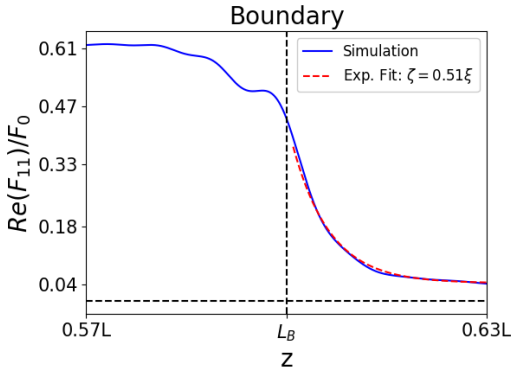

(d) $\alpha = 0, E_0 = 0.3$

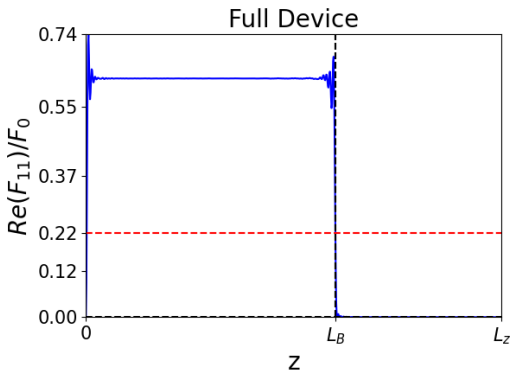

(e) $\alpha = 2, E_0 = 0.05$

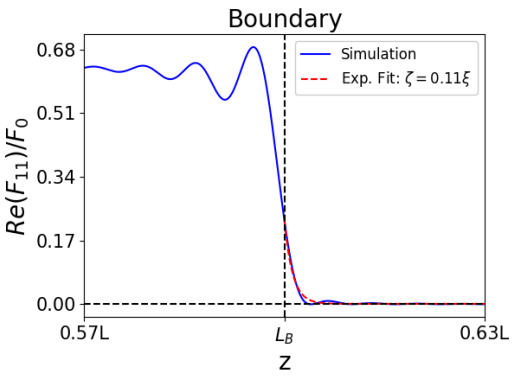

(f) $\alpha = 2, E_0 = 0.05$

Figure 2.3: Real component of F_{11} for a metallic model and host superconductor (left) throughout the device and (right) around the interface, where the parameters are varied to explore the effect of the sharp interface: (a-b) identical on both sides, (c-d) shifted band with mismatch in Fermi surface, and (e-f) broken inversion symmetry in the metallic side. All simulations use $N = 145$ Fourier modes. $\xi = 0.01L$ for the parameters of the simulation.

2.3 Weyl Semimetals

2.3.1 Model

We first consider a device of length L with a boundary at $z = L_B$ separating: (1) A Metallic Superconductor and (2) A WSM with some broken symmetry, as seen in Fig.(2.4); for consistency, we will also consider a Josephson-Junction architecture. We begin with a bulk WSM Hamiltonian [11, 41]:

$$H_{WSM} = \int \mathbf{d^3r} \sum_{ss'} \sum_{\sigma\sigma'} \Psi^{\dagger}_{s\sigma}(\mathbf{r}) \Big[v\sigma_x S_z P_x - v\sigma_y P_y + (m_z P_z^2 - m)\sigma_z - \mu\sigma_0 S_0 \Big] \Psi_{s'\sigma'}(\mathbf{r}) \tag{2.54}$$

Here, $\Psi^{\dagger}_{s\sigma}$ ($\Psi_{s\sigma}$) is a creation (annihilation) operator for an electron with spin $s = \uparrow, \downarrow$ and orbital/sublattice quantum number $\sigma = 1, 2$. The momentum operator is given by $\mathbf{P} = -i\vec{\nabla}$, μ is the chemical potential, and the Pauli matrices σ_i (S_i) act in the orbital (spin) subspace, with S_0 and σ_0 their respective identities. Parity and Time-reversal operators are $P = \sigma_z$ and $T = \imath S_y \mathcal{K}$ where $\mathcal{K}$ performs complex conjugation. Of the four possible terms that break inversion symmetry, but preserve time reversal, two generate nodal rings while the other two generate Weyl nodes in either the $k_x - k_z$ or $k_y - k_z$ plane. Focusing on nodal phenomena, the term that has Weyl nodes in the $k_x - k_z$ plane is given by

$$H_{IB} = \int \mathbf{d^3r} \sum_{ss'} \sum_{\sigma\sigma'} \Psi^{\dagger}_{s\sigma}(\alpha\sigma_x) \Psi_{s'\sigma'}(\mathbf{r}) \tag{2.55}$$

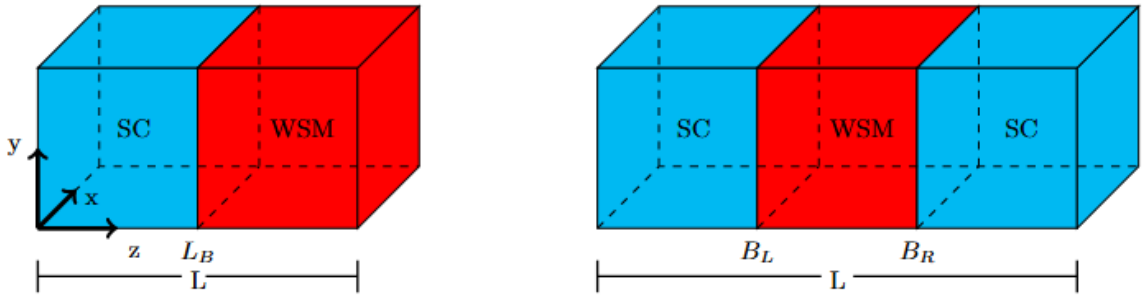

Figure 2.4: (Left) Device consisting of an S-Wave superconductor (SC) in contact with a WSM (WSM); the boundary is located at L_B. (Right) A Josephson Junction architecture with boundaries at B_L and B_R.

The distance between the nodes along the k_x direction is given by 2α which in principle can be determined from data on Weyl semi-metals. We treat it as a phenomenological parameter in our effective model. As discussed previously, for the Fourier basis to be valid, we require the same degrees of freedom and power of the P_z operator throughout the device. Thus, we write the metallic system in the same basis as:

$$H_M = \int \mathbf{d^3 r} \sum_{ss'} \sum_{\sigma\sigma'} \Psi^{\dagger}_{s\sigma}(\mathbf{r}) \Big[(m_z \mathbf{P}^2 + E_0)\sigma_z S_0 - \mu \sigma_0 S_0 \Big] \Psi_{s'\sigma'}(\mathbf{r}) \tag{2.56}$$

where E_0 creates a gap between the conduction ($\sigma = 1$) and valence ($\sigma = 2$) bands. Finally, we add to the metallic model a superconducting piece:

$$H_{SC} = \int \mathbf{d^3 r} \sum_{ss'} \sum_{\sigma\sigma'} (iS_y)_{ss'} \Delta_{\sigma\sigma'}(\mathbf{r}) \Psi^{\dagger}_{s\sigma}(\mathbf{r}) \Psi^{\dagger}_{s'\sigma'}(\mathbf{r}) + H.c. \tag{2.57}$$

where the gap function $\Delta_{\sigma\sigma'}$ is given by:

$$\Delta_{\sigma\sigma'}(\mathbf{r}) = g_{\sigma\sigma'}(\mathbf{r}) F_{\sigma\sigma'}(\mathbf{r}) \tag{2.58}$$

and the interaction strength $g_{\sigma\sigma'}(\mathbf{r})$ is constant within the superconductor, and only nonzero for $\sigma = \sigma' = 1$. The pairing amplitude is as before, with a modification to include the orbital quantum number.

We now obtain the BdG Hamiltonian for the above Bulk Model. We define the Nambu basis:

$$\mathbf{\Psi}_{\mathbf{k}_\perp}(z) = [\Psi_{\mathbf{k}_\perp,1,\uparrow}, \Psi_{\mathbf{k}_\perp,1,\downarrow}, \Psi_{\mathbf{k}_\perp,2,\uparrow}, \Psi_{\mathbf{k}_\perp,2,\downarrow}, \Psi^\dagger_{-\mathbf{k}_\perp,1,\downarrow}, \Psi^\dagger_{-\mathbf{k}_\perp,1,\uparrow}, \Psi^\dagger_{-\mathbf{k}_\perp,2,\downarrow}, \Psi^\dagger_{-\mathbf{k}_\perp,2,\uparrow}]^T \quad (2.59)$$

write our Hamiltonian as:

$$H = \frac{1}{2}\int dz \int d^2\mathbf{k}_\perp \mathbf{\Psi}^\dagger_{\mathbf{k}_\perp}(z)\mathcal{H}_{BdG}(\mathbf{k}_\perp, z)\Psi_{\mathbf{k}_\perp}(z)$$

and obtain the BdG Hamiltonian:

$$\begin{aligned}\mathcal{H}_{BdG}(\mathbf{k}_\perp, z) = {} & \sigma_z\tau_z[m_z\Theta(L_B - z)\mathbf{k}_\perp^2 - m_z\partial_z^2 + E_0(z)] \\ & + \tau_z[v(z)(k_x\sigma_x S_z - k_y\sigma_y) - m(z)\sigma_z + \alpha(z)\sigma_x - \mu] \\ & + (iS_y)\Delta_{11}(z)\sigma_+\sigma_x\tau_+ - (iS_y)\Delta_{11}(z)\sigma_+\sigma_x\tau_- \end{aligned} \quad (2.60)$$

where τ_i are the Pauli matrices in the particle-hole subspace, $\tau_\pm = (\tau_x \pm i\tau_y)/2$, and Δ_{11} is the gap function of the host superconductor. The parameters E_0, m, v, and α have been replaced with piece-wise functions that are nonzero only within their respective regions.

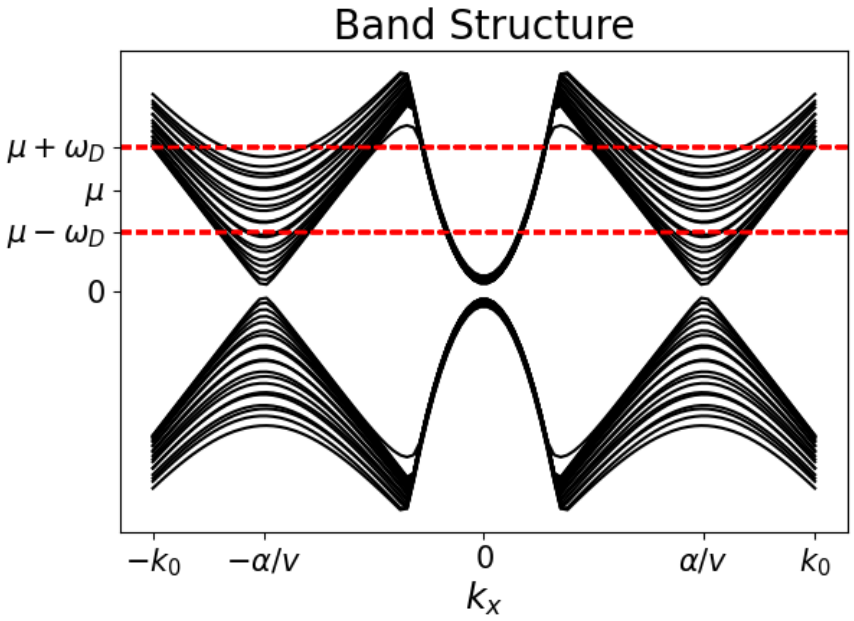

Figure 2.5: Band structure of the proximitized model in the particle subspace. The Debye window, shown as dashed red lines, is chosen such that there is no overlap between the Weyl and Metallic subspaces. The parameters used are: $N = 145$, $E_0 = 0.05$, $\Delta_0 = 0.1$, $\omega_D = 0.3$, $m_z = 3$, $m = 2$, $\alpha = 2$, $v = 1$, and $\mu = 0.71$.

With inversion symmetry broken, and the introduction of the orbital quantum number σ, we expect up to four nonzero pairing amplitudes:

$$F_{11}(z) = -\frac{1}{2}\int d^2\mathbf{k}_\perp \Big[\langle \Psi_{-\mathbf{k}_\perp,1,\downarrow} \Psi_{\mathbf{k}_\perp,1,\uparrow} \rangle + \langle \Psi_{\mathbf{k}_\perp,1,\downarrow} \Psi_{-\mathbf{k}_\perp,1,\uparrow} \rangle \Big] \tag{2.61}$$

$$F_{T}(z) = -\frac{1}{2}\int d^2\mathbf{k}_\perp \Big[\langle \Psi_{-\mathbf{k}_\perp,1,\downarrow} \Psi_{\mathbf{k}_\perp,2,\uparrow} \rangle + \langle \Psi_{\mathbf{k}_\perp,2,\downarrow} \Psi_{-\mathbf{k}_\perp,1,\uparrow} \rangle \Big] \tag{2.62}$$

$$F_{S}(z) = -\frac{1}{2}\int d^2\mathbf{k}_\perp \Big[\langle \Psi_{-\mathbf{k}_\perp,1,\downarrow} \Psi_{\mathbf{k}_\perp,2,\uparrow} \rangle - \langle \Psi_{\mathbf{k}_\perp,2,\downarrow} \Psi_{-\mathbf{k}_\perp,1,\uparrow} \rangle \Big] \tag{2.63}$$

$$F_{22}(z) = -\frac{1}{2}\int d^2\mathbf{k}_\perp \Big[\langle \Psi_{-\mathbf{k}_\perp,2,\downarrow} \Psi_{\mathbf{k}_\perp,2,\uparrow} \rangle + \langle \Psi_{\mathbf{k}_\perp,2,\downarrow} \Psi_{-\mathbf{k}_\perp,2,\uparrow} \rangle \Big] \tag{2.64}$$

where F_S and F_T are orbital singlet (spin triplet) and orbital triplet (spin singlet) pairings.

A cut of the noninteracting band structure in the Fourier basis, cut along $k_y = 0$ in the particle subspace, is shown in Fig.(2.5). With the appropriate choice of parameters and the Debye window (dashed red), the numerical model faithfully approximates a set of Weyl and Metallic bands that couple across the interface.

2.3.2 Results

SC-WSM

We begin by exploring the behavior of the induced pairing amplitudes in a device consisting of one SC-WSM interface with broken inversion symmetry in the WSM. For our initial parameters, we set the chemical potential and Debye window such that $\mu + \omega_D$ falls below the top of the Weyl bands in k_x and k_z space (i.e. $\mu + \omega_D < \alpha, m_1$, respectively). Additionally, the window is adjusted so that it is near the middle of the metallic band (i.e. $\mu - \omega_D > E_0$). The number of modes for this simulation is taken to be $N = 145$ with the boundary at $Z_B = 0.6L$, and the maximum values of k_x and k_y are taken such that $k_y^{max} = k_x^{max}$ with $H_{WSM}(k_x^{max}, 0, 0) = \mu + \omega_D$.

Shown in Fig.(2.6a), Fig.(2.6c) and Fig.(2.6e) are the pairing channels F_{11}, F_{22}, and F_T. The F_S channel has been omitted since it is several orders of magnitude smaller than the others. The upper panels cover the entire device while the lower panels focus on the behavior near the interface. The magnitudes are normalized to $F_0 = \Delta_0/g_{11}$, with $g_{11} \approx 49$ and $F_0 \approx 6.1 \times 10^{-3}$. The broken inversion symmetry implies that a classification in terms of singlets and triplets is not appropriate. This is reflected in the finite amplitude seen in all three pairing channels even though the superconductor is an s-wave spin singlet.

However, the mismatch in symmetry and band structure across the interface leads to a significant reduction in amplitude which decays very quickly as one enters the semi-metal. While the peak and oscillatory behavior near the interface are expected from the finite number of Fourier nodes and the step like change in Hamiltonian, the significant drop-off across the interface is a result of disparity between the semi-metallic and metallic behavior of the low energy electronic states. In sec.2.2.2, we show that, for metallic bands on both sides, the canonical result of a smooth evolution is recovered.

To better characterize the proximity effect, we analyse the momentum dependence of the superconducting gap. Fig.(2.6b) shows the form of the pairing amplitude in the middle of the host SC, whereas Fig.(2.6d) and Fig.(2.6f) show the pairing amplitude on and near the interface on the WSM side. Notably, the majority of weight remains near the Γ point until one gets well inside the WSM. However, the amplitude has essentially decayed to zero by that point. This suggests that the confinement of the superconducting pairing to the interface on the WSM side of the junction is correlated to the degree to which the metallic electronic states penetrate the WSM. In other words, the wave-functions participating in the superconductivity at and near the interface inside the WSM resemble those of the host superconductor.

Superconductor-WSM-Superconductor

While the surface state of the WSM at the interface with the superconductor is accurately captured above, those at the other end of the device are ignored. Since the induced superconductivity is localized to the region around the interface, this approximation

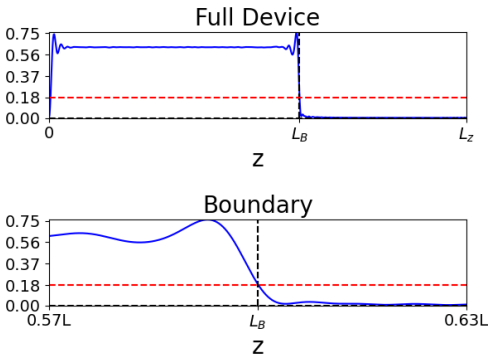

(a) $Re(F_{11})/F_0$

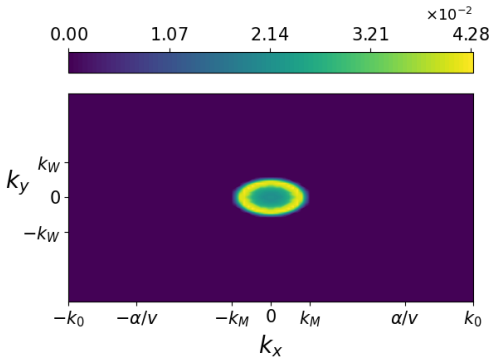

(b) $|F_{11}(\mathbf{k}_\perp, z = 0.30L)|$

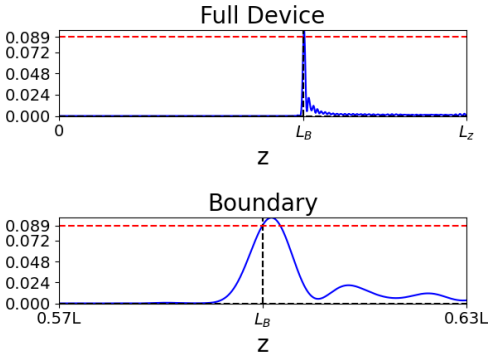

(c) $Re(F_{22})/F_0$

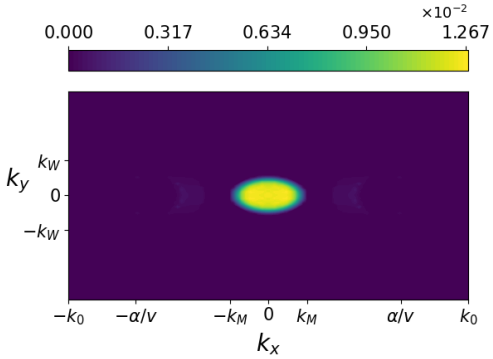

(d) $|F_{11}(\mathbf{k}_\perp, z = 0.60L)|$

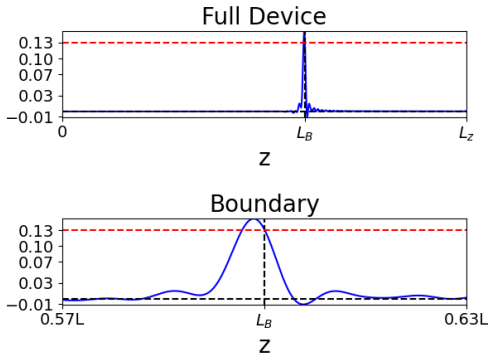

(e) $Re(F_T)/F_0$

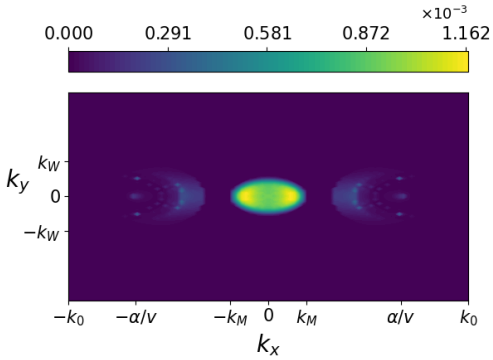

(f) $|F_{11}(\mathbf{k}_\perp, z = 0.61L)|$

Figure 2.6: (Left) Real component of (a) F_{11}/F_0, (c) F_{22}/F_0, and (e) F_T/F_0 throughout the device (top) and around the boundary (bottom). (b,d,f) Momentum space behavior of $|F_{11}|$ (b) in the center of the host SC, (d) on the interface, and (f) just within the interface on the WSM side. The Weyl nodes are marked at $k_x = \pm\alpha/v$, and the edeges of the metallic (Weyl) debye window are marked at $\pm k_M$ ($\pm k_W$). The boundary is placed at $L_B = 0.6L$, and the parameters used are: $N = 145$, $E_0 = 0.05$, $\Delta_0 = 0.1$, $\omega_D = 0.3$, $m_z = 3$, $m = 2$, $\alpha = 2$, $v = 1$, and $\mu = 0.71$.

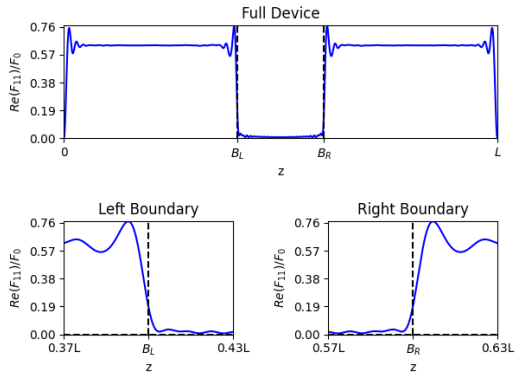

(a) $Re(F_{11})/F_0$

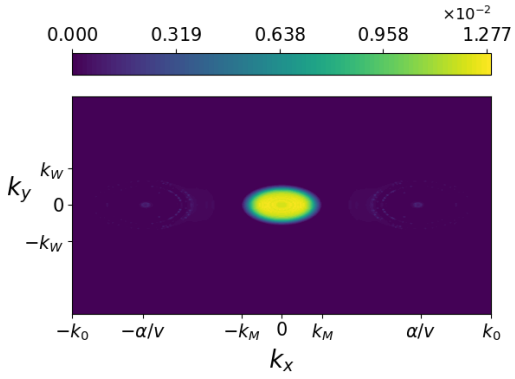

(b) $|F_{11}(\mathbf{k}_\perp, B_L)|$

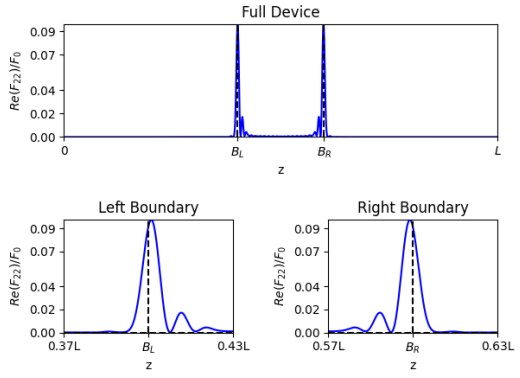

(c) $Re(F_{22})/F_0$

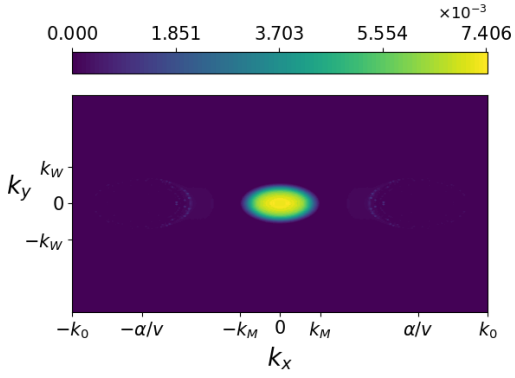

(d) $|F_{22}(\mathbf{k}_\perp, B_L)|$

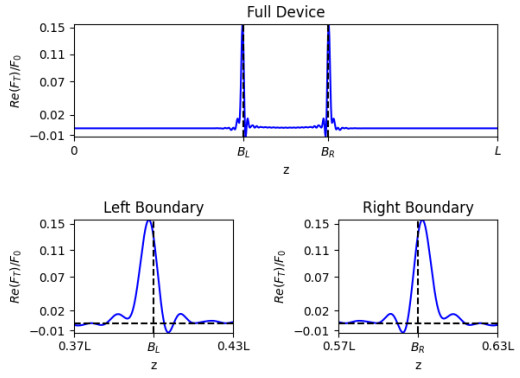

(e) $Re(F_T)/F_0$

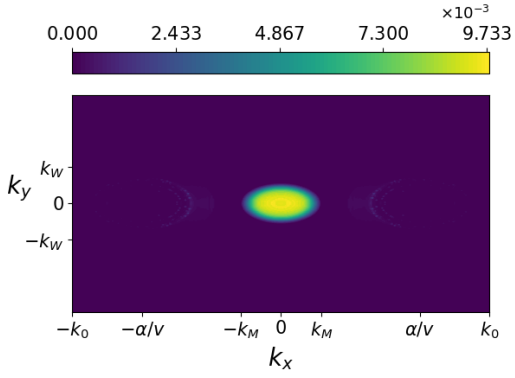

(f) $|F_T(\mathbf{k}_\perp, B_L)|$

Figure 2.7: (Left) Real component of (a) F_{11}/F_0, (c) F_{22}/F_0, and (e) F_T/F_0 of the two Josephson-Junction. (Right) Momentum space behavior on the left boundary of (b) F_{11}, (d) F_{22}, and (f)F_T. The boundaries are placed at $B_L = 0.4L$ and $B_R = 0.6L$, and the parameters used are: $N = 145$, $E_0 = 0.05$, $\Delta_0 = 0.1$, $\omega_D = 0.3$, $m_z = 3$, $m = 2$, $\alpha = 2$, $v = 1$, $\mu = 0.71$, $g_{11} = 48.53$, and $F_0 = 6.18 \times 10^{-3}$.

is expected to be valid. To verify this, we next turn to the behavior of a SC-WSM-SC device. To better capture the physics, a greater momentum space resolution is implemented.

Plotted in Fig.(2.7a) is the real component of the pairing mode F_{11} throughout the device, as well as its behavior near the boundaries. The results are in agreement with those in section 2.3.2 where induced superconductivity is predominantly in the F_{11} channel confined to the interface. The behaviors of F_{22} and F_T are shown in fig.(2.7c) and Fig.(2.7e). The latter are finite as expected by the broken inversion symmetry but are much weaker as compared to the F_{11} channel.

The momentum space dependence at the boundary for F_{11}, F_{22} and F_T are shown in Fig.(2.7b), fig.(2.7d) and Fig.(2.7f) respectively. As in the single interface case the majority of the weight remains near the Γ point in all three channels reflecting the very wek coupling to the Weyl nodes.

Velocity mismatch across the interface

An important determinant of the coupling across the interface is the mismatch in the perpendicular velocity between states of the host superconductor (v_z^{sc}) and the WSM (v_z^w). To understand its impact, we vary the Weyl velocity v and adjust α to keep the Fermi-surfaces separate; all other parameters are fixed. Two limiting values of v are (1) v_ℓ^c, below which the two systems share no states with similar energy and velocity, and (2) v_u^c, above which there are states for which the two systems have the same energy and velocity. To determine these values, we first note the velocity $v_z = \partial_{k_z} E(\mathbf{k})$ for each system is given by:

$$v_z^W = \frac{2m_z k_z(m_z k_z^2 - m)}{\sqrt{v^2(k_x \pm \alpha/v)^2 + v^2 k_y^2 + (m_z k_z^2 - m)^2}} \tag{2.65}$$

$$v_z^M = 2m_z k_z \tag{2.66}$$

It will prove convenient to write the ratio of these two velocities, $R \equiv v_z^W / v_z^M$, in terms of the band energy E, the Weyl wave vector magnitude $k_W^2 = (k_x \pm \alpha/v)^2 + k_y^2$, and the metallic wave vector magnitude $k_M^2 = k_x^2 + k_y^2$:

$$R = \frac{\sqrt{E^2 - v^2 k_W^2}}{E} \sqrt{\frac{\sqrt{E^2 - v^2 k_W^2} + m}{E - E_0 - m_z k_M^2}} \tag{2.67}$$

For $k_W = k_M \equiv k$ with functions $f(k) = \sqrt{E^2 - v^2 k_W^2}$ and $g(k) = E - E_0 - m_z k_M^2$ Eq.(2.67) is:

$$R(k, E) = \frac{f(k)}{E} \sqrt{\frac{f(k) + m}{g(k)}} \tag{2.68}$$

We seek a condition on our parameters that will either forbid or allow $R(k, E) = 1$. A local extreme exists at $k = 0$ which has the value:

$$R(0, E) = \sqrt{\frac{E + m}{E - E_0}} \equiv h_0 \geq 1$$

Determining v_ℓ^c is equivalent to finding v for which the concavity of $R(0,E)$ changes sign:

$$R''(0) = \frac{m_z h_0}{g_0} - \frac{v^2 h_0}{f_0^2}\left[\frac{2g_0 h_0^2 + f_0}{2g_0 h_0^2}\right]$$

$$\implies v_c^\ell = \sqrt{\frac{E+m}{E-E_0}}\sqrt{\frac{2m_z E^2}{3E+2m}} \tag{2.69}$$

For $v < v_\ell^c$, h_0 is a global minimum, and thus the electronic velocities are never equal. However, $v > v_\ell^c$ is not enough to guarantee equal velocities, as seen in Fig.(2.8). We denote k_c^W (k_c^M) to be the root of $f(k)$ ($g(k)$). When $k_c^W < k_c^M$, the ratio function diverges before it can reach one; thus, the value v_u^c is obtained when the two roots are equivalent:

$$v_u^c = \sqrt{\frac{m_z E^2}{E-E_0}} = v_\ell^c\sqrt{\frac{3E+2m}{2E+2m}} \tag{2.70}$$

For $v_\ell^c < v < v_u^c$, it is still possible to have $R(k,E) = 1$ for some value of k; in practice, however, this window is quite small and does not guarantee a ratio of one. Given these expressions, we find the simulation in sections 2.3.2 and 2.3.2 have a Weyl velocity of $v = 0.89v_\ell^c$, which suggests that the states near the chemical potential on the two sides of the interface have very different velocities.

We can now explore the effects of mismatched v_z on induced superconductivity. Shown in Fig.(2.9) are plots of the energy bands for the BdG equations with $k_y = 0$, along with the corresponding momentum space distribution of F_{11} at the interface, for $v = 0.5v_\ell^c$, $v = v_u^c$, and $v = 4.0v_u^c$. The energy band plots have been color weighted by the

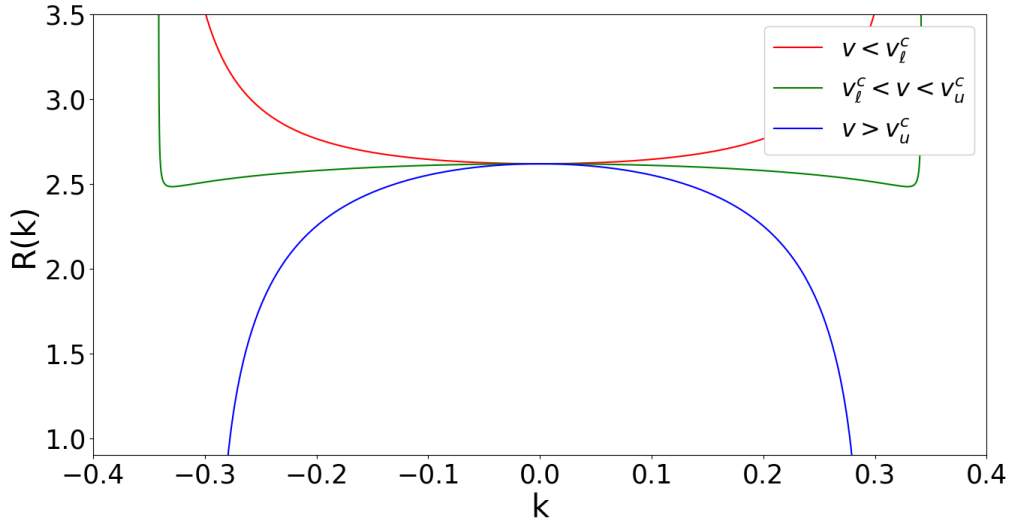

Figure 2.8: Plot of $R(k)$ for (red) $v < v_\ell^c$, (green) $v_\ell^c < v < v_u^c$, and (blue) $v > v_u^c$ using the same parameters as our simulations and $E = \mu - \omega_D = 0.4$. Only $v > v_u^c$ guarantees a ratio of one.

average of their wave function over the device. To ensure that the Fermi surfaces of the two systems remain well separated, we adjust α such that the two band structures still meet at $E = \mu + \omega_D$. Three distinct band structures are observed: (1) Metallic like bands that average to the center of the SC at $0.3L$ (light blue), (2) Weyl like bands that average to the center of the WSM at $0.8L$ (light maroon), and (3) Edge states bridging the two band structures that average to the interface at $0.6L$ (light brown). We find that, below v_ℓ^c, the pairing function is mostly confined to the host superconductor and does not couple to the Weyl or Edge states; this is reflected in the form of $F_{11}(\mathbf{k}_\perp)$ as a function of z. As v is increased to v_u^c, the edge states and the pairing function are able to weakly couple to the Weyl nodes. Finally, at $v = 4.0v_u^c$, the edge states and pairing functions are more evenly distributed between the Weyl nodes and γ point.

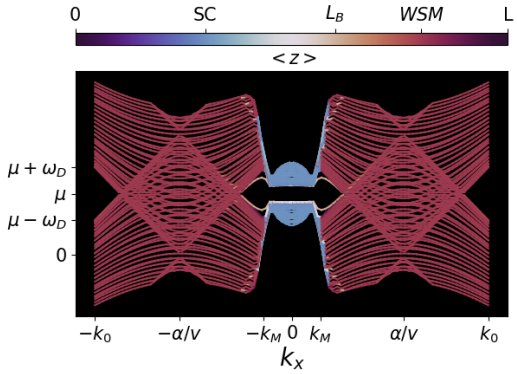

(a) $v = 0.5v_\ell^c$

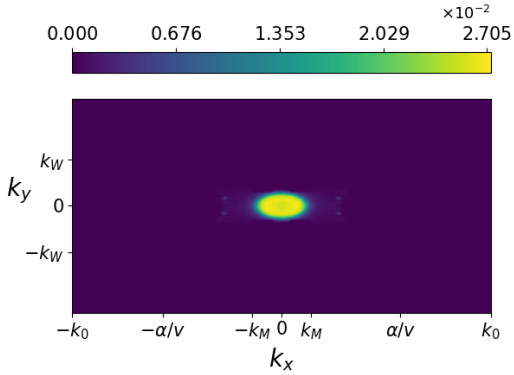

(b) $v = 0.5v_\ell^c$

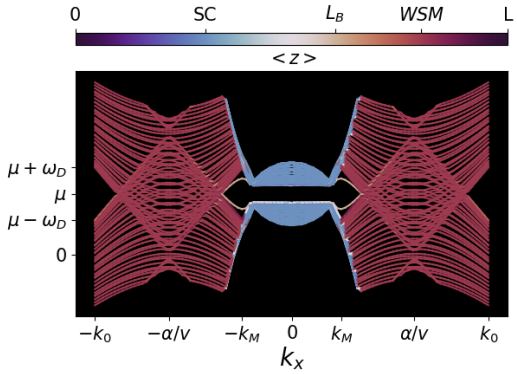

(c) $v = v_u^c$

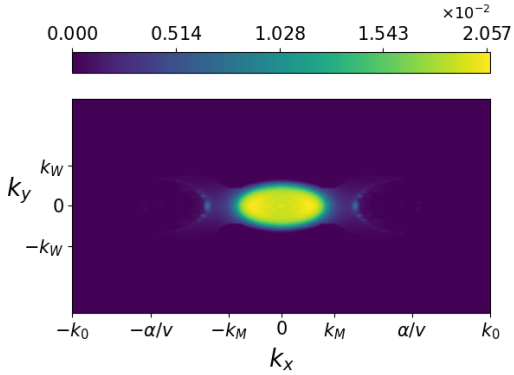

(d) $v = v_u^c$

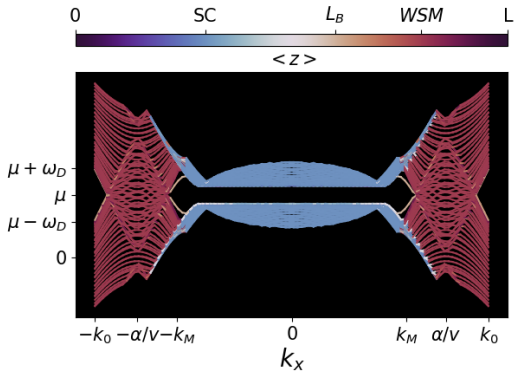

(e) $v = 4.0v_u^c$

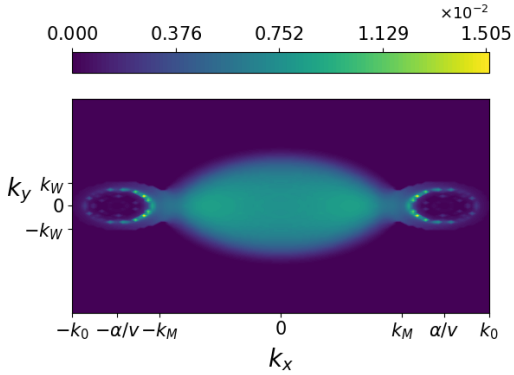

(f) $v = 4.0v_u^c$

Figure 2.9: (Left Column) BdG energy bands of the single SC-WSM system for (a) $v = 0.5v_\ell^c$, (b)$v = v_u^c$, and (c)$v = 4.0v_u^c$. The bands are color weighted by the average of their wave function over the length of the device. (Right Column) Corresponding momentum space distribution for F_{11} at the interface. The model parameters used are: $N = 146$, $E_0 = 0.05$, $\Delta_0 = 0.1$, $\omega_D = 0.3$, $m_z = 2$, $m = 2$, $\mu = 0.7$, $g_{11} = 48.9$, and $F_0 = 6.13 \times 10^{-3}$, with α adjusted based on v.

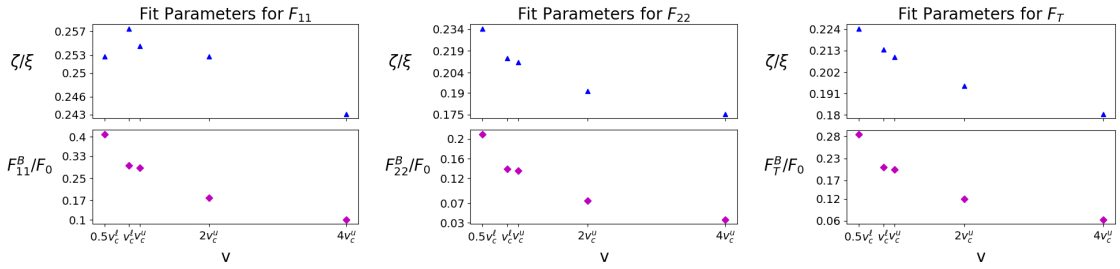

Figure 2.10: Least squares fit calculation of (Blue) Decay length and (Purple) Interface Amplitude as v is increased for (left) F_{11}, (middle) F_{22}, and (right) F_T. $\xi = 0.04L$ for the chosen parameters of the simulation. As the velocity mismatch becomes smaller, both the amplitude at the boundary and the coherence length inside the WSM decrease.

To better understand the behavior of the pairing modes as v is increased, we fit the real component of each mode in real space to extract the penetration depth ζ and the paring amplitude at the interface. These values are plotted and compared to the Cooper pair size $\xi = 2m_z k_F/(\pi\Delta_0)$ and the initial pairing amplitude strength F_0 in Fig.(2.10). For a clean superconductor the coherence length is 0.74ξ. As v is increased, and the pairing amplitudes couple more with the Weyl physics, the amplitude of the pairing modes at the interface and the decay length decrease. This suggests that the mismatch in band structure and loss of inversion symmetry are antagonistic to proximal superconductivity. Even when states with similar velocities and energies exist at the interface the overlap of wave-functions is not sufficient to induce superconductivity well inside the WSM.

2.4 Transition Metal Dichalcogenides

2.4.1 Model

We now consider our previous system, but with a Transition Metal Dichalcogenide (TMDC) replacing the Weyl semimetal. In momentum space, the TMDC has the two dimensional BdG Hamiltonian [42]:

$$H_v^0(\mathbf{k}) = t(vk_x\sigma_x + k_y\sigma_y) + \tfrac{1}{2}E_G\sigma_z - \tfrac{v}{2}E_{soc}(\sigma_z - 1)S_z - \mu_T \tag{2.71}$$

where σ_i are the Pauli matrices in the orbital subspace for the in-plane $|1\rangle_v = \left|d_{x^2-y^2}\right\rangle + iv\left|d_{xy}\right\rangle$ and out-of-plane $|2\rangle = |d_{z^2}\rangle$ orbital states, with valley number $v = \pm 1$. The momenta k_x and k_y are measured relative to the TMDC's K-point denoted by K_0. We seek to apply the spectral method to simulate tunneling between a metallic superconductor and a TMDC. To do this, we model the TMDC as a thin film whose in plane $x-y$ physics is given by Eq.(2.71), with a free particle model along z:

$$H_v(\mathbf{k}) = H_v^0(\mathbf{k}) + mk_z^2\sigma_z \tag{2.72}$$

Additionally, we modify our metallic system by inserting a barrier in the $|2\rangle$ subspace:

$$H_M(\mathbf{k}) = (m\mathbf{k}_\perp^2)\sigma_1 + (mk_z^2\sigma_z + E_0)\sigma_z - (V_0 - \mu_T)\sigma_2 - \mu_M \tag{2.73}$$

where $\mathbf{k}_\perp = k_x\hat{x} + k_y\hat{y}$ is the momentum perpendicular to the normal of the interface and σ_1 and σ_2 project onto their respective orbital subspace. This model is designed to better

represent a single band metallic system while still allowing for the Fourier expansion, as the barrier term forbids electrons in the orbital $|2\rangle$ state from entering the metallic system. The new BdG Hamiltonian is given by:

$$\begin{aligned}\mathcal{H}_{BdG}(\mathbf{k}_\perp, z) = \tau_z[\sigma_1 m\Theta(L_B - z)\mathbf{k}_\perp^2 - \sigma_z m\partial_z^2 + \sigma_z E_0(z) - \mu(z)] \\ + \tau_z[t(z)\{v(k_x, z)k_x\sigma_x + k_y\sigma_y\} + \tfrac{1}{2}E_G(z)\sigma_z - \tfrac{v}{2}(k_x, z)E_{soc}(\sigma_z - 1)S_z] \\ + (iS_y)\Delta_{11}(z)\sigma_1\tau_+ - (iS_y)\Delta_{11}(z)\sigma_1\tau_- \end{aligned} \tag{2.74}$$

To account for the valley physics, which cannot be replicated in the metallic model, we have introduced the parameter $v(k_x, z) \equiv sgn(k_x)\Theta(z - L_B)$. Because of this, there will be a discontinuity in the physics of the TMDC when its Fermi momentum is near the Γ point; our parameters are chosen to avoid this issue. The correlation functions are the same as before, and we can proceed as we did with the Weyl semimetal.

2.4.2 Results

We explore the induced pairing functions in both the conduction and valence bands by adjusting the chemical potential of the TMDC. As was the case for the Weyl Semimetal, the spin triplet pairing is several orders of magnitude weaker than its counterparts, and will be ignored in this analysis. Our results from the Weyl Semimetal simulations suggest that only momentum states near the superconductor's Debye window will have an induced gap; we test this by constructing the TMDC model in two regimes: 1) Strong overlap, where K_0 is such that the Fermi momentum of the TMDC lies within the Debye window of the superconductor, and 2) Weak overlap, where K_0 puts the Fermi momentum outside the

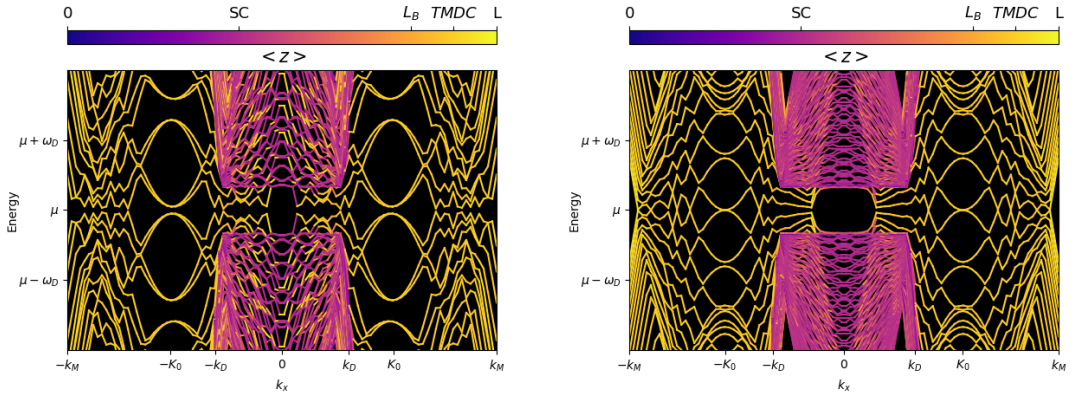

(a) $\mu_T = 3.0$ (b) $\mu_T = -2.1$

Figure 2.11: Color weighted bands at $K_0 = 1.8$ for (a) conduction bands ($\mu_T = 3.0$) and (b) Valence bands ($\mu_T = -2.1$). Both cases place the TMDC's Fermi momentum within the Debye window of the superconductor.

Debye window of the superconductor. For these simulations, all parameters (excluding μ_T and K_0) are fixed to be: $\mu_M = 2$, $E_0 = 0.1$, $V_0 = 30.0$, $m = 2$, $\Delta_0 = 0.1$, $\omega_D = 0.3$, $t = 3$, $E_G = 3.0$, and $E_{soc} = 1.0$. The boundary is fixed at $L_B = 0.80L$.

Strong Overlap

We first take $K_0 = 1.8$, with $\mu_T = 3.0$ and $\mu_T = -2.1$ for the conduction and valence bands, respectively. A plot of the full band structure, color weighted by average position within the device, is shown in Fig.(2.11). The simulated band structure captures the TMDC and superconductor physics with the TMDC's Fermi momentum placed within the superconductor's Debye window. Shown in Fig.(2.12) (Fig.(2.13)) are the induced pairings of the conduction (valence) bands (left) throughout the device and (right) in momentum space at the center of the TMDC ($z = 0.90L$).

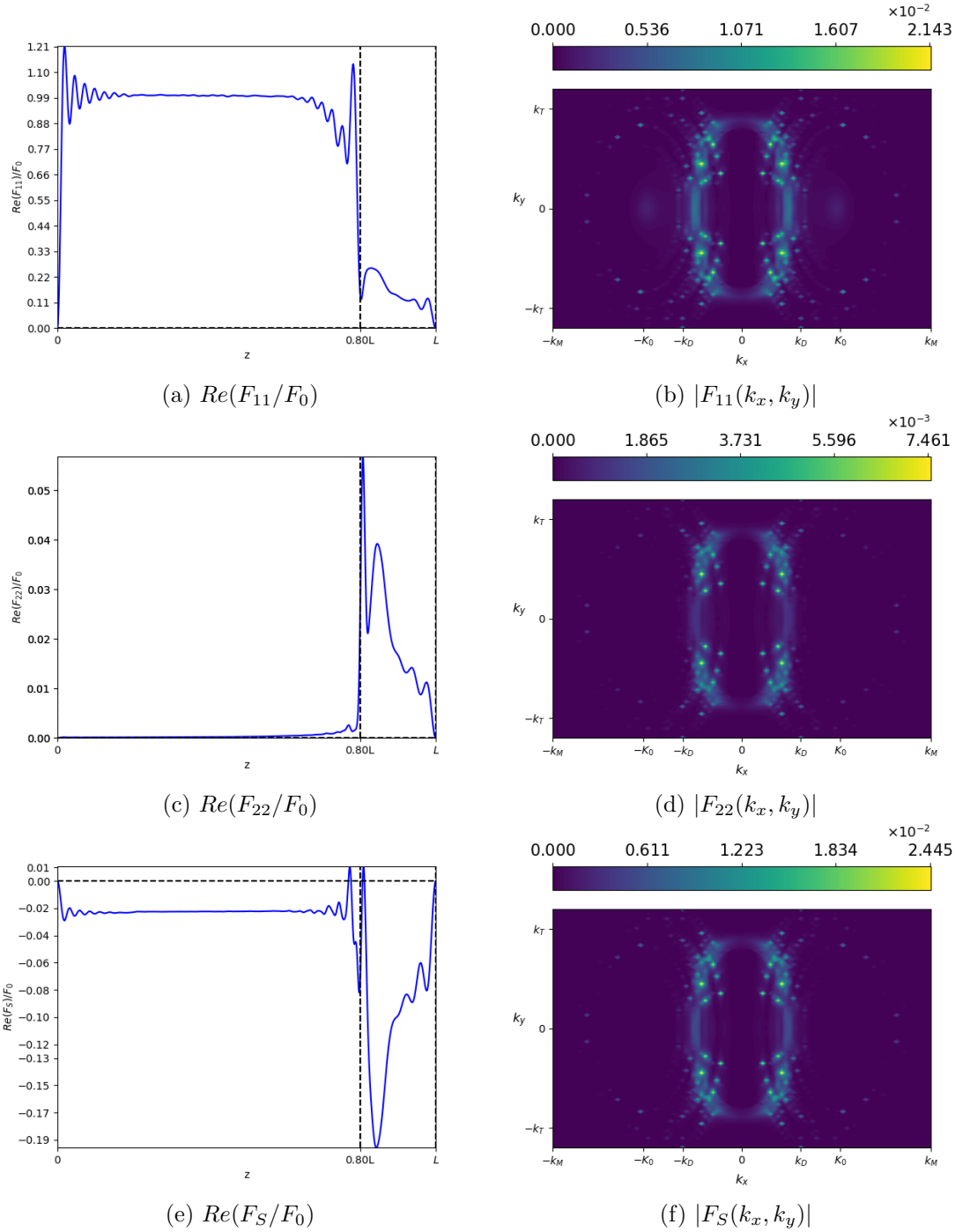

(a) $Re(F_{11}/F_0)$ (b) $|F_{11}(k_x, k_y)|$

(c) $Re(F_{22}/F_0)$ (d) $|F_{22}(k_x, k_y)|$

(e) $Re(F_S/F_0)$ (f) $|F_S(k_x, k_y)|$

Figure 2.12: (Left) Real part of the correlation functions in the conduction bands for (a) F_{11}, (c) F_{22}, and (e) F_S. (Right) Corresponding magnitude of the correlation functions in momentum space at the center of the TMDC. The momentum space correlations are only nonzero near the superconductor's Debye window.

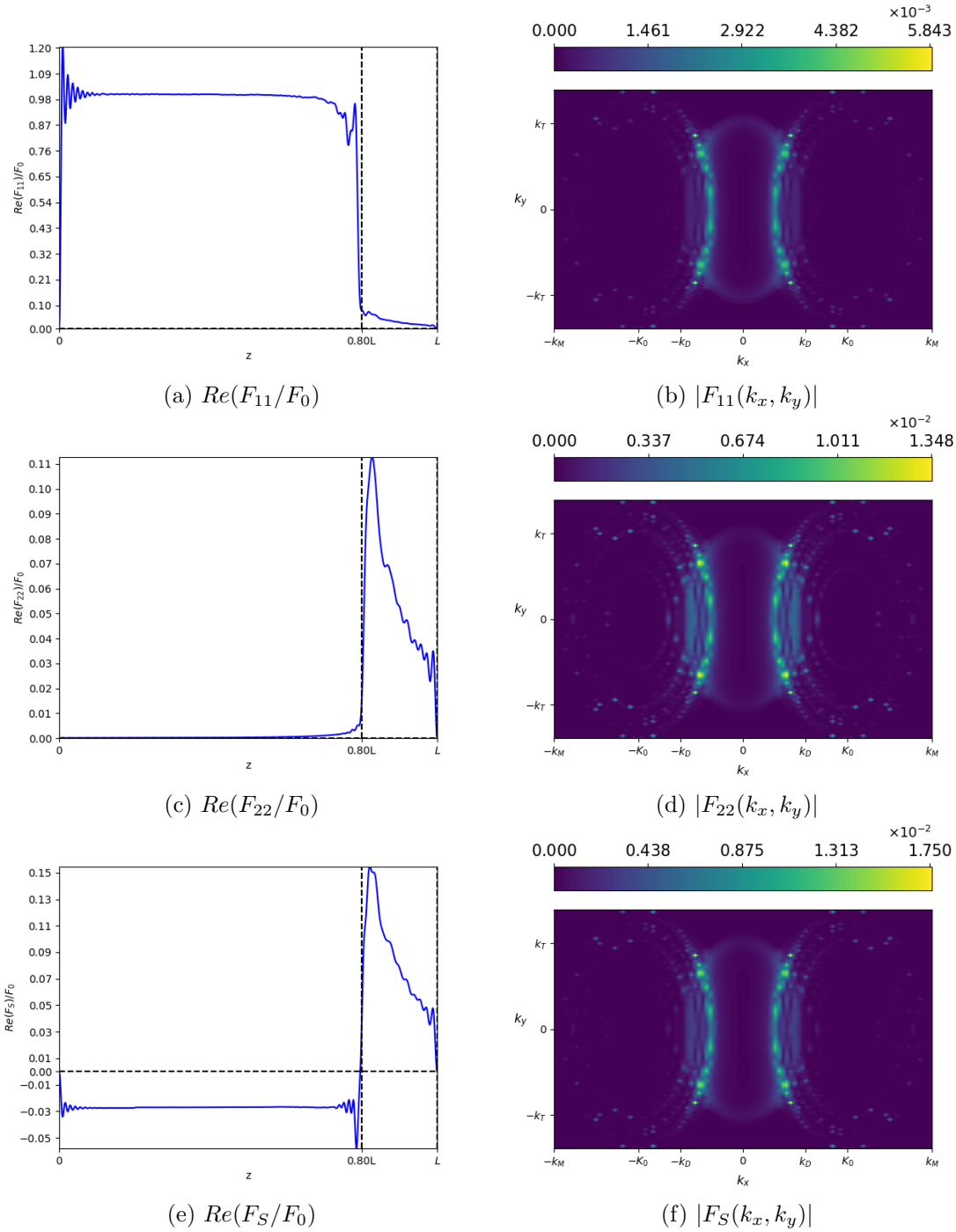

(a) $Re(F_{11}/F_0)$ (b) $|F_{11}(k_x, k_y)|$

(c) $Re(F_{22}/F_0)$ (d) $|F_{22}(k_x, k_y)|$

(e) $Re(F_S/F_0)$ (f) $|F_S(k_x, k_y)|$

Figure 2.13: (Left) Real part of the correlation functions in the valence band for (a) F_{11}, (c) F_{22}, and (e) F_S. (Right) Corresponding magnitude of the correlation functions in momentum space at the center of the TMDC.

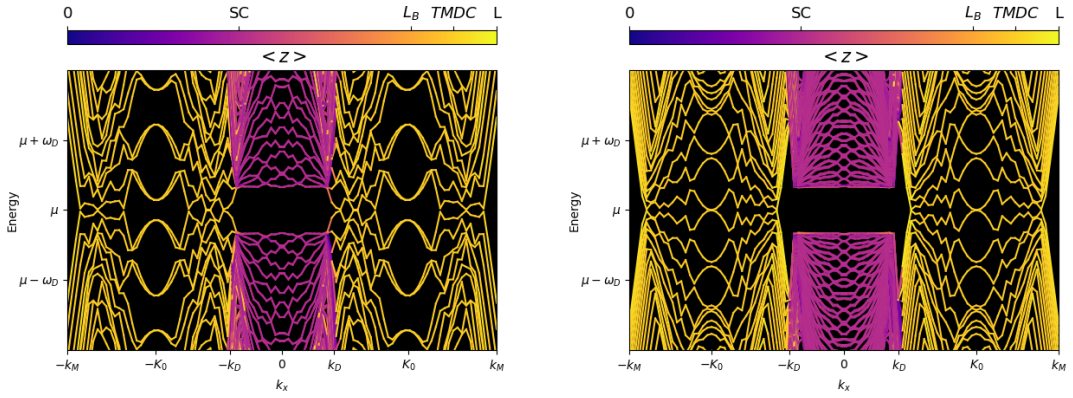

(a) $\mu_T = 3.0$ (b) $\mu_T = -2.1$

Figure 2.14: Color weighted bands at $K_0 = 2.6$ for (a) conduction bands ($\mu_T = 3.0$) and (b) Valence bands ($\mu_T = -2.1$). Both cases place the TMDC's Fermi momentum outside the Debye window of the superconductor.

Weak Overlap

We now take $K_0 = 2.6$, with the same chemical potentials. A plot of the full band structure, color weighted by average position within the device, is shown in Fig.(2.14). The simulated band structure captures the TMDC and superconductor physics with the TMDC's Fermi momentum placedoutside the superconductor's Debye window.

Shown in Fig.(2.15) are the induced F_{11}, F_{22}, and F_S pairings of the conduction bands (left) throughout the device and (right) in momentum space at the center of the TMDC ($z = 0.90L$). For both strong and weak overlap, only momentum states near the Debye window of the superconductor have a nonzero pairing.

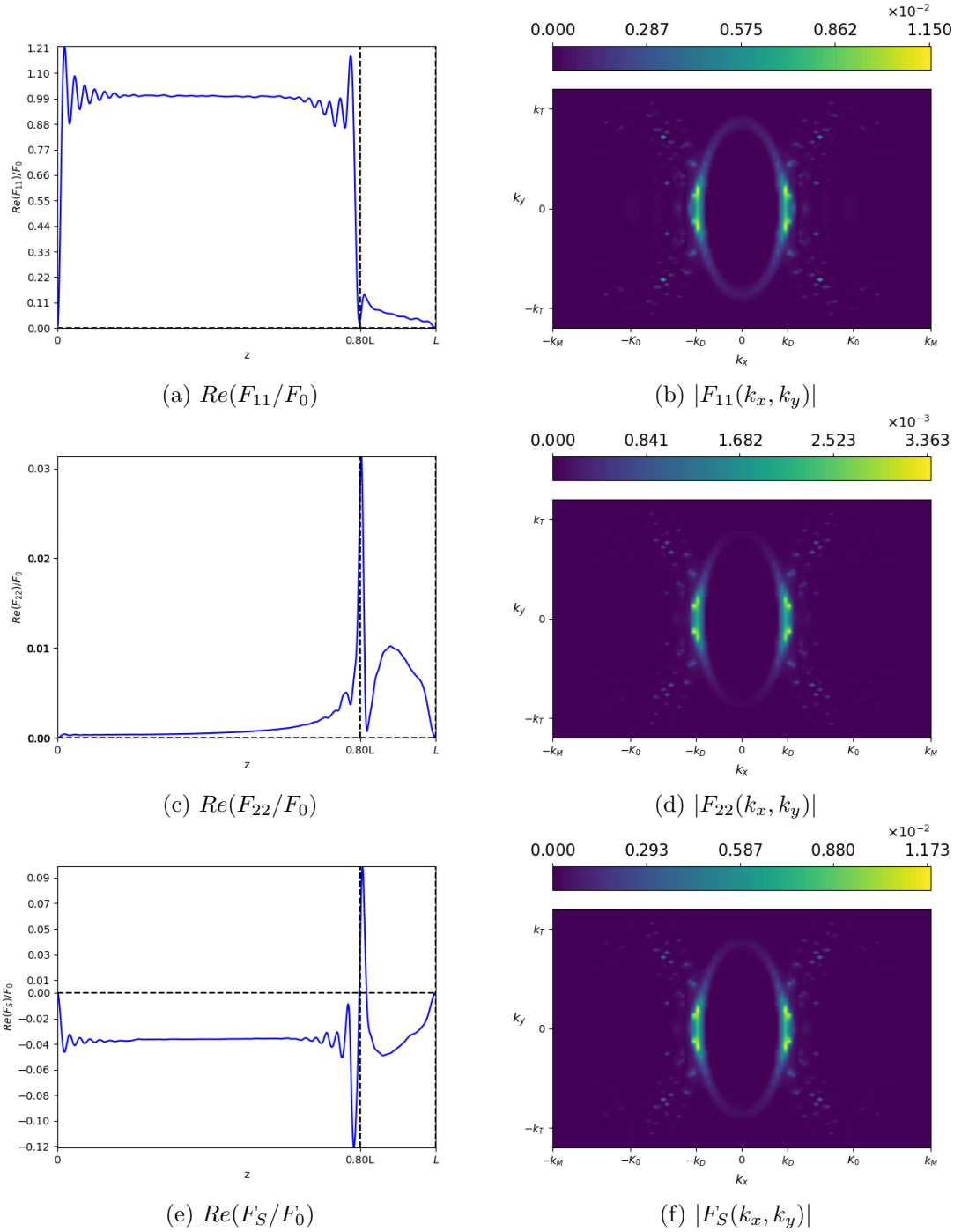

(a) $Re(F_{11}/F_0)$ (b) $|F_{11}(k_x, k_y)|$

(c) $Re(F_{22}/F_0)$ (d) $|F_{22}(k_x, k_y)|$

(e) $Re(F_S/F_0)$ (f) $|F_S(k_x, k_y)|$

Figure 2.15: (Left) Real part of the correlation functions in the conduction bands for (a) F_{11}, (c) F_{22}, and (e) F_S. (Right) Corresponding magnitude of the correlation functions in momentum space at the center of the TMDC. The momentum space correlations are only nonzero near the superconductor's Debye window.

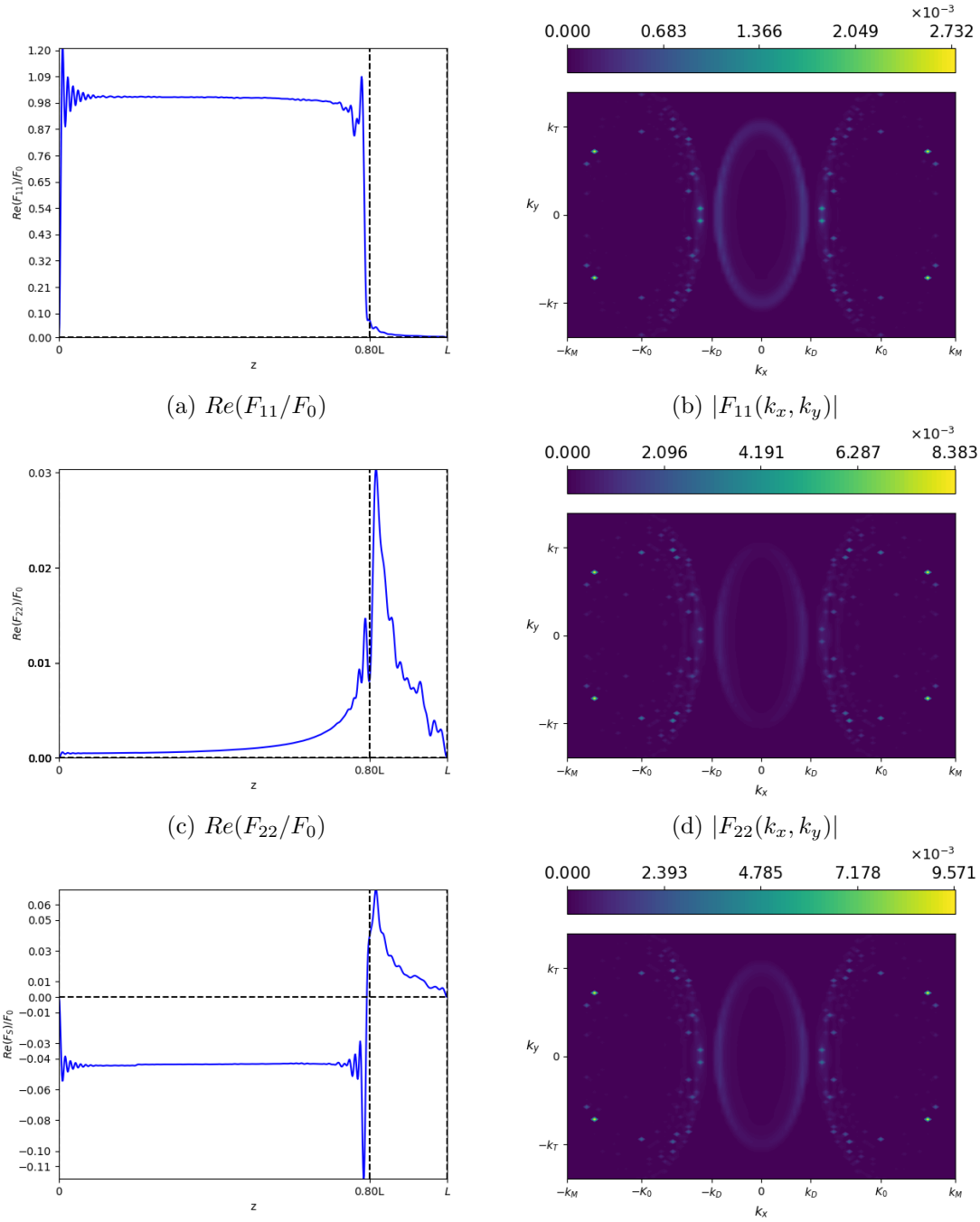

(a) $Re(F_{11}/F_0)$ (b) $|F_{11}(k_x, k_y)|$

(c) $Re(F_{22}/F_0)$ (d) $|F_{22}(k_x, k_y)|$

(e) $Re(F_S/F_0)$ (f) $|F_S(k_x, k_y)|$

Figure 2.16: (Left) Real part of the correlation functions in the valence band for (a) F_{11}, (c) F_{22}, and (e) F_S. (Right) Corresponding magnitude of the correlation functions in momentum space at the center of the TMDC.

2.5 Conclusions

A promising architecture often proposed to realize unconventional, and potentially topological, superconductivity is proximal coupling of an s-wave superconductor to materials such as WSMs, TMDCs, and other unconventional systems. Theoretical models providing support to this approach employ tunneling models across the interface where the parameters are phenomenological inputs. Of interest for experimental implementation are design principles which inform on an optimal choice of material properties to achieve proximal superconductivity. This study elucidates the effects of proximitized superconductivity in an architecture without assuming new physics at the interface beyond quantum tunneling. This is achieved by a numerical calculation of the electronic wave functions and their correlations by expanding the respective Hamiltonians in a common Fourier basis.

Our simulations show that the degree to which the superconductivity and Weyl physics couple is dependent on mismatches in electronic velocity normal to the interface. The two systems are only able to sufficiently couple once the Weyl velocity v reaches some minimum value v_c^u; however, all three pairing channels show a negative correlation between the Weyl velocity and their respective decay length and interface amplitude. This suggests that the induced pairing is unable to penetrate far into the bulk of the WSM. Within a continuum model, with quantum tunneling across the interface, predominantly surface superconducting state is induced by proximity. In other words ensuring continuity of wavefunction and probability current at a sharp boundary separating two regions is not enough. Other treatments implement the same boundary assuming tunneling [43] across the interface but cannot capture the decay of the amplitude in the superconductor. Additional physics

involving electronic states near the boundary is needed to induce superconductivity inside the bulk of the WSM. These can be implemented by adding an interface potential or using an alternative approach based on transmission/reflection coefficients [44, 45]. Determining the boundary conditions that allow for efficient proximity effect in Weyl semi-metals is an interesting next step and beyond the scope of this work.

The momentum space pairings for WSMs reveal higher weight near the Γ point while the edge state is distributed around the Weyl Nodes. The inability of the pairing amplitude to penetrate into the bulk of the WSM likely stems from a mismatch in the momentum of their low energy physics. The same result is found for simulations involving TMDCs, suggesting that the often desired pairings (i.e. those distributed around the Weyl Nodes or TMDC valleys) require some form of interface scattering in either the momentum space, electron spin, or both.

Chapter 3

Phonon Assisted Optical Absorption

3.1 Introduction

In semiconductors, there is a finite band gap between the valence and conduction bands that prevents current from flowing freely. Unlike an insulator, however, the gap is small enough that it is possible to excite electrons from the valence band into the conduction band by the absorption of a photon of the appropriate length. The excited electron experiences an attractive Coulomb interaction with the hole left behind in the valence band, forming a bound state known as an exciton [46]. Finally, after some delay, the electron decays back to the valence band, releasing a photon in a process known as photo-luminescence. The photo-luminescent spectrum of semiconductors is often used to determine the band gap (exciton energy) [47]; however, a recent experiment has captured photo-current absorption

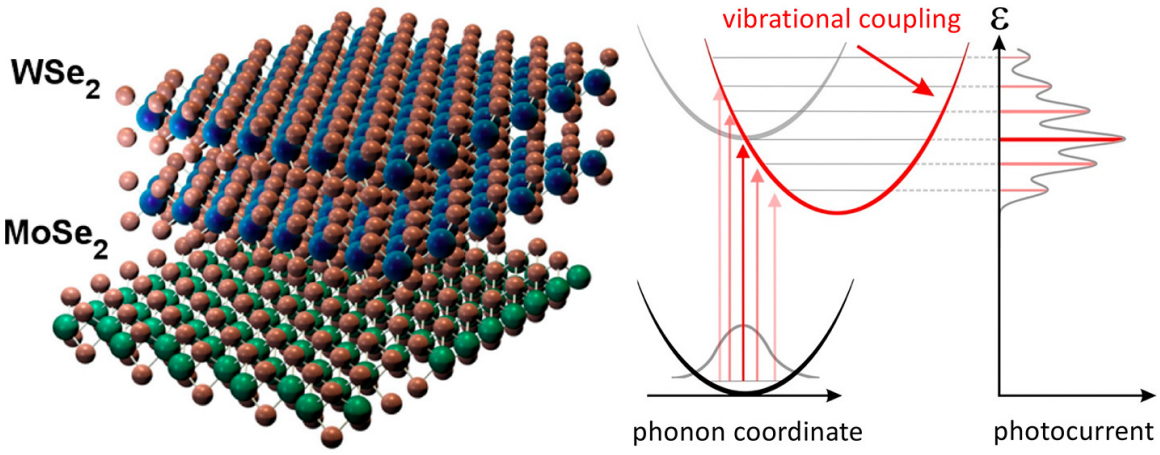

Figure 3.1: Layered TMDC structure and a sketch of the observed side-bands in the absorption photo-current. (Barati et. al., 2022).

data to measure the inter-layer excitation energy of the layered TMDC structure shown in Fig.(3.1) [48]. Their measurements, shown in Fig. (3.2), depict a collection of absorption peaks, suggesting that the vibrational states of the system allowed for simultaneous phonon absorption event(s). They corroborate this by confirming that the side-band energy splitting, which is roughly 30 meV, is consistent with density functional theory calculations of the system's phonon dispersions (as seen in Fig.(3.4)). Since such phonon side-bands have historically been explored in the context of photo-luminescence spectra [47, 49–53], our goal will be to obtain a model that captures this physics in the context of an optical absorption spectrum.

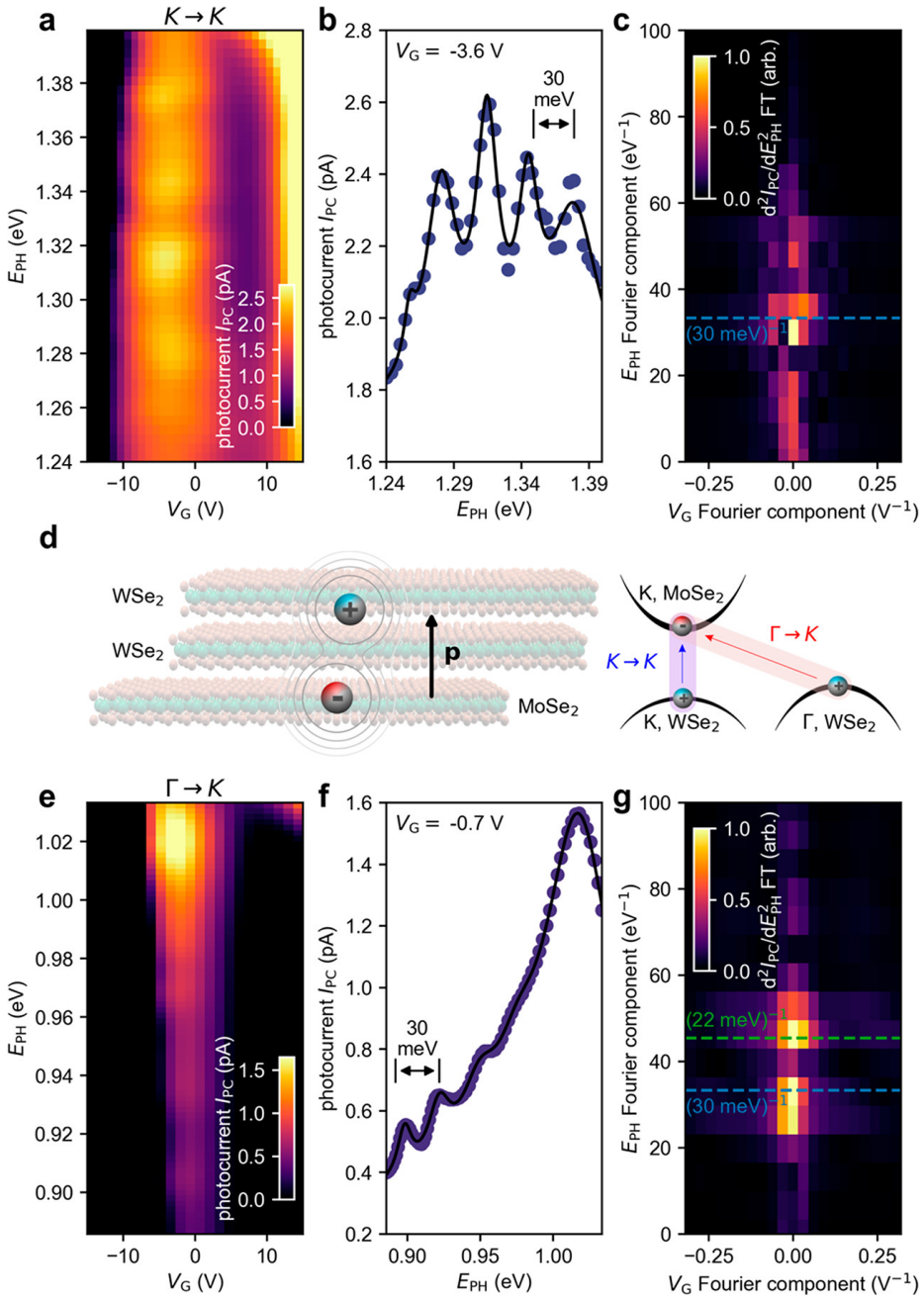

Figure 3.2: Absorption photo-current for (a-c) direct momentum ($K \rightarrow K$) and (e-g) indirect momentum ($\Gamma \rightarrow K$) inter-layer transitions. (Barati et. al., 2022).

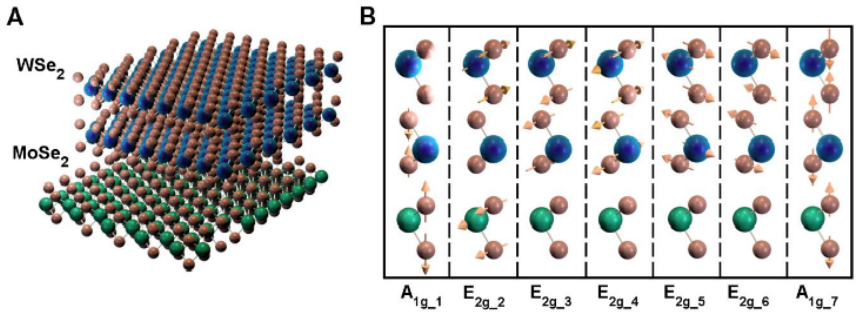

Figure 3.3: (Left) The schematic device and (Right) its predicted vibrational states. (Barati et. al. Supplementary information, 2022).

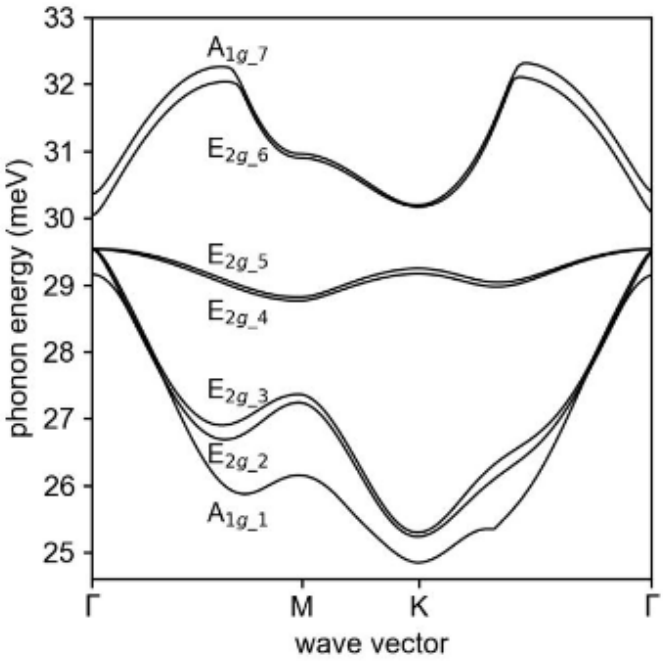

Figure 3.4: Density Functional Theory calculations of the phonon dispersions for the vibrational modes in Fig.(3.3) (Barati et. al. Supplementary information, 2022).

3.2 Initial Model

We first consider a basic model of interacting electrons, phonons, and photons:

$$\begin{aligned} H_0 &= H_{el} + H_{latt} + H_{em} \\ &= \sum_{\lambda,\mathbf{k}} \varepsilon_{\lambda,\mathbf{k}} P^{\lambda,\lambda}_{\mathbf{k},\mathbf{k}} + \sum_{\mathbf{q}} \hbar\Omega_{\mathbf{q}} (D^\dagger_{\mathbf{q}} D_{\mathbf{q}} + \tfrac{1}{2}) + \sum_{\mathbf{q}} \hbar\omega_{\mathbf{q}} (B^\dagger_{\mathbf{q}} B_{\mathbf{q}} + \tfrac{1}{2}) \end{aligned} \tag{3.1}$$

$$H_{el-el} = \tfrac{1}{2} \sum_{\lambda,\lambda'} \sum_{\mathbf{k},\mathbf{k}'} \sum_{\mathbf{q}\neq 0} V^{\lambda,\lambda'}_{\mathbf{q}} \Psi^\dagger_{\lambda,\mathbf{k}} \Psi^\dagger_{\lambda',\mathbf{k}'} \Psi_{\lambda',\mathbf{k}'+\mathbf{q}} \Psi_{\lambda,\mathbf{k}-\mathbf{q}} \tag{3.2}$$

$$H_{el-ph} = \sum_{\lambda,\mathbf{k}} \sum_{\mathbf{q}} \hbar\Omega_{\mathbf{q}} g^\lambda_{\mathbf{q}} P^{\lambda,\lambda}_{\mathbf{k}-\mathbf{q},\mathbf{k}} (D_{-\mathbf{q}} + D^\dagger_{\mathbf{q}}) \tag{3.3}$$

$$H_{el-em} = -i \sum_{\lambda,\lambda'} \sum_{\mathbf{k}} F^{\lambda,\lambda'} P^{\lambda,\lambda'}_{\mathbf{k},\mathbf{k}} B^{\lambda,\lambda'} \tag{3.4}$$

where $P^{\lambda,\lambda'}_{\mathbf{k},\mathbf{q}} = \Psi^\dagger_{\lambda,\mathbf{k}} \Psi_{\lambda',\mathbf{q}}$ is a shorthand for the electronic polarization operator, and $B^\dagger_{\mathbf{q}}$ ($B_{\mathbf{q}}$) and $D^\dagger_{\mathbf{q}}$ ($D_{\mathbf{q}}$) are creation (annihilation) operators for photons and phonons with wave vector $\mathbf{q}$, respectively. The parameters $\varepsilon_{\lambda,\mathbf{k}}$, $g^\lambda_{\mathbf{q}}$, and $F^{\lambda,\lambda'}$ represent the electronic band structure, Frölich Hamiltonian matrix element (scaled by the phonon energy), and dipole matrix element for vertical transitions, respectively. Additionally, we allow for band dependence in the coulomb interaction $V^{\lambda,\lambda'}_{\mathbf{q}}$, which will prove necessary when considering layered 2-D materials. The operator $B^{\lambda,\lambda'}$ is defined to be B_0 for $\varepsilon_{\lambda,\mathbf{k}} > \varepsilon_{\lambda',\mathbf{k}}$ and $B^\dagger_0$ for $\varepsilon_{\lambda,\mathbf{k}} < \varepsilon_{\lambda',\mathbf{k}}$. There are two approaches to determine the absorption spectrum for such a system: 1) Obtain the retarded electronic polarization function [54], and 2) Obtain the

Heisenberg Equation of Motion for the photon occupation number $\langle B^\dagger B \rangle$. For the purposes of this work, we will only consider the latter, but note that the results are identical. To that end, require an expression for the general polarization commutator:

$$[P^{c,v}_{\mathbf{k},\mathbf{q}}, P^{\lambda,\lambda'}_{\mathbf{k}',\mathbf{q}'}] = \delta_{v,\lambda}\delta_{\mathbf{q},\mathbf{k}'}P^{c,\lambda'}_{\mathbf{k},\mathbf{q}'} - \delta_{c,\lambda'}\delta_{\mathbf{k},\mathbf{q}'}P^{\lambda,v}_{\mathbf{k}',\mathbf{q}} \tag{3.5}$$

Using the Heisenberg picture, one can show that the average photon occupation number obeys [46, 47]:

$$\frac{d}{dt}\left\langle B^\dagger_{\mathbf{q}} B_{\mathbf{q}} \right\rangle = \frac{1}{\hbar}\Big[\langle A_{\mathbf{q}}(t)\rangle - \langle L_{\mathbf{q}}(t)\rangle \Big] \tag{3.6}$$

where $A_{\mathbf{q}}(t)$ ($L_{\mathbf{q}}(t)$) describe changes in the photon number due to absorption (emission) events. Focusing on the absorption term, we define the polarization function:

$$\bar{\Pi}^{\lambda,\lambda'}(\mathbf{k}) \equiv \left\langle B P^{\lambda,\lambda'}_{\mathbf{k},\mathbf{k}} \right\rangle \tag{3.7}$$

and find:

$$\langle A_{\mathbf{q}}(t)\rangle = \sum_{\varepsilon_\lambda > \varepsilon_{\lambda'}} \sum_{\mathbf{k}} F^{\lambda,\lambda'} \bar{\Pi}^{\lambda,\lambda'}(\mathbf{k}) \tag{3.8}$$

To determine the absorption spectrum, we must solve the equation of motion of the polarization function. However, we must be careful with how we determine the average of an operator $\langle A \rangle$. Note that, when calculating the equation of motion for the two particle correlation function $\left\langle B^\dagger_{\mathbf{q}} B_{\mathbf{q}} \right\rangle$, we obtained an expression involving the three particle correlation

function $\left\langle B\Psi^{\dagger}_{\lambda,\mathbf{k}}\Psi_{\lambda',\mathbf{q}}\right\rangle$. In general, the equation of motion of an N particle correlation function requires knowledge of an $N+1$ particle correlation function. This leads to a hierarchy problem that can only be solved by truncating the resulting coupled equations at a chosen particle number. The solution is to follow the *cluster expansion* procedure outlined in Kira and Koch [55], where the $N+1$ particle correlation function is written in terms of its composite correlations. In a zeroth order cluster expansion, we keep terms up to order N in the equation of motion, and evaluate them with respect to the system's initial ground state. Applying the cluster expansion, the polarization function's equation of motion obeys *the Wannier Equation* [46, 47]:

$$\{i\hbar\tfrac{d}{dt} + (e_{c,\mathbf{k}} - e_{v,\mathbf{k}}) - \hbar\omega\}\bar{\Pi}^{c,v}_{\alpha,\beta}(\mathbf{k},t) = \{f^{v}_{\mathbf{k}} - f^{c}_{\mathbf{k}}\}\sum_{\mathbf{k}'} V_{\mathbf{k}-\mathbf{k}'}\bar{\Pi}^{c,v}(\mathbf{k}') - iS(\mathbf{k},t) \qquad (3.9)$$

where $e_{\lambda,\mathbf{k}}$ is a modified band structure accounting for the Coulomb self-energy, $f^{\lambda}_{\mathbf{k}}$ is the average electronic occupation number for energy $\varepsilon_{\lambda,\mathbf{k}}$, and $S(\mathbf{k},t) = F^{v,c}\left\langle B^{\dagger}B\right\rangle(f^{c}_{\mathbf{k}-\mathbf{q}} - f^{v}_{\mathbf{k}})$ acts as a source term for the excitations. Note that solutions to Eq.(3.9) describe bound states created by the attractive Coulomb interaction between the excited electron and the (positively charged) hole left behind in the valence band, as previously mentioned.

While Eq.(3.9) reveals the well established optical properties of a traditional exciton, it notably lacks any contribution from the electron-phonon interactions. This is due to the prescription of the zeroth order cluster expansion, which allows only terms of the same particle order as the correlation function. In order to introduce the Nth order phonon side-band, we would need to take the cluster expansion to Nth order, requiring us to solve $N+1$ coupled differential equations. This is impractical, and we will need to find some

method to simplify the calculation before we can obtain the desired phonon side-bands. In the next section we present a model containing the phonon side-bands, and explore its derivation in subsequent sections.

3.3 Fitting of Data

In the following sections, we will discuss a transformation that allows us to obtain the phonon side-bands to arbitrary order within the optical absorption spectrum without needing to take the cluster expansion to the same order. In the simplest case in which phonons are emitted/absorbed from optical branch ν with energy $\hbar\Omega_\nu$, we find the absorption coefficient as a function of the photon frequency ω to be:

$$\alpha(\omega) = \sum_{\varepsilon_c > \varepsilon_v} |F^{c,v}|^2 \sum_{\{m_\nu \epsilon \mathbb{Z}\}} \sum_n \frac{\prod_\nu D_\nu^{c,v} \Gamma_\nu^{c,v}}{(\tilde{E}_g^\nu + \sum_\nu m_\nu \hbar\Omega_\nu - \hbar\omega - E_{n,\nu})^2 + (\Gamma_{m_\nu}^{c,v})^2} \tag{3.10}$$

In this expression, $\tilde{E}_g^\nu$ represents a modified band gap resulting from corrections due to the electron-phonon interaction, $E_{n,\nu}$ is the Wannier energy, and $\Gamma_{m_\nu}^{c,v}$ is the effective exciton lifetime for transitions between the conduction and valence band. The side-band amplitude is given by:

$$D_\nu^{c,v} = e^{-|g_\nu^{c,v}|^2(1+2n_\nu)} e^{\frac{1}{2}m_\nu \beta\Omega_\nu} I_{m_\nu}\left(\frac{|g_\nu^{c,v}|^2}{sinh(\beta\hbar\Omega_\nu/2)}\right) \tag{3.11}$$

where $g_\nu^{c,v} = g_\nu^c - g_\nu^v$ is the difference between the electron-phonon matrix elements for the two bands, and I_{m_ν} is the first Bessel Function of imaginary argument. For simplicity, we will assume only one phonon mode contributes to the optical spectra. Furthermore, since

the difference between Wannier energies is typically larger than spectrum bandwidth, we will restrict the summation over Wannier energies to a single energy, which will be included within the fitting. Finally, there are three key unknown parameters in the experimental data: 1) the effective temperature of the system, 2) the zero phonon line, and 3) the exciton lifetime. For this reason, we fit the data in three distinct ways: 1) all parameters freely determined by the curve fit algorithm, 2) the exciton energy fixed near the predicted literature values ($\sim$1.3 eV for the $K-K$ transitions [48, 56, 57] and $\sim$0.9 eV for the $\Gamma-K$ transitions [48, 58]), and 3) temperature fixed to zero kelvin, preventing the model from considering phonon absorption side-bands.

Shown in FIG.(3.5) are fittings for the $K-K$ transitions for: 1) arbitrary parameters, 2) fixed phonon (30 meV) and exciton (1.278 eV) energies, 3) fixed phonon (30 meV) and exciton (1.313 eV) energies, and 4) fixed temperature (0K). All values have chi-squared values of approximately 0.12, suggesting that all four fits are in good agreement with the data. However, the fits with fixed exciton energy have fitting temperatures of 1538 K and 4626 K, respectively, which are significantly higher than the reported cryogenic temperature of 20 K of the experiment. Fits (1) and (4) are consistent with one another and the expected cryogenic temperature, but predict an exciton energy of about 0.78 eV.

Shown in FIG.(3.6) are fittings for the $\Gamma-K$ transitions for: 1) arbitrary parameters, 2) fixed phonon (30 meV) and exciton (0.94 eV) energies, 3) fixed phonon (30 meV) and exciton (1.02 eV) energies, and 4) fixed temperature (0K). All three arbitrary temperature plots suggest an ambient temperature of about 456 K, while the 0 K plot suggests a phonon energy of 50 meV and exciton energy of 0.58 eV.

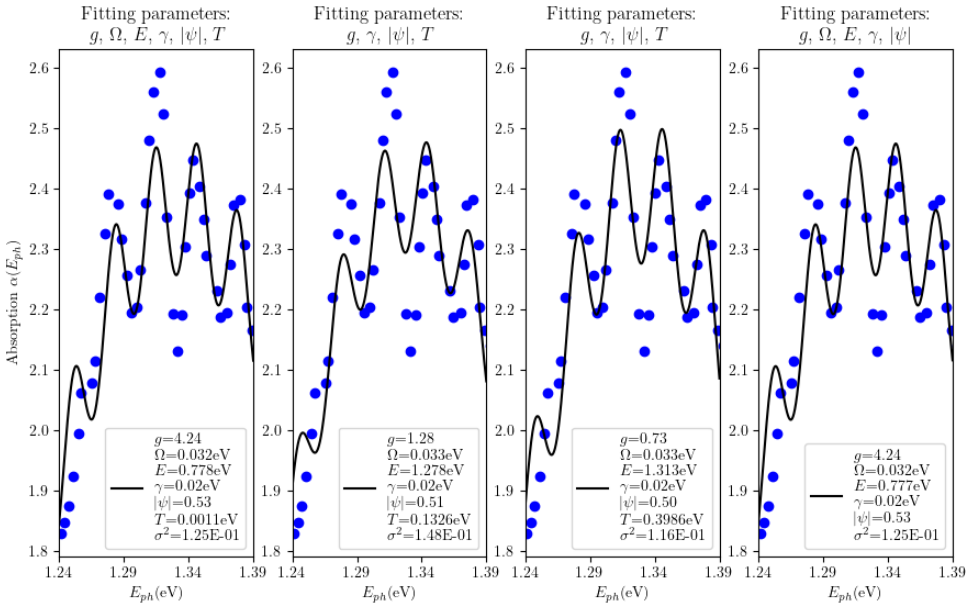

Figure 3.5: Fitting of Eq.(3.86) to $K-K$ absorption data from reference [48] for (Left) all model parameters, (Middle) all model parameters with energy fixed to 1.278 ev and 1.313 ev, respectively, and (Right) all model parameters in the zero temperature limit.

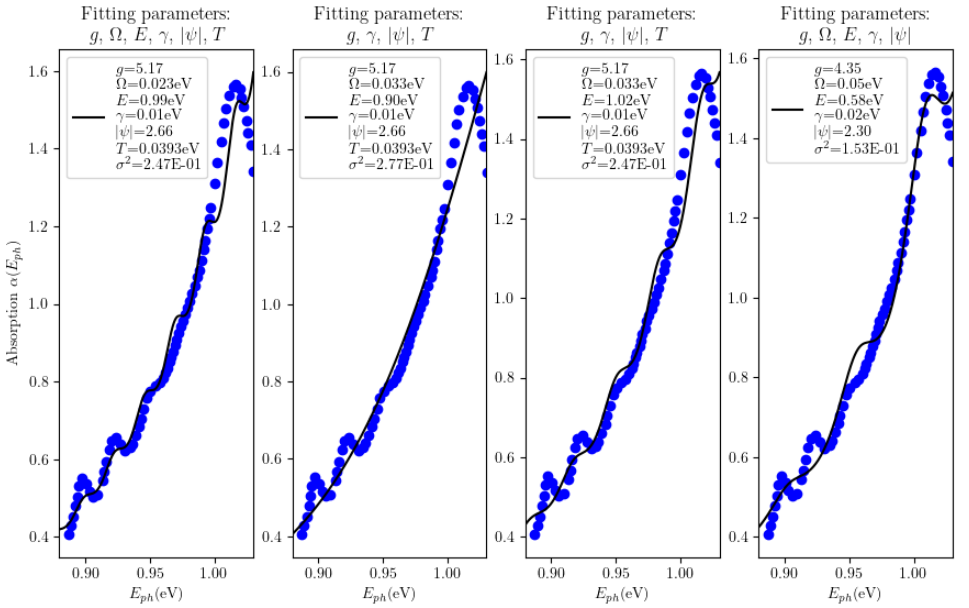

Figure 3.6: Fitting of Eq.(3.86) to $\Gamma-K$ absorption data from reference [48] for (Left) all model parameters, (Middle) all model parameters with energy fixed to 0.90 ev and 1.02 ev, respectively, and (Right) all model parameters in the zero temperature limit.

3.3.1 Discussion

Let us first examine the fittings that fix the exciton energy to the literature values of 0.9 eV and 1.3 eV. In both cases, the fittings suggest a phonon temperature well above that of the cryogenics. While it is possible that some effective temperature was introduced in the experiment, given that the literature values are themselves estimates based off of photo-luminescent experiments, we must also explore the possibility that these values are inaccurate. For this reason, we turn to the 0 K fits, which have the lowest and second lowest chi-squared values for the $\Gamma - k$ and $K - K$ transitions, respectively. For the $K - K$ transitions, the fit predicts a zero-phonon line of about 0.78 eV, differing from the literature value by about 50%. For the $\Gamma - K$ transitions, a zero-phonon line energy of 0.58 eV is predicted, differing from the literature value by about 43%.

Ultimately, our model serves as an additional method for calculating the exciton energy. Critically, it accounts for two perturbations of the bare exciton energy (i.e. in the absence of a phonon bath) by 1) determining the effective polaron band structure due to the Frölich interactions (Eq.(A.10)), and 2) allowing for an effective Coulomb interaction that shifts the Wannier energy. Such corrections are crucial for an optical spectrum with phonon side-bands, since they would be necessary for determining whether or not the side-bands are from phonon absorption, emission, or some combination of the two. Finally, it is worth noting that, to simplify the fitting, some key details of the model were omitted. Due to the complexity of the exact model (see Eq.(3.80), the above fitting assumes a single vibrational state with flat dispersion and Frölich matrix elements. While the experimental fits are consistent with the data, a more sophisticated fitting algorithm paired with the

more detailed model could yield a more precise calculation of the exciton energies.

3.4 Interacting Polaron Model

We now follow Feldtmann et. al. [47] and define a unitary transformation that casts the system as an effective interacting Polaron model:

$$T = exp\Big[\sum_{\lambda,\mathbf{k},\mathbf{q}} g^{\lambda}_{\mathbf{q}} P^{\lambda,\lambda}_{\mathbf{k}-\mathbf{q},\mathbf{k}} Q_{\mathbf{q}}\Big] \equiv exp\Big[\sum_{\lambda,\mathbf{k},\mathbf{q}} U^{\lambda}_{\mathbf{k},\mathbf{q}}\Big] \equiv e^{U} \tag{3.12}$$

where $Q_{\mathbf{q}} \equiv D^{\dagger}_{\mathbf{q}} - D_{-\mathbf{q}}$. The following commutators will prove useful:

$$\begin{aligned}
[Q_{\mathbf{q}}, Q_{\mathbf{q}'}] &= [D^{\dagger}_{\mathbf{q}} - D_{-\mathbf{q}}, D^{\dagger}_{\mathbf{q}'} - D_{-\mathbf{q}'}] \\
&= -[D^{\dagger}_{\mathbf{q}}, D_{-\mathbf{q}'}] - [D_{-\mathbf{q}}, D^{\dagger}_{\mathbf{q}'}] = 0
\end{aligned} \tag{3.13}$$

$$\begin{aligned}
[U^{\lambda}_{\mathbf{k},\mathbf{q}}, P^{\alpha,\beta}_{\mathbf{k}',\mathbf{q}'}] &= g^{\lambda}_{q} Q_{\mathbf{q}} [P^{\lambda,\lambda}_{\mathbf{k}-\mathbf{q},\mathbf{k}}, P^{\alpha,\beta}_{\mathbf{k}',\mathbf{q}'}] \\
&= g^{\lambda}_{\mathbf{q}} (\delta_{\lambda,\alpha}\delta_{\mathbf{k},\mathbf{k}'} P^{\lambda,\beta}_{\mathbf{k}-\mathbf{q},\mathbf{q}'} - \delta_{\lambda,\beta}\delta_{\mathbf{k}-\mathbf{q},\mathbf{q}'} P^{\alpha,\lambda}_{\mathbf{k}',\mathbf{k}}) Q_{\mathbf{q}}
\end{aligned} \tag{3.14}$$

$$\begin{aligned}
[U^{\lambda}_{\mathbf{k},\mathbf{q}}, U^{\lambda'}_{\mathbf{k}',\mathbf{q}'}] &= g^{\lambda}_{\mathbf{q}} g^{\lambda'}_{\mathbf{q}'} \{P^{\lambda',\lambda'}_{\mathbf{k}'-\mathbf{q}',\mathbf{k}'} P^{\lambda,\lambda}_{\mathbf{k}-\mathbf{q},\mathbf{k}} [Q_{\mathbf{q}}, Q_{\mathbf{q}'}] + [P^{\lambda,\lambda}_{\mathbf{k}-\mathbf{q},\mathbf{k}}, P^{\lambda',\lambda'}_{\mathbf{k}'-\mathbf{q}',\mathbf{k}'}] Q_{\mathbf{q}} Q_{\mathbf{q}'}\} \\
&= g^{\lambda}_{\mathbf{q}} g^{\lambda'}_{\mathbf{q}'} (\delta_{\lambda,\lambda'}\delta_{\mathbf{k},\mathbf{k}'-\mathbf{q}'} P^{\lambda,\lambda'}_{\mathbf{k}-\mathbf{q},\mathbf{k}'} - \delta_{\lambda,\lambda'}\delta_{\mathbf{k}-\mathbf{q},\mathbf{k}'} P^{\lambda',\lambda}_{\mathbf{k}'-\mathbf{q}',\mathbf{k}}) Q_{\mathbf{q}} Q_{\mathbf{q}'}
\end{aligned} \tag{3.15}$$

We now obtain the Polaron picture using the Baker-Campbell-Hausdorff (BCH) lemma. Note that $[U, B_{\mathbf{q}}] = 0$, leaving the photon operator and H_{em} unchanged under the transfor-

mation. To first order, the phonon Hamiltonian transforms as:

$$\begin{aligned}
[U, H_{latt}] &= \sum_{\mathbf{q}'} \sum_{\lambda,\mathbf{k},\mathbf{q}} \hbar\omega_{\mathbf{q}'} [U^{\lambda}_{\mathbf{k},\mathbf{q}}, D^{\dagger}_{\mathbf{q}'} D_{\mathbf{q}'}] \\
&= \sum_{\mathbf{q}'} \sum_{\lambda,\mathbf{k},\mathbf{q}} \hbar\omega_{\mathbf{q}'} g^{\lambda}_{\mathbf{q}} P^{\lambda,\lambda}_{\mathbf{k}-\mathbf{q},\mathbf{k}} \{[D^{\dagger}_{\mathbf{q}}, D^{\dagger}_{\mathbf{q}'} D_{\mathbf{q}'}] - [D_{-\mathbf{q}}, D^{\dagger}_{\mathbf{q}'} D_{\mathbf{q}'}]\} \\
&= \sum_{\mathbf{q}'} \sum_{\lambda,\mathbf{k},\mathbf{q}} \hbar\omega_{\mathbf{q}'} g^{\lambda}_{\mathbf{q}} P^{\lambda,\lambda}_{\mathbf{k}-\mathbf{q},\mathbf{k}} \{-\delta_{\mathbf{q},\mathbf{q}'} D^{\dagger}_{\mathbf{q}'} - \delta_{\mathbf{q},-\mathbf{q}'} D_{\mathbf{q}'}\} \\
&= -H_{el-ph}
\end{aligned} \tag{3.16}$$

This eliminates H_{el-ph} in the BCH expansion, and reduces the first order expression to $[U, H_{el-ph}]/2$. All higher orders of the BCH expansion for H_{latt} can thus be found from calculating $[U, H_{el-ph}]$:

$$\begin{aligned}
[U, H_{el-ph}] &= \sum_{\lambda,\lambda'} \sum_{\mathbf{k},\mathbf{k}'} \sum_{\mathbf{q},\mathbf{q}'} (\hbar\Omega_{\mathbf{q}'}) [U^{\lambda}_{\mathbf{k},\mathbf{q}}, U^{\lambda'}_{\mathbf{k}',\mathbf{q}'} + 2 g^{\lambda'}_{\mathbf{q}'} P^{\lambda',\lambda'}_{\mathbf{k}'-\mathbf{q}',\mathbf{k}'} D_{-\mathbf{q}'}] \\
&= \sum_{\lambda} \sum_{\mathbf{k}} \sum_{\mathbf{q},\mathbf{q}'} g^{\lambda'}_{\mathbf{q}'} g^{\lambda}_{\mathbf{q}} (\hbar\Omega_{\mathbf{q}'}) (P^{\lambda,\lambda}_{\mathbf{k}-\mathbf{q},\mathbf{k}+\mathbf{q}'} - P^{\lambda,\lambda}_{\mathbf{k}-\mathbf{q}-\mathbf{q}',\mathbf{k}}) Q_{\mathbf{q}} Q_{\mathbf{q}'} \\
&+ 2 \sum_{\lambda,\lambda'} \sum_{\mathbf{k},\mathbf{k}'} \sum_{\mathbf{q},\mathbf{q}'} g^{\lambda'}_{\mathbf{q}'} g^{\lambda}_{\mathbf{q}} (\hbar\Omega_{\mathbf{q}'}) [P^{\lambda,\lambda}_{\mathbf{k}-\mathbf{q},\mathbf{k}} Q_{\mathbf{q}}, P^{\lambda',\lambda'}_{\mathbf{k}'-\mathbf{q}',\mathbf{k}'} D_{-\mathbf{q}'}]
\end{aligned}$$

The first term can be cancelled with a momentum transformation $\mathbf{k}' = \mathbf{k} - \mathbf{q}'$. The remaining commutator is found to be:

$$\begin{aligned}
[P^{\lambda,\lambda}_{\mathbf{k}-\mathbf{q},\mathbf{k}} Q_{\mathbf{q}}, P^{\lambda',\lambda'}_{\mathbf{k}'-\mathbf{q}',\mathbf{k}'} D_{-\mathbf{q}'}] &= P^{\lambda,\lambda}_{\mathbf{k}-\mathbf{q},\mathbf{k}} P^{\lambda',\lambda'}_{\mathbf{k}'-\mathbf{q}',\mathbf{k}'} [Q_{\mathbf{q}}, D_{-\mathbf{q}'}] + [P^{\lambda,\lambda}_{\mathbf{k}-\mathbf{q},\mathbf{k}}, P^{\lambda',\lambda'}_{\mathbf{k}'-\mathbf{q}',\mathbf{k}'}] D_{-\mathbf{q}'} Q_{\mathbf{q}} \\
&= -\delta_{\mathbf{q}',-\mathbf{q}} P^{\lambda,\lambda}_{\mathbf{k}-\mathbf{q},\mathbf{k}} P^{\lambda',\lambda'}_{\mathbf{k}'-\mathbf{q}',\mathbf{k}'} \\
&+ \delta_{\lambda\lambda'} (\delta_{\mathbf{k}'-\mathbf{q}',\mathbf{k}} P^{\lambda,\lambda'}_{\mathbf{k}-\mathbf{q},\mathbf{k}'} - \delta_{\mathbf{k}',\mathbf{k}-\mathbf{q}} P^{\lambda',\lambda}_{\mathbf{k}'-\mathbf{q}',\mathbf{k}}) D_{-\mathbf{q}'} Q_{\mathbf{q}}
\end{aligned}$$

which gives:

$$[U, H_{el-ph}] = -2\sum_{\lambda,\lambda'}\sum_{\mathbf{k},\mathbf{k}'}\sum_{\mathbf{q}} g^{\lambda}_{\mathbf{q}} g^{\lambda'}_{-\mathbf{q}} (\hbar\Omega_{\mathbf{q}}) P^{\lambda,\lambda}_{\mathbf{k}-\mathbf{q},\mathbf{k}} P^{\lambda',\lambda'}_{\mathbf{k}'+\mathbf{q},\mathbf{k}'}$$
$$- 2\sum_{\lambda}\sum_{\mathbf{k}}\sum_{\mathbf{q},\mathbf{q}'} g^{\lambda}_{\mathbf{q}} g^{\lambda'}_{\mathbf{q}'} (\hbar\Omega_{\mathbf{q}'}) \{P^{\lambda,\lambda}_{\mathbf{k}-\mathbf{q},\mathbf{k}+\mathbf{q}} - P^{\lambda,\lambda}_{\mathbf{k}-\mathbf{q}-\mathbf{q}',\mathbf{k}}\} D_{-\mathbf{q}'} Q_{\mathbf{q}}$$

The second term is eliminated by the same momentum transformation, yielding:

$$[U, H_{el-ph}] = -2\sum_{\lambda\lambda'}\sum_{\mathbf{k},\mathbf{k}'}\sum_{\mathbf{q}} g^{\lambda}_{\mathbf{q}} g^{\lambda'}_{-\mathbf{q}} (\hbar\Omega_{\mathbf{q}}) \{\Psi^{\dagger}_{\lambda,\mathbf{k}-\mathbf{q}} (\delta_{\lambda,\lambda'}\delta_{\mathbf{k}'+\mathbf{q},\mathbf{k}} - \Psi^{\dagger}_{\lambda',\mathbf{k}'+\mathbf{q}} \Psi_{\lambda,\mathbf{k}}) \Psi_{\lambda',\mathbf{k}'}\}$$
$$= -2\sum_{\lambda,\mathbf{k},\mathbf{q}} \hbar\Omega_{\mathbf{q}} |g^{\lambda}_{\mathbf{q}}|^2 P^{\lambda,\lambda}_{\mathbf{k}-\mathbf{q},\mathbf{k}-\mathbf{q}}$$
$$- 2\sum_{\lambda,\lambda'}\sum_{\mathbf{k},\mathbf{k}'}\sum_{\mathbf{q}} \hbar\Omega_{\mathbf{q}}\, g^{\lambda}_{-\mathbf{q}} g^{\lambda'}_{\mathbf{q}} \Psi^{\dagger}_{\lambda,\mathbf{k}} \Psi^{\dagger}_{\lambda',\mathbf{k}'} \Psi_{\lambda',\mathbf{k}'+\mathbf{q}} \Psi_{\lambda,\mathbf{k}-\mathbf{q}} \tag{3.17}$$

The first term in in Eq.(3.17) couples to the electronic band structure, while the second term modifies the Coulomb interaction. Finally, we note that when the coefficients in the Hamiltonian do not depend on the electronic momentum $\mathbf{k}$, the following commutators vanish:

$$[P^{\lambda,\lambda}_{\mathbf{k}-\mathbf{q},\mathbf{k}}, P^{\lambda',\lambda'}_{\mathbf{k}',\mathbf{k}'}] = \delta_{\lambda,\lambda'}(\delta_{\mathbf{k},\mathbf{k}'} P^{\lambda,\lambda'}_{\mathbf{k}-\mathbf{q},\mathbf{k}'} - \delta_{\mathbf{k}',\mathbf{k}-\mathbf{q}} P^{\lambda',\lambda}_{\mathbf{k}',\mathbf{k}}) \tag{3.18}$$

$$[P^{\lambda,\lambda}_{\mathbf{k}-\mathbf{q},\mathbf{k}}, \Psi^{\dagger}_{\lambda',\mathbf{k}'} \Psi^{\dagger}_{\lambda'',\mathbf{k}''} \Psi_{\lambda'',\mathbf{k}''+\mathbf{q}'} \Psi_{\lambda',\mathbf{k}'-\mathbf{q}'}] = [P^{\lambda,\lambda}_{\mathbf{k}-\mathbf{q},\mathbf{k}}, \delta_{\mathbf{q}',0} P^{\lambda',\lambda'}_{\mathbf{k}',\mathbf{k}'-\mathbf{q}'} - P^{\lambda',\lambda''}_{\mathbf{k}',\mathbf{k}''+\mathbf{q}'} P^{\lambda'',\lambda'}_{\mathbf{k}'',\mathbf{k}'-\mathbf{q}'}]$$
$$= \delta_{\mathbf{q}',0}\delta_{\lambda',\lambda}\{\delta_{\mathbf{k}',\mathbf{k}} P^{\lambda,\lambda'}_{\mathbf{k}-\mathbf{q},\mathbf{k}'-\mathbf{q}'} - \delta_{\mathbf{k}'-\mathbf{q}',\mathbf{k}-\mathbf{q}} P^{\lambda',\lambda}_{\mathbf{k}',\mathbf{k}}\}$$
$$- \delta_{\lambda'',\lambda}\{\delta_{\mathbf{k}'',\mathbf{k}} P^{\lambda',\lambda''}_{\mathbf{k}',\mathbf{k}''+\mathbf{q}'} P^{\lambda'',\lambda'}_{\mathbf{k}-\mathbf{q},\mathbf{k}'-\mathbf{q}'} - \delta_{\mathbf{k}'+\mathbf{q}',\mathbf{k}-\mathbf{q}} P^{\lambda',\lambda}_{\mathbf{k}',\mathbf{k}} P^{\lambda'',\lambda'}_{\mathbf{k}'',\mathbf{k}'-\mathbf{q}'}\}$$
$$- \delta_{\lambda',\lambda}\{\delta_{\mathbf{k}',\mathbf{k}} P^{\lambda,\lambda''}_{\mathbf{k}-\mathbf{q},\mathbf{k}''+\mathbf{q}'} P^{\lambda'',\lambda'}_{\mathbf{k}'',\mathbf{k}'-\mathbf{q}'} - \delta_{\mathbf{k}'-\mathbf{q}',\mathbf{k}-\mathbf{q}} P^{\lambda',\lambda''}_{\mathbf{k}',\mathbf{k}''+\mathbf{q}'} P^{\lambda'',\lambda}_{\mathbf{k}'',\mathbf{k}}\} \tag{3.19}$$

Thus $[U, H_{el-el}] = 0$ and $[U[U, H_{el-ph}] = 0$. The Coulomb interaction remains unchanged, and the higher order terms in the BCH expansion of H_{latt} and H_{el-ph} vanish. We are left to calculate the transformations for H_{el} and H_{el-em}. We begin with the band structure terms at first order:

$$\begin{aligned}
[U, H_{el}] &= \sum_{\lambda,\lambda'} \sum_{\mathbf{k},\mathbf{k}'} \sum_{\mathbf{q}} \varepsilon_{\lambda',\mathbf{k}'} g^{\lambda}_{\mathbf{q}} [P^{\lambda,\lambda}_{\mathbf{k}-\mathbf{q},\mathbf{k}}, P^{\lambda',\lambda'}_{\mathbf{k}',\mathbf{k}'}] Q_{\mathbf{q}} \\
&= \sum_{\lambda,\mathbf{k},\mathbf{q}} \{\varepsilon_{\lambda,\mathbf{k}} - \varepsilon_{\lambda,\mathbf{k}-\mathbf{q}}\} g^{\lambda}_{\mathbf{q}} P^{\lambda,\lambda}_{\mathbf{k}-\mathbf{q},\mathbf{k}} Q_{\mathbf{q}} \\
&= \sum_{\lambda,\mathbf{k},\mathbf{q}} \{\varepsilon_{\lambda,\mathbf{k}} - \varepsilon_{\lambda,\mathbf{k}-\mathbf{q}}\} U^{\lambda}_{\mathbf{k},\mathbf{q}}
\end{aligned} \tag{3.20}$$

At second order, we obtain:

$$[U, [U, H_{el}]] = \sum_{\lambda,\lambda'} \sum_{\mathbf{k},\mathbf{k}'} \sum_{\mathbf{q},\mathbf{q}'} \{\varepsilon_{\lambda',\mathbf{k}'} - \varepsilon_{\lambda',\mathbf{k}'-\mathbf{q}'}\} [U^{\lambda}_{\mathbf{k},\mathbf{q}}, U^{\lambda'}_{\mathbf{k}',\mathbf{q}'}]$$

Using Eq.(3.15), this reduces to:

$$\sum_{\lambda} \sum_{\mathbf{k},\mathbf{q}} \sum_{\mathbf{q}'} g^{\lambda}_{\mathbf{q}} g^{\lambda}_{\mathbf{q}'} \{(\varepsilon_{\lambda,\mathbf{k}+\mathbf{q}'} - \varepsilon_{\lambda,\mathbf{k}}) P^{\lambda,\lambda}_{\mathbf{k}-\mathbf{q},\mathbf{k}+\mathbf{q}'} - (\varepsilon_{\lambda,\mathbf{k}-\mathbf{q}} - \varepsilon_{\lambda,\mathbf{k}-\mathbf{q}-\mathbf{q}'}) P^{\lambda,\lambda}_{\mathbf{k}-\mathbf{q}-\mathbf{q}',\mathbf{k}}\} Q_{\mathbf{q}} Q_{\mathbf{q}'}$$

Defining $\mathbf{q}'' = \mathbf{q} + \mathbf{q}'$, we obtain:

$$[U, [U, H_{el}]] = \sum_{\lambda} \sum_{\mathbf{k},\mathbf{q}} \sum_{\mathbf{q}'} \{\varepsilon_{\lambda,\mathbf{k}} - 2\varepsilon_{\lambda,\mathbf{k}-\mathbf{q}+\mathbf{q}'} + \varepsilon_{\lambda,\mathbf{k}-\mathbf{q}}\} g^{\lambda}_{\mathbf{q}-\mathbf{q}'} Q_{\mathbf{q}-\mathbf{q}'} U^{\lambda}_{\mathbf{k}-\mathbf{q},\mathbf{k}} \tag{3.21}$$

The form of Eq.(3.21) suggests higher order terms will be of the same form. Using the matrix product notation $(MN)_{\mathbf{k},\mathbf{k}'} = \sum_{\mathbf{k}_1} M_{\mathbf{k},\mathbf{k}_1} N_{\mathbf{k}_1,\mathbf{k}}$, the transformed Hamiltonian is:

$$\bar{H}_{el} = \sum_{\lambda} \sum_{\mathbf{k},\mathbf{q}} \left(e^{-C_\lambda} \mathcal{E}_\lambda e^{C_\lambda} \right)_{\mathbf{k},\mathbf{k}-\mathbf{q}} P^{\lambda,\lambda}_{\mathbf{k}-\mathbf{q},\mathbf{k}}$$

where $C^{\lambda}_{\mathbf{k},\mathbf{k}'} \equiv g^{\lambda}_{\mathbf{k}-\mathbf{k}'} Q_{\mathbf{k}-\mathbf{k}'}$ and $(\mathcal{E}_\lambda)_{\mathbf{k},\mathbf{k}'} = \varepsilon_{\lambda,\mathbf{k}} \delta_{\mathbf{k},\mathbf{k}'}$. First and second order transformations of H_{el-em} are similar. We have:

$$\begin{aligned}
[U, H_{el-em}] &= -i \sum_{\lambda} \sum_{\mathbf{k},\mathbf{q}} \sum_{\lambda',\lambda''} \sum_{\mathbf{k}'} F^{\lambda',\lambda''} [U^{\lambda}_{\mathbf{k},\mathbf{q}}, P^{\lambda',\lambda''}_{\mathbf{k}',\mathbf{k}'}] B^{\lambda',\lambda''} \\
&= -i \sum_{\lambda,\lambda'} \sum_{\mathbf{k},\mathbf{q}} F^{\lambda,\lambda'} \{ g^{\lambda}_{\mathbf{q}} - g^{\lambda'}_{\mathbf{q}} \} Q_{\mathbf{q}} P^{\lambda,\lambda'}_{\mathbf{k}-\mathbf{q},\mathbf{k}} B^{\lambda,\lambda'}
\end{aligned}$$

and:

$$\begin{aligned}
[U, [U, H_{el-em}]] &= -i \sum_{\lambda} \sum_{\mathbf{k},\mathbf{q}} \sum_{\lambda',\lambda''} \sum_{\mathbf{k}',\mathbf{q}'} F^{\lambda',\lambda''} g^{\lambda}_{\mathbf{q}} Q_{\mathbf{q}} \{ g^{\lambda'}_{\mathbf{q}'} - g^{\lambda''}_{\mathbf{q}'} \} Q_{\mathbf{q}'} [P^{\lambda,\lambda}_{\mathbf{k}-\mathbf{q},\mathbf{k}}, P^{\lambda',\lambda''}_{\mathbf{k}'-\mathbf{q}',\mathbf{k}'}] B^{\lambda',\lambda''} \\
&= -i \sum_{\lambda,\lambda'} \sum_{\mathbf{k},\mathbf{q}} \sum_{\mathbf{q}'} F^{\lambda,\lambda'} \{ g^{\lambda}_{\mathbf{q}} Q_{\mathbf{q}} (g^{\lambda}_{\mathbf{q}'} - g^{\lambda'}_{\mathbf{q}'}) Q_{\mathbf{q}'} P^{\lambda,\lambda'}_{\mathbf{k}-\mathbf{q},\mathbf{k}+\mathbf{q}'} - g^{\lambda'}_{\mathbf{q}} Q_{\mathbf{q}} (g^{\lambda}_{\mathbf{q}'} - g^{\lambda'}_{\mathbf{q}'}) Q_{\mathbf{q}'} P^{\lambda,\lambda'}_{\mathbf{k}-\mathbf{q}-\mathbf{q}',\mathbf{k}} \} B^{\lambda,\lambda'} \\
&= -i \sum_{\lambda,\lambda'} \sum_{\mathbf{k},\mathbf{q}} \sum_{\mathbf{q}'} F^{\lambda,\lambda'} \{ (g^{\lambda}_{\mathbf{q}'} - g^{\lambda'}_{\mathbf{q}'}) (g^{\lambda}_{\mathbf{q}-\mathbf{q}'} - g^{\lambda'}_{\mathbf{q}-\mathbf{q}'}) Q_{\mathbf{q}} Q_{\mathbf{q}-\mathbf{q}'} \} P^{\lambda,\lambda'}_{\mathbf{k}-\mathbf{q},\mathbf{k}} B^{\lambda,\lambda'}
\end{aligned}$$

This allows us to write the interacting polaron picture as:

$$\bar{H}_{pol} = \sum_{\lambda,\mathbf{k},\mathbf{q}} \left\{ \left(e^{-C_\lambda} \mathcal{E}_\lambda e^{C_\lambda} \right)_{\mathbf{k},\mathbf{k}-\mathbf{q}} P^{\lambda,\lambda}_{\mathbf{k}-\mathbf{q},\mathbf{k}} - \hbar\Omega_{\mathbf{q}} |g^\lambda_{\mathbf{q}}|^2 P^{\lambda,\lambda}_{\mathbf{k},\mathbf{k}} \right\} \tag{3.22}$$

$$\bar{H}_{latt} = \sum_{\mathbf{q}} \hbar\Omega_{\mathbf{q}} (D^\dagger_{\mathbf{q}} D_{\mathbf{q}} + \tfrac{1}{2}) \tag{3.23}$$

$$\bar{H}_{em} = \sum_{\mathbf{q}} \hbar\omega_{\mathbf{q}} (B^\dagger_{\mathbf{q}} B_{\mathbf{q}} + \tfrac{1}{2}) \tag{3.24}$$

$$\bar{H}_{pol-pol} = \tfrac{1}{2} \sum_{\lambda,\lambda'} \sum_{\mathbf{k},\mathbf{k}'} \sum_{\mathbf{q}} \tilde{V}^{\lambda,\lambda'} \Psi^\dagger_{\lambda,\mathbf{k}} \Psi^\dagger_{\lambda',\mathbf{k}'} \Psi_{\lambda',\mathbf{k}'+\mathbf{q}} \Psi_{\lambda,\mathbf{k}-\mathbf{q}} \tag{3.25}$$

$$\bar{H}_{pol-em} = -i \sum_{\lambda,\lambda'} \sum_{\mathbf{k},\mathbf{q}} F^{\lambda,\lambda'} \left(e^{C_\lambda - C_{\lambda'}} \right)_{\mathbf{q},0} P^{\lambda,\lambda'}_{\mathbf{k}-\mathbf{q},\mathbf{k}} B^{\lambda,\lambda'} \tag{3.26}$$

where we have defined $\tilde{V}^{\lambda,\lambda'}_{\mathbf{q}} = V^{\lambda,\lambda'}_{\mathbf{q}} - 2\hbar\Omega_{\mathbf{q}} (g^\lambda_{\mathbf{q}})^* g^{\lambda'}_{\mathbf{q}}$. Crucially, we see that the EM-field interaction has been modified and now couples the dipole matrix element with the Frölich matrix elements.

We further simplify $\bar{H}_{pol}$ by replacing all powers of C_λ with their thermal average, reducing it to:

$$\bar{H}_{pol} = \sum_{\lambda,\mathbf{k}} e_{\lambda,\mathbf{k}} P^{\lambda,\lambda}_{\mathbf{k},\mathbf{k}} \tag{3.27}$$

The energies $e_{\lambda,\mathbf{k}}$ are found from evaluating the thermal expectation values.

3.4.1 Photon Emission and Absorption Spectra

Using Eqs.(3.23-3.27), we are now able to write the equation of motion for the photon number operator $\left\langle B^{\dagger}_{\mathbf{q}} B_{\mathbf{q}} \right\rangle$. Using the Heisenberg picture, we obtain:

$$\begin{aligned}
[B^{\dagger}_{\mathbf{q}} B_{\mathbf{q}}, \bar{H}] &= -i \sum_{\lambda\lambda'} \sum_{\mathbf{k},\mathbf{q}'} F^{\lambda,\lambda'} \left(e^{C_{\lambda} - C_{\lambda'}} \right)_{\mathbf{q}',0} P^{\lambda,\lambda'}_{\mathbf{k}-\mathbf{q}',\mathbf{k}} [B^{\dagger}_{\mathbf{q}} B_{\mathbf{q}}, B^{\lambda,\lambda'}] \\
&= i \sum_{\varepsilon_{\lambda} > \varepsilon_{\lambda'}} \sum_{\mathbf{k},\mathbf{q}'} F^{\lambda,\lambda'} \left(e^{C_{\lambda} - C_{\lambda'}} \right)_{\mathbf{q}',0} P^{\lambda,\lambda'}_{\mathbf{k}-\mathbf{q}',\mathbf{k}} B_{\mathbf{q}} \delta_{\mathbf{q},0} \\
&\quad - i \sum_{\varepsilon_{\lambda} < \varepsilon_{\lambda'}} \sum_{\mathbf{k},\mathbf{q}'} F^{\lambda,\lambda'} \left(e^{C_{\lambda} - C_{\lambda'}} \right)_{\mathbf{q}',0} P^{\lambda,\lambda'}_{\mathbf{k}-\mathbf{q}',\mathbf{k}} B^{\dagger}_{\mathbf{q}} \delta_{\mathbf{q},0}
\end{aligned} \tag{3.28}$$

which can be re-written as:

$$\frac{d}{dt} B^{\dagger}_{\mathbf{q}} B_{\mathbf{q}} = \frac{1}{\hbar} \Big[A_{\mathbf{q}}(t) - L_{\mathbf{q}}(t) \Big] \tag{3.29}$$

where:

$$A_{\mathbf{q}}(t) = \sum_{\varepsilon_{\lambda} > \varepsilon_{\lambda'}} \sum_{\mathbf{k},\mathbf{q}'} F^{\lambda,\lambda'} \left(e^{C_{\lambda} - C_{\lambda'}} \right)_{\mathbf{q}',0} P^{\lambda,\lambda'}_{\mathbf{k}-\mathbf{q}',\mathbf{k}} B_{\mathbf{q}} \delta_{\mathbf{q},0} \tag{3.30}$$

$$L_{\mathbf{q}}(t) = \sum_{\varepsilon_{\lambda} < \varepsilon_{\lambda'}} \sum_{\mathbf{k},\mathbf{q}'} F^{\lambda,\lambda'} \left(e^{C_{\lambda} - C_{\lambda'}} \right)_{\mathbf{q}',0} P^{\lambda,\lambda'}_{\mathbf{k}-\mathbf{q}',\mathbf{k}} B^{\dagger}_{\mathbf{q}} \delta_{\mathbf{q},0} \tag{3.31}$$

describe changes in the photon number due to optical absorption and emission, respectively. We are primarily concerned with phonon side-bands in the absorption spectrum, and will thus focus our efforts on Eq.(3.30). By normal ordering the phonon operators, we are able

to define the polaron polarization function:

$$\Pi^{\lambda,\lambda'}_{\alpha,\beta}(\mathbf{k},\mathbf{q}) \equiv BP^{\lambda,\lambda'}_{\mathbf{k}-\mathbf{q},\mathbf{k}}([d^{\dagger}_{\lambda,\lambda'}]^{\alpha}[d^{T}_{\lambda,\lambda'}]^{\beta})_{\mathbf{q},0} \tag{3.32}$$

with $(d^{\dagger}_{\lambda,\lambda'})_{\mathbf{k},\mathbf{k}'} = (g^{\lambda}_{\mathbf{k}-\mathbf{k}'} - g^{\lambda'}_{\mathbf{k}-\mathbf{k}'})D^{\dagger}_{\mathbf{k}-\mathbf{k}'}$ and $(d^{T}_{\lambda,\lambda'})_{\mathbf{k},\mathbf{k}'} = (g^{\lambda}_{\mathbf{k}-\mathbf{k}'} - g^{\lambda'}_{\mathbf{k}-\mathbf{k}'})D_{\mathbf{k}'-\mathbf{k}}$. The absorption spectrum is now given by:

$$A(t) = \sum_{\varepsilon_{\lambda}>\varepsilon_{\lambda'}} \sum_{\mathbf{k},\mathbf{q}} F^{\lambda,\lambda'} \sum_{\alpha,\beta} C^{\alpha,\beta}_{\lambda,\lambda'} \Pi^{\lambda,\lambda'}_{\alpha,\beta}(\mathbf{k},\mathbf{q}) \tag{3.33}$$

where $C^{\alpha,\beta}_{\lambda,\lambda'}$ is a coefficient accounting for the normal ordering of the phonon operators. We will assume the interaction $g^{\lambda}_{\mathbf{q}}$ arises from an optical phonon such that $\Omega_{\mathbf{q}} = \Omega \, \forall \mathbf{q}$. We can find the dynamics of the polarization function by once again using the Heisenberg picture:

$$i\hbar \frac{d}{dt} \Pi^{c,v}_{\alpha,\beta}(\mathbf{k},\mathbf{q}) = [\Pi^{c,v}_{\alpha,\beta}(\mathbf{k},\mathbf{q}), \bar{H}] \tag{3.34}$$

Commutators for $\bar{H}_{pol}$ and $\bar{H}_{em}$ are:

$$\begin{aligned} [\Pi^{c,v}_{\alpha,\beta}(\mathbf{k},\mathbf{q}), \bar{H}_{pol}] &= \sum_{\lambda',\mathbf{k}'} e_{\lambda',\mathbf{k}'} [\Pi^{c,v}_{\alpha,\beta}(\mathbf{k},\mathbf{q}), P^{\lambda',\lambda'}_{\mathbf{k}',\mathbf{k}'}] \\ &= (e_{v,\mathbf{k}} - e_{c,\mathbf{k}-\mathbf{q}}) \Pi^{c,v}_{\alpha,\beta}(\mathbf{k},\mathbf{q}) \end{aligned} \tag{3.35}$$

$$\begin{aligned} [\Pi^{c,v}_{\alpha,\beta}(\mathbf{k},\mathbf{q}), \bar{H}_{em}] &= \sum_{\mathbf{q}'} \hbar\omega_{\mathbf{q}'} [\Pi^{c,v}_{\alpha,\beta}(\mathbf{k},\mathbf{q}), B^{\dagger}_{\mathbf{q}'} B_{\mathbf{q}'}] \\ &= \hbar\omega \Pi^{c,v}_{\alpha,\beta}(\mathbf{k},\mathbf{q}) \end{aligned} \tag{3.36}$$

For $\bar{H}_{latt}$, we first note:

$$\sum_{\mathbf{q}'}[(d^T_{c,v})_{\mathbf{q},0}, D^\dagger_{\mathbf{q}'}]D_{\mathbf{q}'} = \sum_{\mathbf{q}'}\delta_{\mathbf{q}',-\mathbf{q}}(g^c_{\mathbf{q}} - g^v_{\mathbf{q}})^* D_{\mathbf{q}'} = (d^T_{c,v})_{\mathbf{q},0}$$

Assuming:

$$\sum_{\mathbf{q}'}[(d^T_{c,v})^\beta_{\mathbf{q},0}, D^\dagger_{\mathbf{q}'}]D_{\mathbf{q}'} = \beta(d^T_{c,v})^\beta_{\mathbf{q},0}$$

we find:

$$\begin{aligned}
\sum_{\mathbf{q}'}[(d^T_{c,v})^{\beta+1}_{\mathbf{q},0}, D^\dagger_{\mathbf{q}'}]D_{\mathbf{q}'} &= \sum_{\mathbf{q}',\mathbf{q}''}[(d^T_{c,v})^\beta_{\mathbf{q},\mathbf{q}''}(d^T_{c,v})_{\mathbf{q}'',0}, D^\dagger_{\mathbf{q}'}]D_{\mathbf{q}'} \\
&= \sum_{\mathbf{q}',\mathbf{q}''}\{[(d^T_{c,v})^\beta_{\mathbf{q},\mathbf{q}''}, D^\dagger_{\mathbf{q}'}]D_{\mathbf{q}'',0} + (d^T_{c,v})^\beta_{\mathbf{q},\mathbf{q}''}[d_{\mathbf{q}'',0}, D^\dagger_{\mathbf{q}'}]\}D_{\mathbf{q}'} \\
&= \sum_{\mathbf{q}''}\{\beta(d^T_{c,v})^\beta_{\mathbf{q},\mathbf{q}''}D_{\mathbf{q}'',0} + (d^T_{c,v})^\beta_{\mathbf{q},\mathbf{q}''}D_{\mathbf{q}'',0}\} \\
&= (\beta+1)(d^T_{c,v})^{\beta+1}_{\mathbf{q},0}
\end{aligned}$$

Thus, by induction:

$$\begin{aligned}
[\Pi^{c,v}_{\alpha,\beta}(\mathbf{k},\mathbf{q}), \bar{H}_{latt}] &= \sum_{\mathbf{q}',\mathbf{q}''}\hbar\Omega B P^{\lambda,\lambda'}_{\mathbf{k}-\mathbf{q},\mathbf{k}}\{(d^\dagger_{c,v})^\alpha_{\mathbf{q},\mathbf{q}''}[(d^T_{c,v})^\beta_{\mathbf{q}'',0}, D^\dagger_{\mathbf{q}'}]D_{\mathbf{q}'} \\
&\qquad + D^\dagger_{\mathbf{q}'}[(d^\dagger_{c,v})^\alpha_{\mathbf{q},\mathbf{q}''}, D_{\mathbf{q}'}](d^T_{c,v})^\beta_{\mathbf{q}'',0}\} \\
&= (\beta-\alpha)(\hbar\Omega)\Pi^{c,v}_{\alpha,\beta}(\mathbf{k},\mathbf{q}) \qquad (3.37)
\end{aligned}$$

where, for now, we have assumed the phonon dispersion to be flat; we will discuss how to generalize to non-flat bands later. The first term of the inter-polaron interaction becomes:

$$\tfrac{1}{2}\sum_{\lambda,\lambda'}\sum_{\mathbf{k}',\mathbf{k}''}\tilde{V}_0^{\lambda,\lambda'}[P^{c,v}_{\mathbf{k}-\mathbf{q},\mathbf{k}},P^{\lambda,\lambda}_{\mathbf{k}',\mathbf{k}'}]=\tfrac{1}{2}\sum_{\lambda,\mathbf{k}'}(\tilde{V}_0^{v,\lambda}-\tilde{V}_0^{c,\lambda})P^{c,v}_{\mathbf{k}-\mathbf{q},\mathbf{k}} \tag{3.38}$$

For the second term, we note:

$$\begin{aligned}[P^{c,v}_{\mathbf{k}-\mathbf{q},\mathbf{k}},P^{\lambda,\lambda'}_{\mathbf{k}',\mathbf{k}'+\mathbf{q}'}P^{\lambda',\lambda}_{\mathbf{k}'',\mathbf{k}'-\mathbf{q}'}]&=P^{\lambda,\lambda'}_{\mathbf{k}',\mathbf{k}''+\mathbf{q}'}[P^{c,v}_{\mathbf{k}-\mathbf{q},\mathbf{k}},P^{\lambda',\lambda}_{\mathbf{k}'',\mathbf{k}'-\mathbf{q}'}]+[P^{c,v}_{\mathbf{k}-\mathbf{q},\mathbf{k}},P^{\lambda,\lambda'}_{\mathbf{k}',\mathbf{k}''+\mathbf{q}'}]P^{\lambda',\lambda}_{\mathbf{k}'',\mathbf{k}'-\mathbf{q}'}\\&=P^{\lambda,\lambda'}_{\mathbf{k}',\mathbf{k}''+\mathbf{q}'}(\delta_{\lambda',v}\delta_{\mathbf{k}'',\mathbf{k}}P^{c,\lambda}_{\mathbf{k}-\mathbf{q},\mathbf{k}'-\mathbf{q}'}-\delta_{\lambda,c}\delta_{\mathbf{k}'-\mathbf{q}',\mathbf{k}-\mathbf{q}}P^{\lambda',v}_{\mathbf{k}'',\mathbf{k}})\\&+(\delta_{\lambda,v}\delta_{\mathbf{k}',\mathbf{k}}P^{c,\lambda'}_{\mathbf{k}-\mathbf{q},\mathbf{k}''+\mathbf{q}'}-\delta_{\lambda',c}\delta_{\mathbf{k}''+\mathbf{q}',\mathbf{k}-\mathbf{q}}P^{\lambda,v}_{\mathbf{k}',\mathbf{k}})P^{\lambda',\lambda}_{\mathbf{k}'',\mathbf{k}'-\mathbf{q}'}\end{aligned}$$

which reduces the second term to:

$$\sum_{\lambda}\sum_{\mathbf{k}',\mathbf{q}'}\left(\tilde{V}^{\lambda,v}_{\mathbf{q}'}\tfrac{1}{2}\{P^{\lambda,v}_{\mathbf{k}',\mathbf{k}+\mathbf{q}'},P^{c,\lambda}_{\mathbf{k}-\mathbf{q},\mathbf{k}'-\mathbf{q}'}\}-\tilde{V}^{c,\lambda}_{\mathbf{q}'}\tfrac{1}{2}\{P^{c,\lambda}_{\mathbf{k}-\mathbf{q}+\mathbf{q}',\mathbf{k}'+\mathbf{q}'},P^{\lambda,v}_{\mathbf{k}',\mathbf{k}}\}\right) \tag{3.39}$$

We replace the commutator and obtain:

$$\sum_{\lambda}\sum_{\mathbf{k}',\mathbf{q}'}\{\tilde{V}^{\lambda,v}_{\mathbf{q}'}P^{\lambda,v}_{\mathbf{k}',\mathbf{k}'+\mathbf{q}'}P^{c,\lambda}_{\mathbf{k}-\mathbf{q},\mathbf{k}'-\mathbf{q}'}-\tilde{V}^{c,\lambda}_{\mathbf{q}'}P^{c,\lambda}_{\mathbf{k}-\mathbf{q}+\mathbf{q}',\mathbf{k}'+\mathbf{q}'}P^{\lambda,v}_{\mathbf{k}',\mathbf{k}}\} \tag{3.40}$$

$$-\sum_{\lambda}\sum_{\mathbf{k}',\mathbf{q}'}\left(\tilde{V}^{\lambda,v}_{\mathbf{q}'}\tfrac{1}{2}[P^{\lambda,v}_{\mathbf{k}',\mathbf{k}+\mathbf{q}'},P^{c,\lambda}_{\mathbf{k}-\mathbf{q},\mathbf{k}'-\mathbf{q}'}]-\tilde{V}^{c,\lambda}_{\mathbf{q}'}\tfrac{1}{2}[P^{c,\lambda}_{\mathbf{k}-\mathbf{q}+\mathbf{q}',\mathbf{k}'+\mathbf{q}'},P^{\lambda,v}_{\mathbf{k}',\mathbf{k}}]\right) \tag{3.41}$$

The second term reduces to:

$$\sum_{\lambda}\sum_{\mathbf{k}',\mathbf{q}'}\left(\tilde{V}^{\lambda,v}_{\mathbf{q}'}\tfrac{1}{2}\{P^{\lambda,v}_{\mathbf{k}',\mathbf{k}+\mathbf{q}'},P^{c,\lambda}_{\mathbf{k}-\mathbf{q},\mathbf{k}'-\mathbf{q}'}\}-\tilde{V}^{c,\lambda}_{\mathbf{q}'}\tfrac{1}{2}\{P^{c,\lambda}_{\mathbf{k}-\mathbf{q}+\mathbf{q}',\mathbf{k}'+\mathbf{q}'},P^{\lambda,v}_{\mathbf{k}',\mathbf{k}}\}\right)$$

Which cancels with Eq.(3.38), leaving:

$$[\Pi^{c,v}_{\alpha,\beta}(\mathbf{k},\mathbf{q}),\bar{H}_{pol-pol}] = \sum_{\lambda}\sum_{\mathbf{k}',\mathbf{q}'} B([d^{\dagger}_{c,v}]^{\alpha}[d^{T}_{c,v}]^{\beta})_{\mathbf{q},0}\{\tilde{V}^{c,\lambda}_{\mathbf{q}'}P^{c,\lambda}_{\mathbf{k}-\mathbf{q}+\mathbf{q}',\mathbf{k}'+\mathbf{q}'}P^{\lambda,v}_{\mathbf{k}',\mathbf{k}} - \tilde{V}^{\lambda,v}_{\mathbf{q}'}P^{\lambda,v}_{\mathbf{k}',\mathbf{k}'+\mathbf{q}'}P^{c,\lambda}_{\mathbf{k}-\mathbf{q},\mathbf{k}'-\mathbf{q}'}\} \tag{3.42}$$

Finally, we evaluate the commutator with $\bar{H}_{pol-em}$:

$$\begin{aligned}[\Pi^{c,v}_{\alpha,\beta}(\mathbf{k},\mathbf{q}),\bar{H}_{pol-em}] &= -i\sum_{\lambda,\lambda'}\sum_{\mathbf{k}',\mathbf{q}'} F^{\lambda,\lambda'}[BP^{c,v}_{\mathbf{k}-\mathbf{q},\mathbf{k}}([d^{\dagger}_{c,v}]^{\alpha}[d^{T}_{c,v}]^{\beta})_{\mathbf{q},0}, B^{\lambda,\lambda'}P^{\lambda,\lambda'}_{\mathbf{k}'-\mathbf{q}',\mathbf{k}'}(e^{C_{\lambda}-C_{\lambda'}})_{\mathbf{q}',0}] \\ &= -i\sum_{\lambda,\lambda'}\sum_{\mathbf{k}',\mathbf{q}'} F^{\lambda,\lambda'}\Big\{BP^{c,v}_{\mathbf{k}-\mathbf{q},\mathbf{k}}B^{\lambda,\lambda'}P^{\lambda,\lambda'}_{\mathbf{k}'-\mathbf{q}',\mathbf{k}'}[([d^{\dagger}_{c,v}]^{\alpha}[d^{T}_{c,v}]^{\beta})_{\mathbf{q},0},(e^{C_{\lambda}-C_{\lambda'}})_{\mathbf{q}',0}] \\ &\quad + [BP^{c,v}_{\mathbf{k}-\mathbf{q},\mathbf{k}},B^{\lambda,\lambda'}P^{\lambda,\lambda'}_{\mathbf{k}'-\mathbf{q}',\mathbf{k}'}](e^{C_{\lambda}-C_{\lambda'}})_{\mathbf{q}',0}([d^{\dagger}_{c,v}]^{\alpha}[d^{T}_{c,v}]^{\beta})_{\mathbf{q},0}\Big\}\end{aligned}$$

The absorption spectrum is found from the thermal average $\bar{\Pi}^{c,v}_{\alpha,\beta}(\mathbf{k},\mathbf{q}) = \langle\Pi\rangle^{c,v}_{\alpha,\beta}(\mathbf{k},\mathbf{q})$. We can reduce Eq.(3.42) into two terms:

$$(1)\sum_{\lambda}\sum_{\mathbf{k}',\mathbf{q}'}\Big\{\tilde{V}^{c,\lambda}_{\mathbf{q}'}\Big\langle P^{c,\lambda}_{\mathbf{k}-\mathbf{q}+\mathbf{q}',\mathbf{k}'+\mathbf{q}'}\Big\rangle\Big\langle P^{\lambda,v}_{\mathbf{k}',\mathbf{k}}B([d^{\dagger}_{c,v}]^{\alpha}[d^{T}_{c,v}]^{\beta})_{\mathbf{q},0}\Big\rangle - \tilde{V}^{\lambda,v}_{\mathbf{q}'}\Big\langle P^{\lambda,v}_{\mathbf{k}',\mathbf{k}+\mathbf{q}'}\Big\rangle\Big\langle P^{c,\lambda}_{\mathbf{k}-\mathbf{q},\mathbf{k}'-\mathbf{q}'}B([d^{\dagger}_{c,v}]^{\alpha}[d^{T}_{c,v}]^{\beta})_{\mathbf{q},0}\Big\rangle\Big\} \tag{3.43}$$

$$(2)\sum_{\lambda}\sum_{\mathbf{k}',\mathbf{q}'}\Big\{\tilde{V}^{c,\lambda}_{\mathbf{q}'}\Big\langle P^{c,\lambda}_{\mathbf{k}-\mathbf{q}+\mathbf{q}',\mathbf{k}'+\mathbf{q}'}B([d^{\dagger}_{c,v}]^{\alpha}[d^{T}_{c,v}]^{\beta})_{\mathbf{q},0}\Big\rangle\Big\langle P^{\lambda,v}_{\mathbf{k}',\mathbf{k}}\Big\rangle - \tilde{V}^{\lambda,v}_{\mathbf{q}'}\Big\langle P^{\lambda,v}_{\mathbf{k}',\mathbf{k}+\mathbf{q}'}B([d^{\dagger}_{c,v}]^{\alpha}[d^{T}_{c,v}]^{\beta})_{\mathbf{q},0}\Big\rangle\Big\langle P^{c,\lambda}_{\mathbf{k}-\mathbf{q},\mathbf{k}'-\mathbf{q}'}\Big\rangle\Big\} \tag{3.44}$$

The first term reduces to:

$$\sum_{\mathbf{q}'} \left\{ \tilde{V}^{c,c}_{\mathbf{k}-\mathbf{q}-\mathbf{q}'} f^{c}_{\mathbf{q}'} - \tilde{V}^{v,v}_{\mathbf{k}-\mathbf{q}'} f^{\nu}_{\mathbf{q}'} \right\} \bar{\Pi}^{c,v}_{\alpha,\beta}(\mathbf{k},\mathbf{q}) \tag{3.45}$$

whereas the second term reduces to:

$$\sum_{\mathbf{q}'} \tilde{V}^{v,c}_{\mathbf{k}-\mathbf{q}'} \{ f^{v}_{\mathbf{k}} - f^{c}_{\mathbf{k}-\mathbf{q}} \} \bar{\Pi}^{c,v}_{\alpha,\beta}(\mathbf{q}',\mathbf{q}) \tag{3.46}$$

where $f^{\lambda}_{\mathbf{k}}$ is the Fermi-distribution. The first term consists of contributions from the Polaron self energy, thus we define:

$$\tilde{e}_{\lambda,\mathbf{k}} = e_{\lambda,\mathbf{k}} - \sum_{\mathbf{k}'} \tilde{V}^{\lambda,\lambda}_{\mathbf{k}-\mathbf{k}'} f^{\lambda}_{\mathbf{k}'}$$

The equation of motion for the polaron correlation function becomes:

$$\begin{aligned}
&\{ i\hbar \tfrac{d}{dt} + (\tilde{e}_{c,\mathbf{k}-\mathbf{q}} - \tilde{e}_{v,\mathbf{k}}) + (\alpha-\beta)\hbar\omega_{\mathbf{q}} - \hbar\omega \} \bar{\Pi}^{c,v}_{\alpha,\beta}(\mathbf{k},\mathbf{q}) \\
&= \{ f^{v}_{\mathbf{k}} - f^{c}_{\mathbf{k}-\mathbf{q}} \} \sum_{\mathbf{k}'} \tilde{V}^{v,c}_{\mathbf{k}-\mathbf{k}'} \bar{\Pi}^{c,v}_{\alpha,\beta}(\mathbf{k}',\mathbf{q}) \\
&= -i \sum_{\lambda,\lambda'} \sum_{\mathbf{k}',\mathbf{q}'} F^{\lambda,\lambda'} \Big\{ BP^{c,v}_{\mathbf{k}-\mathbf{q},\mathbf{k}} B^{\lambda,\lambda'} P^{\lambda,\lambda'}_{\mathbf{k}'-\mathbf{q}',\mathbf{k}'} [([d^{\dagger}_{c,v}]^{\alpha}[d^{T}_{c,v}]^{\beta})_{\mathbf{q},0}, (e^{C_\lambda - C_{\lambda'}})_{\mathbf{q}',0}] \\
&\qquad\qquad + [BP^{c,v}_{\mathbf{k}-\mathbf{q},\mathbf{k}}, B^{\lambda,\lambda'} P^{\lambda,\lambda'}_{\mathbf{k}'-\mathbf{q}',\mathbf{k}'}] (e^{C_\lambda - C_{\lambda'}})_{\mathbf{q}',0} ([d^{\dagger}_{c,v}]^{\alpha}[d^{T}_{c,v}]^{\beta})_{\mathbf{q},0} \Big\}
\end{aligned} \tag{3.47}$$

We now begin reducing the remaining expectation values in Eq.(3.47). Denoting the phonon operator combination as $D^{\lambda,\lambda'}_{\alpha,\beta}(\mathbf{q}')$, we have:

$$
\begin{aligned}
&-i\sum_{\lambda,\lambda'}\sum_{\mathbf{k}',\mathbf{q}'} F^{\lambda,\lambda'}[BP^{c,v}_{\mathbf{k}-\mathbf{q},\mathbf{k}}, B^{\lambda,\lambda'}P^{\lambda,\lambda'}_{\mathbf{k}'-\mathbf{q}',\mathbf{k}'}]D^{\lambda,\lambda'}_{\alpha,\beta}(\mathbf{q}') \\
&= -i\sum_{\lambda,\lambda'}\sum_{\mathbf{k}',\mathbf{q}'} F^{\lambda,\lambda'}\Big\{B^{\lambda,\lambda'}B[P^{c,v}_{\mathbf{k}-\mathbf{q},\mathbf{k}}, P^{\lambda,\lambda'}_{\mathbf{k}'-\mathbf{q}',\mathbf{k}'}] + [B, B^{\lambda,\lambda'}]P^{c,v}_{\mathbf{k}-\mathbf{q},\mathbf{k}}P^{\lambda,\lambda'}_{\mathbf{k}'-\mathbf{q}',\mathbf{k}'}\Big\}D^{\lambda,\lambda'}_{\alpha,\beta}(\mathbf{q}')
\end{aligned}
$$

which splits into:

$$
\begin{aligned}
-i\sum_{\varepsilon_\lambda<\varepsilon_{\lambda'}}\sum_{\mathbf{k}',\mathbf{q}'} F^{\lambda,\lambda'}\Big\{&B^\dagger B(\delta_{\mathbf{k}'-\mathbf{q}',\mathbf{k}}\delta_{\lambda,v}P^{c,\lambda'}_{\mathbf{k}-\mathbf{q},\mathbf{k}'} - \delta_{\mathbf{k}',\mathbf{k}-\mathbf{q}}\delta_{\lambda',c}P^{\lambda,v}_{\mathbf{k}'-\mathbf{q}',\mathbf{k}}) \\
&- [B, B^\dagger]P^{c,v}_{\mathbf{k}-\mathbf{q},\mathbf{k}}P^{\lambda,\lambda'}_{\mathbf{k}'-\mathbf{q}',\mathbf{k}'}\Big\}D^{\lambda,\lambda'}_{\alpha,\beta}(\mathbf{q}')
\end{aligned} \tag{3.48}
$$

and:

$$
-i\sum_{\varepsilon_\lambda>\varepsilon_{\lambda'}}\sum_{\mathbf{k}',\mathbf{q}'} F^{\lambda,\lambda'}B^2(\delta_{\mathbf{k}'-\mathbf{q}',\mathbf{k}}\delta_{\lambda,v}P^{c,\lambda'}_{\mathbf{k}-\mathbf{q},\mathbf{k}'} - \delta_{\mathbf{k}',\mathbf{k}-\mathbf{q}}\delta_{\lambda',c}P^{\lambda,v}_{\mathbf{k}'-\mathbf{q}',\mathbf{k}})D^{\lambda,\lambda'}_{\alpha,\beta}(\mathbf{q}') \tag{3.49}
$$

Taking an expectation value, Eq.(3.48) takes the form:

$$
\begin{aligned}
&-i\left\langle B^\dagger B\right\rangle\sum_{\mathbf{q}'}\left\{\sum_{\varepsilon_\lambda>\varepsilon_v} F^{\nu,\lambda}\left\langle P^{c,\lambda}_{\mathbf{k}-\mathbf{q},\mathbf{k}+\mathbf{q}'}\right\rangle\left\langle D^{v,\lambda}_{\alpha,\beta}(\mathbf{q}')\right\rangle - \sum_{\varepsilon_\lambda<\varepsilon_c} F^{\lambda,c}\left\langle P^{\lambda,v}_{\mathbf{k}-\mathbf{q}-\mathbf{q}',\mathbf{k}}\right\rangle\left\langle D^{\lambda,c}_{\alpha,\beta}(\mathbf{q}')\right\rangle\right\} \\
&-i\sum_{\varepsilon_\lambda<\varepsilon_{\lambda'}}\sum_{\mathbf{k}',\mathbf{q}'} F^{\lambda,\lambda'}\left\langle P^{c,v}_{\mathbf{k}-\mathbf{q},\mathbf{k}}P^{\lambda,\lambda'}_{\mathbf{k}'-\mathbf{q}',\mathbf{k}'}\right\rangle\left\langle D^{v,\lambda}_{\alpha,\beta}(\mathbf{q}')\right\rangle
\end{aligned}
$$

Noting:

$$\left\langle P^{c,v}_{\mathbf{k-q},\mathbf{k}} P^{\lambda,\lambda'}_{\mathbf{k'-q'},\mathbf{k'}} \right\rangle = \left\langle \Psi^{\dagger}_{c,\mathbf{k-q}} (\delta_{\lambda,v}\delta_{\mathbf{k'-q'},\mathbf{k}} - \Psi^{\dagger}_{\lambda,\mathbf{k'-q'}} \Psi_{v,\mathbf{k}}) \Psi_{\lambda',\mathbf{k'}} \right\rangle$$
$$= \delta_{\lambda,v}\delta_{\lambda',c}\delta_{\mathbf{k'},\mathbf{k-q}}\delta_{\mathbf{k'},\mathbf{k+q'}} f^{c}_{\mathbf{k-q}}(1 - f^{v}_{\mathbf{k}}) \tag{3.50}$$

where we have ignored the term proportional to $\delta_{c,v}$ since we only consider absorption events for $\varepsilon_c > \varepsilon_v$. Thus, Eq.(3.48) reduces to:

$$-iF^{v,c}\Big\{ f^{c}_{\mathbf{k-q}}(1 - f^{v}_{\mathbf{k}}) + \left\langle B^{\dagger}B \right\rangle (f^{c}_{\mathbf{k-q}} - f^{v}_{\mathbf{k}}) \Big\} \left\langle (e^{C_v - C_c})_{\mathbf{q'},0} ([d^{\dagger}_{c,v}]^{\alpha} [d^{T}_{c,v}]^{\beta})_{\mathbf{q},0} \right\rangle \tag{3.51}$$

Eq.(3.49) reduces to:

$$-i \left\langle B^2 \right\rangle \sum_{\mathbf{q'}} \left\{ \sum_{\varepsilon_\lambda < \varepsilon_v} F^{\nu,\lambda} \left\langle P^{c,\lambda}_{\mathbf{k-q},\mathbf{k+q'}} \right\rangle \left\langle D^{v,\lambda}_{\alpha,\beta}(\mathbf{q'}) \right\rangle - \sum_{\varepsilon_\lambda > \varepsilon_c} F^{\lambda,c} \left\langle P^{\lambda,v}_{\mathbf{k-q-q'},\mathbf{k}} \right\rangle \left\langle D^{\lambda,c}_{\alpha,\beta}(\mathbf{q'}) \right\rangle \right\}$$

which vanishes for the ground state. The first commutator of Eq.(3.47) has the general form:

$$-i \sum_{\lambda,\lambda'} \sum_{\mathbf{k'},\mathbf{q'}} F^{\lambda,\lambda'} B P^{c,v}_{\mathbf{k-q},\mathbf{k}} B^{\lambda,\lambda'} P^{\lambda,\lambda'}_{\mathbf{k'-q'},\mathbf{k'}} \sum_{n,m} C^{\lambda,\lambda'}_{nm} [([d^{\dagger}_{c,v}]^{\alpha} [d^{T}_{c,v}]^{\beta})_{\mathbf{q},0}, ([d^{\dagger}_{\lambda,\lambda'}]^{n} [d^{T}_{\lambda,\lambda'}]^{m})_{\mathbf{q'},0}] \tag{3.52}$$

We split this expressions' contributions to the EOM into two pieces: 1) a product of correlations with particle order less than the polarization function, and 2) a product of two correlations with particle order equal to the polarization function. Due to the form of Eq.(3.52), terms of the first form must be proportional to $F^{\lambda,\lambda'}\delta_{\lambda,\lambda'} = 0$. For terms of the

second form, Eq.(3.52) becomes:

$$
\begin{aligned}
&- i \sum_{\lambda,\lambda'} \sum_{\mathbf{k}',\mathbf{q}'} \sum_{n,m} F^{\lambda,\lambda'} C^{\lambda,\lambda'}_{n,m} \left\langle B P^{c,v}_{\mathbf{k}-\mathbf{q},\mathbf{k}} D^{c,v}_{\alpha,\beta}(\mathbf{q}) B^{\lambda,\lambda'} P^{\lambda,\lambda'}_{\mathbf{k}'-\mathbf{q}',\mathbf{k}'} D^{\lambda,\lambda'}_{n,m}(\mathbf{q}') \right\rangle \\
&+ i \sum_{\lambda,\lambda'} \sum_{\mathbf{k}',\mathbf{q}'} \sum_{n,m} F^{\lambda,\lambda'} C^{\lambda,\lambda'}_{n,m} \left\langle B P^{c,v}_{\mathbf{k}-\mathbf{q},\mathbf{k}} D^{\lambda,\lambda'}_{n,m}(\mathbf{q}') B^{\lambda,\lambda'} P^{\lambda,\lambda'}_{\mathbf{k}'-\mathbf{q}',\mathbf{k}'} D^{c,v}_{\alpha,\beta}(\mathbf{q}) \right\rangle
\end{aligned}
\tag{3.53}
$$

The polaron polarization function must be band consistent since our Fröhlich matrix elements only scatter electrons within one band, and the displacement momentum of the exciton must match that of the phonons. Thus, Eq.(3.53) can only be nonzero when $\{\lambda, \lambda'\} = \{c, v\}$ and $\mathbf{q}' = \mathbf{q}$, yielding:

$$
i \sum_{\mathbf{k}'} \sum_{n,m} F^{c,v} C^{c,v}_{n,m} \left(\bar{\Pi}^{c,v}_{n,m}(\mathbf{k}, \mathbf{q}) \bar{\Pi}^{c,v}_{\alpha,\beta}(\mathbf{k}', \mathbf{q}) - \bar{\Pi}^{c,v}_{\alpha,\beta}(\mathbf{k}, \mathbf{q}) \bar{\Pi}^{c,v}_{n,m}(\mathbf{k}', \mathbf{q}) \right) \tag{3.54}
$$

which is only nonzero for $\{n, m\} \neq \{\alpha, \beta\}$ and $\mathbf{k}' \neq \mathbf{k}$. In general, the first term is a correction to the Coulomb piece in Eq.(3.46), and the second term contributes to the absorption spectrum's broadening. However, their contributions to the full absorption spectrum are of the form:

$$
i \sum_{\mathbf{k}'} F^{c,v} \sum_{\alpha,\beta} \sum_{n,m} C^{c,v}_{\alpha,\beta} C^{c,v}_{n,m} \left(\bar{\Pi}^{c,v}_{n,m}(\mathbf{k}, \mathbf{q}) \bar{\Pi}^{c,v}_{\alpha,\beta}(\mathbf{k}', \mathbf{q}) - \bar{\Pi}^{c,v}_{\alpha,\beta}(\mathbf{k}, \mathbf{q}) \bar{\Pi}^{c,v}_{n,m}(\mathbf{k}', \mathbf{q}) \right) \tag{3.55}
$$

Which vanishes.

In the quasi-static limit, we set $(d/dt)\bar{\Pi}^{c,v}_{\alpha,\beta}(\mathbf{k},\mathbf{q}) = 0$ and obtain:

$$\begin{aligned}&\{(\tilde{e}_{c,\mathbf{k}-\mathbf{q}} - \tilde{e}_{v,\mathbf{k}}) + (\alpha-\beta)\hbar\Omega - \hbar\omega\}\bar{\Pi}^{c,v}_{\alpha,\beta}(\mathbf{k},\mathbf{q},t)\\ &= \{f^v_{\mathbf{k}} - f^c_{\mathbf{k}-\mathbf{q}}\}\sum_{\mathbf{k}'}\tilde{V}^{v,c}_{\mathbf{k}-\mathbf{k}'}\bar{\Pi}^{c,v}_{\alpha,\beta}(\mathbf{k}',\mathbf{q}) - iS(\mathbf{k},\mathbf{q},t)\end{aligned} \tag{3.56}$$

where the source term is given by:

$$S(\mathbf{k};\mathbf{q},t) = F^{v,c}\Big\{f^c_{\mathbf{k}-\mathbf{q}}(1-f^v_{\mathbf{k}}) + \Big\langle B^\dagger B\Big\rangle (f^c_{\mathbf{k}-\mathbf{q}} - f^v_{\mathbf{k}})\Big\}\Big\langle (e^{C_v - C_c})_{-\mathbf{q},0}([d^\dagger_{c,v}]^\alpha [d^T_{c,v}]^\beta)_{\mathbf{q},0}\Big\rangle \tag{3.57}$$

The solutions to Eq.(3.56) gives a set of zero width Lorentzian distributions; however, in practice, these peaks have a finite width owing to the exciton lifetime. Thus, a better approximation for the time derivative is given by:

$$\frac{d}{dt}\bar{\Pi}^{c,v}_{\alpha,\beta}(\mathbf{k},\mathbf{q}) = -\Gamma_{\alpha,\beta}\bar{\Pi}^{c,v}_{\alpha,\beta}(\mathbf{k},\mathbf{q})$$

which yields:

$$\begin{aligned}&\{-i\hbar\Gamma_{\alpha,\beta} + (\tilde{e}_{c,\mathbf{k}-\mathbf{q}} - \tilde{e}_{v,\mathbf{k}}) + (\alpha-\beta)\hbar\omega_{\mathbf{q}} - \hbar\omega\}\bar{\Pi}^{c,v}_{\alpha,\beta}(\mathbf{k},\mathbf{q},t)\\ &= \{f^v_{\mathbf{k}} - f^c_{\mathbf{k}-\mathbf{q}}\}\sum_{\mathbf{k}'}\tilde{V}^{v,c}_{\mathbf{k}-\mathbf{k}'}\bar{\Pi}^{c,v}_{\alpha,\beta}(\mathbf{k}',\mathbf{q}) - iS(\mathbf{k},\mathbf{q},t)\end{aligned} \tag{3.58}$$

and the excited polaron decay rate $\Gamma_{\alpha,\beta}$ is given by the inverse of the average life time $\tau_{\alpha,\beta}$:

$$\Gamma_{\alpha,\beta} = (\tau_{\alpha,\beta})^{-1} = \Big|\frac{2}{\hbar}Im(\Sigma_{\alpha,\beta})\Big|$$

where $\Sigma_{\alpha,\beta}$ is the self energy of an electron, which has emitted (absorbed) α (β) phonons, absorbing and re-emitting a photon. For now, we will focus on solving the quasi-static solutions to Eq.(3.56), and we will treat the broadening as a fitting parameter.

3.4.2 Wannier Equation

Derivation in 2-D

We focus our attention on the quasi-static EOM, noting that the Lorentzian broadening can always be added later. The inhomogeneous Eq.(3.56) can be solved by expanding in the basis of its homogeneous equivalent. To do so, we must make some approximations. We write the polaron dispersion as:

$$\begin{aligned}\tilde{e}_{\lambda,\mathbf{k}} &= e_{\lambda,\mathbf{k}} - \Sigma_{\lambda} \\ &\equiv \tilde{m}_{\lambda} k^2 + \tilde{E}_{\lambda}\end{aligned}$$

where $\tilde{m}_{\lambda}$ and $\tilde{E}_{\lambda}$ are modifications to the original electron effective mass and band shift caused by the Fröhlich interaction and Coulomb self energy. The main assumption here is that the Coulomb self energy and Fröhlich interaction do not change the quadratic dispersion of the original band structure. We now define the inverse transform of the multi-particle

correlation function:

$$\bar{\Pi}^{c,v}_{\alpha,\beta}(\mathbf{k};\mathbf{q}) = \frac{1}{V_d}\int d^d\mathbf{r} e^{i\mathbf{k}\cdot\mathbf{r}}\bar{\Pi}^{c,v}_{\alpha,\beta}(\mathbf{r},\mathbf{q})$$

$$\bar{\Pi}^{c,v}_{\alpha,\beta}(\mathbf{r},\mathbf{q}) = \frac{V_d}{(2\pi)^d}\int d^d\mathbf{k} e^{-i\mathbf{k}\cdot\mathbf{r}}\bar{\Pi}^{c,v}_{\alpha,\beta}(\mathbf{k},\mathbf{q})$$

Thus, inverse transforming Eq.(3.56), we obtain:

$$\Big\{\tilde{m}_c(-i\nabla-\mathbf{q})^2 + \tilde{m}_v\nabla^2 - \tilde{V}^{v,c}(\mathbf{r})\Big\}\bar{\Pi}^{c,v}_{\alpha,\beta}(\mathbf{r},\mathbf{q}) = E^{c,v}_{\alpha,\beta}\bar{\Pi}^{c,v}_{\alpha,\beta}(\mathbf{r},\mathbf{q}) - iS(\mathbf{q},t)V_d\delta^d(\mathbf{r}) \quad (3.59)$$

Where $E^{c,v}_{\alpha,\beta} = (\tilde{E}_c - \tilde{E}_v + (\alpha-\beta)\hbar\omega_{\mathbf{q}} - \hbar(\omega + i\Gamma_{\alpha,\beta}))$. To reduce clutter, we temporarily drop the unnecessary subscripts and define:

$$\Pi(\mathbf{r}) = f(\mathbf{r})\Psi(\mathbf{r})$$

We first solve the homogeneous equation with $S(\mathbf{q}) = 0$. Our goal is to eliminate the first order gradient operators in Eq.(3.59). We expand the differential terms as:

$$\tilde{m}_c(-i\nabla-\mathbf{q})^2\Pi = \tilde{m}_c\{[-f\nabla^2\Psi - 2(\boldsymbol{\nabla}f)\cdot(\boldsymbol{\nabla}\Psi) - \Psi\nabla^2 f + 2i\mathbf{q}\cdot[f\boldsymbol{\nabla}\Psi + \Psi\boldsymbol{\nabla}f] + q^2 f\Psi\}$$

$$\tilde{m}_v\nabla^2\Pi = \tilde{m}_v\{f\nabla^2\Psi + 2(\boldsymbol{\nabla}f)\cdot(\boldsymbol{\nabla}\Psi) + \Psi\nabla^2 f\}$$

We seek to eliminate the linear order $\boldsymbol{\nabla}\Gamma$ terms. Thus:

$$\tilde{m}_c\{-2(\boldsymbol{\nabla}f)\cdot(\boldsymbol{\nabla}\Psi)+2i\mathbf{q}\cdot f\boldsymbol{\nabla}\Psi\}+\tilde{m}_v\{2(\boldsymbol{\nabla}f)\cdot(\boldsymbol{\nabla}\Psi)\}=0$$

$$\implies(\tilde{m}_c-\tilde{m}_v)(\boldsymbol{\nabla}f)=i\tilde{m}_c\mathbf{q}f$$

yielding:

$$f=e^{i\eta_{c,v}\mathbf{q}\cdot\mathbf{r}},\ \eta_{c,v}=\frac{\tilde{m}_c}{\tilde{m}_c-\tilde{m}_v}$$

Eq.(3.59) is now reduced to:

$$\Big\{\tilde{m}_c\Big[-\nabla^2\Psi+\Psi(\eta_{c,v}^2q^2)+\Psi q^2-\Psi(2\eta_{c,v}\mathbf{q}^2)\Big]+\tilde{m}_v\Big[\nabla^2\Psi-\Psi\eta_{c,v}^2q^2\Big]-\tilde{V}^{v,c}(\mathbf{r})\Big\}\Psi=E_{\alpha,\beta}^{c,v}\Psi$$

Combining the first and second terms yields:

$$\Big\{-\tilde{M}_{c,v}\nabla^2-\tilde{V}^{v,c}(\mathbf{r})\Big\}\Gamma=\Big(E_{\alpha,\beta}^{c,v}-\tilde{m}_c(1-\eta_{c,v})\mathbf{q}^2\Big)\Psi$$

where $\tilde{M}_{c,v}\equiv\tilde{m}_c-\tilde{m}_v$. We can absorb the extra energy term into the definition of $E_{\alpha,\beta}^{c,v}$ and re-introduce our band and phonon number subscripts to obtain the general solution:

$$\bar{\Pi}_{\alpha,\beta}^{c,v}(\mathbf{r},\mathbf{q})=\Big(e^{i\eta_{c,v}\mathbf{q}\cdot\mathbf{r}}\Big)\Psi_{\alpha,\beta}^{c,v}(\mathbf{r}),\ \eta_{c,v}=\tilde{m}_c/\tilde{M}_{c,v}$$

Where:

$$\Big\{ -\tilde{M}_{c,v}\nabla^2 - V^{v,c}(r) - 2\hbar\Omega g_v^* g_c \frac{V_d \delta^d(\mathbf{r})}{(2\pi)^d} \Big\} \Psi^{c,v}_{\alpha,\beta}(\mathbf{r}) = E\Psi^{c,v}_{\alpha,\beta}(\mathbf{r}) \tag{3.60}$$

and E is the Wannier energy. The solutions for Γ are those of the d-dimensional Wannier wave functions with a Darwin perturbation arising from the Fröhlich interaction.

Absorption Spectrum from Wannier Series Expansion

There is a resonance whenever the photon energy allows $E^{c,v}_{\alpha,\beta}$ to equal the Wannier Energy E_n. Following the work of Haug and Koch [46], we write the correlation function as a linear combination of the solutions to the homogeneous Wannier Equation $\Psi^{c,v}_n(\mathbf{r})$[46]:

$$\Psi^{c,v}(\mathbf{r}) = \sum_n b^{c,v}_n \Psi^{c,v}_n(\mathbf{r})$$

Inserting this into Eq.(3.59), multiplying by $[\Gamma^{c,v}_m(\mathbf{r})]^*$, and integrating over real space, we obtain:

$$\sum_n b^{c,v}_n [E_n - E^{c,v}_{\alpha,\beta}] \int d^d\mathbf{r} [\Psi^{c,v}_m(\mathbf{r})]^* \Psi^{c,v}_n(\mathbf{r}) = -iS(\mathbf{q},t) V_d [\Psi^{c,v}_m(0)]^*$$

Thus:

$$b^{c,v}_n = \frac{S(\mathbf{q},t) V_d [\Psi^{c,v}_n(0)]^*}{E^{c,v}_{\alpha,\beta} - E_n} \tag{3.61}$$

which gives the momentum space correlation function:

$$\bar{\Pi}^{c,v}_{\alpha,\beta}(\mathbf{k};\mathbf{q}) = \sum_n \frac{iS(\mathbf{q},t)[\Psi^{c,v}_n(0)]^*}{E^{c,v}_{\alpha,\beta} - E_n} \int d^d\mathbf{r}\Psi^{c,v}_n(\mathbf{r})e^{-i(\mathbf{k}-\eta_{c,v}\mathbf{q})\cdot\mathbf{r}}$$

Recalling that the raw absorption spectrum is given by:

$$A(\omega) = \sum_{\varepsilon_c>\varepsilon_v}\sum_{\alpha,\beta}\sum_{\mathbf{q}} C^{\alpha,\beta}_{c,v}F^{c,v}\sum_{\mathbf{k}}\Pi^{c,v}_{\alpha,\beta}(\mathbf{k};\mathbf{q})$$

and noting:

$$\sum_{\mathbf{k}}\int d^d\mathbf{r}F(\mathbf{r})e^{-i\mathbf{k}\cdot\mathbf{r}} = F(\mathbf{r}=0)$$

we obtain:

$$A(\omega) = \sum_{\varepsilon_c>\varepsilon_v}\sum_{\alpha,\beta}\sum_{\mathbf{q}} C^{\alpha,\beta}_{c,v}F^{c,v}\sum_n \frac{iS(\mathbf{q},t)|\Psi^{c,v}_n(0)|^2}{E^{c,v}_{\alpha,\beta} - E_n} \tag{3.62}$$

The photon occupation number cane be recast as $\partial_t\left\langle B^\dagger B\right\rangle = -(\alpha(\omega) - e(\omega))\left\langle B^\dagger B\right\rangle$, such that the absorption coefficient $\alpha(\omega)$ can be defined in terms of the absorption spectrum as $\alpha(\omega) \equiv -\operatorname{Re}\{A(\omega,t)/\left\langle B^\dagger B\right\rangle\}$. Since $S(\mathbf{q},t) \propto (F^{c,v})^*\left\langle B^\dagger B\right\rangle$, the absorption coefficient is given by:

$$\alpha(\omega) = \sum_{\varepsilon_c>\varepsilon_v}\sum_{\alpha,\beta}\sum_{\mathbf{q}} C^{\alpha,\beta}_{c,v}|F^{c,v}|^2\sum_n \frac{D^{c,v}_{\alpha,\beta}(\mathbf{q},T)|\Psi^{c,v}_n(0)|^2\Gamma^{c,v}_{\alpha,\beta}}{(\tilde{E}^g_{\mathbf{q}} + (\alpha-\beta)\hbar\omega_{\mathbf{q}} - \hbar\omega - E_n)^2 + (\Gamma^{c,v}_{\alpha,\beta})^2} \tag{3.63}$$

Where $\tilde{E}^g_{\mathbf{q}} = \tilde{E}_c - \tilde{E}_v + \tilde{m}_c\tilde{m}_v\mathbf{q}^2/\tilde{M}_{c,v}$, $\Gamma_{\alpha,\beta}$ and the phonon contribution to the absorption amplitude is given by the thermal average $D^{c,v}_{\alpha,\beta}(\mathbf{q},T) = \left\langle (e^{C_v - C_c})_{-\mathbf{q},0}([d^\dagger_{c,v}]^\alpha [d^T_{c,v}]^\beta)_{\mathbf{q},0} \right\rangle$.

3.5 Generalized Interacting Polaron Model

We now consider a more realistic material, one which contains multiple phonon branches. Furthermore, we will relax the constraint that the Phonon dispersion is constant. Our new lattice and Frölich Hamiltonians are:

$$H_{latt} = \sum_{\nu,\mathbf{q}} (\hbar\Omega^\nu_{\mathbf{q}})(D^\dagger_{\nu,\mathbf{q}} D_{\nu,\mathbf{q}} + \tfrac{1}{2}) \tag{3.64}$$

$$H_{el-ph} = \sum_{\nu,\lambda} \sum_{\mathbf{k},\mathbf{q}} (\hbar\omega_{\nu,\mathbf{q}}) g^\lambda_{\nu,\mathbf{q}} P^{\lambda,\lambda}_{\mathbf{k}-\mathbf{q},\mathbf{k}} (D_{\nu,-\mathbf{q}} + D^\dagger_{\nu,\mathbf{q}}) \tag{3.65}$$

With ν the phonon branch. We adjust our unitary transformation to account for the new quantum number:

$$T \equiv \exp\left[\sum_{\lambda,\nu} \sum_{\mathbf{k},\mathbf{q}} g^\lambda_{\nu,\mathbf{q}} P^{\lambda,\lambda}_{\mathbf{k}-\mathbf{q},\mathbf{k}} Q^\nu_{\mathbf{q}} \right] \equiv exp\left[\sum_{\lambda,\nu} \sum_{\mathbf{k},\mathbf{q}} U^{\lambda,\nu}_{\mathbf{k},\mathbf{q}} \right] \equiv e^U$$

We note the obvious relation between our previous transformation and our current one: $U^\lambda_{\mathbf{k},\mathbf{q}} = \sum_\nu U^{\lambda,\nu}_{\mathbf{k},\mathbf{q}}$. We'll find this to be a common theme when applying this new transfor-

mation. For the transformation of H_{latt}, we find:

$$\begin{aligned}
[U, H_{latt}] &= \sum_{\nu',\mathbf{q}'} \sum_{\nu,\lambda} \sum_{\mathbf{k},\mathbf{q}} (\hbar\Omega^{\nu'}_{\mathbf{q}'}) g^{\lambda}_{\nu,\mathbf{q}} P^{\lambda,\lambda}_{\mathbf{k}-\mathbf{q},\mathbf{k}} [Q^{\nu}_{\mathbf{q}}, D^{\dagger}_{\nu',\mathbf{q}'} D_{\nu',\mathbf{q}'}] \\
&= \sum_{\nu',\mathbf{q}'} \sum_{\nu,\lambda} \sum_{\mathbf{k},\mathbf{q}} (\hbar\Omega^{\nu'}_{\mathbf{q}'}) g^{\lambda}_{\nu,\mathbf{q}} P^{\lambda,\lambda}_{\mathbf{k}-\mathbf{q},\mathbf{k}} (-\delta_{\nu,\nu'}) (D_{\nu',\mathbf{q}'} \delta_{\mathbf{q}',-\mathbf{q}} + D^{\dagger}_{\nu',\mathbf{q}'} \delta_{\mathbf{q}',\mathbf{q}}) \\
&= -\sum_{\nu,\lambda} \sum_{\mathbf{k},\mathbf{q}} (\hbar\omega_{\nu,\mathbf{q}}) g^{\lambda}_{\nu,\mathbf{q}} P^{\lambda,\lambda}_{\mathbf{k}-\mathbf{q},\mathbf{k}} (D_{\nu,-\mathbf{q}} + D^{\dagger}_{\nu,\mathbf{q}}) \\
&= -H_{el-ph}
\end{aligned}$$

We also have:

$$\begin{aligned}
[U, H_{el-ph}] &= \sum_{\lambda,\lambda'} \sum_{\mathbf{k},\mathbf{k}'} \sum_{\mathbf{q},\mathbf{q}'} \sum_{\nu,\nu'} (\hbar\Omega^{\nu'}_{\mathbf{q}'}) [U^{\lambda,\nu}_{\mathbf{k},\mathbf{q}}, U^{\lambda',\nu'}_{\mathbf{k}',\mathbf{q}'} + 2 g^{\lambda'}_{\nu',\mathbf{q}'} P^{\lambda',\lambda'}_{\mathbf{k}'-\mathbf{q}',\mathbf{k}'} D_{\nu',-\mathbf{q}'}] \\
&= \sum_{\lambda,\mathbf{k}} \sum_{\mathbf{q},\mathbf{q}'} \sum_{\nu,\nu'} (\hbar\Omega^{\nu'}_{\mathbf{q}'}) (g^{\lambda}_{\nu,\mathbf{q}} - g^{\lambda'}_{\nu',\mathbf{q}'}) (P^{\lambda,\lambda}_{\mathbf{k}-\mathbf{q},\mathbf{k}+\mathbf{q}'} - P^{\lambda,\lambda}_{\mathbf{k}-\mathbf{q}-\mathbf{q}',\mathbf{k}}) Q^{\nu}_{\mathbf{q}} Q^{\nu'}_{\mathbf{q}'} \\
&+ \sum_{\lambda,\lambda'} \sum_{\mathbf{k},\mathbf{k}'} \sum_{\mathbf{q},\mathbf{q}'} \sum_{\nu,\nu'} (\hbar\Omega^{\nu'}_{\mathbf{q}'}) (g^{\lambda}_{\nu,\mathbf{q}} g^{\lambda'}_{\nu',\mathbf{q}'}) [P^{\lambda,\lambda}_{\mathbf{k}-\mathbf{q},\mathbf{k}} Q^{\nu}_{\mathbf{q}}, P^{\lambda',\lambda'}_{\mathbf{k}'-\mathbf{q}',\mathbf{k}'} D_{\nu',-\mathbf{q}'}]
\end{aligned}$$

The first term vanishes with a momentum transformation. The commutator in the second term is:

$$\begin{aligned}
[P^{\lambda,\lambda}_{\mathbf{k}-\mathbf{q},\mathbf{k}} Q^{\nu}_{\mathbf{q}}, P^{\lambda',\lambda'}_{\mathbf{k}'-\mathbf{q}',\mathbf{k}'} D_{\nu',-\mathbf{q}'}] &= P^{\lambda,\lambda}_{\mathbf{k}-\mathbf{q},\mathbf{k}} P^{\lambda',\lambda'}_{\mathbf{k}'-\mathbf{q}',\mathbf{k}'} [Q^{\nu}_{\mathbf{q}}, D_{\nu',-\mathbf{q}'}] + [P^{\lambda,\lambda}_{\mathbf{k}-\mathbf{q},\mathbf{k}}, P^{\lambda',\lambda'}_{\mathbf{k}'-\mathbf{q}',\mathbf{k}'}] D_{\nu',-\mathbf{q}'} Q^{\nu}_{\mathbf{q}} \\
&= -\delta_{\mathbf{q}',-\mathbf{q}} \delta_{\nu',\nu} P^{\lambda,\lambda}_{\mathbf{k}-\mathbf{q},\mathbf{k}} P^{\lambda',\lambda'}_{\mathbf{k}'-\mathbf{q}',\mathbf{k}'} \\
&+ \delta_{\lambda\lambda'} (\delta_{\mathbf{k}'-\mathbf{q}',\mathbf{k}} P^{\lambda,\lambda'}_{\mathbf{k}-\mathbf{q},\mathbf{k}'} - \delta_{\mathbf{k}',\mathbf{k}-\mathbf{q}} P^{\lambda',\lambda}_{\mathbf{k}'-\mathbf{q}',\mathbf{k}}) D^{\nu'}_{-\mathbf{q}'} Q^{\nu}_{\mathbf{q}}
\end{aligned}$$

The second term is eliminated by the same momentum transformation, thus:

$$
\begin{aligned}
[U, H_{el-ph}] &= -2\sum_{\lambda\lambda'}\sum_{\mathbf{k},\mathbf{k}'}\sum_{\nu,\mathbf{q}} g^{\lambda}_{\nu,\mathbf{q}} g^{\lambda'}_{\nu,-\mathbf{q}} (\hbar\omega_{\nu,\mathbf{q}}) \{\Psi^{\dagger}_{\lambda,\mathbf{k}-\mathbf{q}} (\delta_{\lambda,\lambda'}\delta_{\mathbf{k}'+\mathbf{q},\mathbf{k}} - \Psi^{\dagger}_{\lambda',\mathbf{k}'+\mathbf{q}}\Psi_{\lambda,\mathbf{k}})\Psi_{\lambda',\mathbf{k}'}\} \\
&= -2\sum_{\lambda,\mathbf{k},\mathbf{q}} \Big(\sum_{\nu} \hbar\omega_{\nu,\mathbf{q}} |g^{\lambda}_{\nu,\mathbf{q}}|^2\Big) P^{\lambda,\lambda}_{\mathbf{k}-\mathbf{q},\mathbf{k}-\mathbf{q}} \\
&\quad - 2\sum_{\lambda,\lambda'}\sum_{\mathbf{k},\mathbf{k}'}\sum_{\mathbf{q}} \Big(\sum_{\nu} \hbar\omega_{\nu,\mathbf{q}}\, g^{\lambda}_{\nu,-\mathbf{q}} g^{\lambda'}_{\nu,\mathbf{q}}\Big) \Psi^{\dagger}_{\lambda,\mathbf{k}} \Psi^{\dagger}_{\lambda',\mathbf{k}'} \Psi_{\lambda',\mathbf{k}'+\mathbf{q}} \Psi_{\lambda,\mathbf{k}-\mathbf{q}}
\end{aligned}
$$

The other Hamiltonians transform as before, and the general interacting polaron model is:

$$\bar{H}_{pol} = \sum_{\lambda,\mathbf{k},\mathbf{q}} \Big\{ \Big(e^{-C_\lambda} \mathcal{E}_\lambda e^{C_\lambda}\Big)_{\mathbf{k},\mathbf{k}-\mathbf{q}} P^{\lambda,\lambda}_{\mathbf{k}-\mathbf{q},\mathbf{k}} - \Big(\sum_{\nu} \hbar\omega_{\nu,\mathbf{q}} |g^{\lambda}_{\nu,\mathbf{q}}|^2\Big) P^{\lambda,\lambda}_{\mathbf{k},\mathbf{k}} \Big\} \tag{3.66}$$

$$\bar{H}_{latt} = \sum_{\nu,\mathbf{q}} \hbar\omega_{\nu,\mathbf{q}} (D^{\dagger}_{\nu,\mathbf{q}} D_{\nu,\mathbf{q}} + \tfrac{1}{2}) \tag{3.67}$$

$$\bar{H}_{em} = \sum_{\mathbf{q}} \hbar\omega_{\mathbf{q}} (B^{\dagger}_{\mathbf{q}} B_{\mathbf{q}} + \tfrac{1}{2}) \tag{3.68}$$

$$\bar{H}_{pol-pol} = \tfrac{1}{2}\sum_{\lambda,\lambda'}\sum_{\mathbf{k},\mathbf{k}'}\sum_{\mathbf{q}} \tilde{V}^{\lambda,\lambda'}_{\mathbf{q}} \{\delta_{\mathbf{q},0} P^{\lambda,\lambda}_{\mathbf{k},\mathbf{k}-\mathbf{q}} - P^{\lambda,\lambda'}_{\mathbf{k},\mathbf{k}'+\mathbf{q}} P^{\lambda',\lambda}_{\mathbf{k}',\mathbf{k}-\mathbf{q}}\} \tag{3.69}$$

$$\bar{H}_{pol-em} = -i\sum_{\lambda,\lambda'}\sum_{\mathbf{k},\mathbf{q}} F^{\lambda,\lambda'} \Big(e^{C_\lambda - C_{\lambda'}}\Big)_{\mathbf{q},0} P^{\lambda,\lambda'}_{\mathbf{k}-\mathbf{q},\mathbf{k}} B^{\lambda,\lambda'} \tag{3.70}$$

where we have re-defined C_λ:

$$C^{\lambda}_{\mathbf{k}-\mathbf{k}'} \equiv \sum_{\nu} C^{\lambda}_{\nu,\mathbf{k}-\mathbf{k}'} = \sum_{\nu} g^{\lambda}_{\nu,\mathbf{k}-\mathbf{k}'} Q^{\nu}_{\mathbf{k}-\mathbf{k}'} \tag{3.71}$$

and the modified Coulomb potential is now:

$$\tilde{V}_{\mathbf{q}}^{\lambda,\lambda'} = \sum_{\nu} \tilde{V}_{\nu,\mathbf{q}}^{\lambda,\lambda'} \tag{3.72}$$

$$= V_{\mathbf{q}}^{\lambda,\lambda'} - \sum_{\nu} (2\hbar\omega_{\nu,\mathbf{q}})(g_{\nu,\mathbf{q}}^{\lambda})^* g_{\nu,\mathbf{q}}^{\lambda'} \tag{3.73}$$

As for the Absorption spectrum, we must be careful in how we define the multi-particle correlation function. We have:

$$A_{\mathbf{q}}(t) = \sum_{\varepsilon_\lambda > \varepsilon_{\lambda'}} \sum_{\mathbf{k},\mathbf{q}'} F^{\lambda,\lambda'} \left(e^{C_\lambda - C_{\lambda'}} \right)_{\mathbf{q}',0} P_{\mathbf{k}-\mathbf{q}',\mathbf{k}}^{\lambda,\lambda'} B_{\mathbf{q}} \delta_{\mathbf{q},0} \tag{3.74}$$

We define:

$$(d_{\lambda,\lambda'}^{\dagger})_{\mathbf{k},\mathbf{k}'} = \sum_{\nu} (g_{\nu,\mathbf{k}-\mathbf{k}'}^{\lambda} - g_{\nu,\mathbf{k}-\mathbf{k}'}^{\lambda'}) D_{\nu,\mathbf{k}-\mathbf{k}'}^{\dagger}$$

$$\equiv \sum_{\nu} [(d_{\lambda,\lambda'}^{\dagger})_{\nu}]_{\mathbf{k},\mathbf{k}'} \tag{3.75}$$

and obtain:

$$A(t) = \sum_{\varepsilon_\lambda > \varepsilon_{\lambda'}} \sum_{\mathbf{k},\mathbf{q}} F^{\lambda,\lambda'} \sum_{\alpha,\beta} C_{\lambda,\lambda'}^{\alpha,\beta} \left(B P_{\mathbf{k}-\mathbf{q},\mathbf{k}}^{\lambda,\lambda'} \right) ([d_{\lambda,\lambda'}^{\dagger}]^{\alpha} [d_{\lambda,\lambda'}^{T}]^{\beta})_{\mathbf{q},0} \tag{3.76}$$

Unlike before, we must expand the phonon contributions to account for the phonon branch:

$$\begin{aligned}([d^{\dagger}_{\lambda,\lambda'}]^{\alpha}[d^{T}_{\lambda,\lambda'}]^{\beta})_{\mathbf{q},0} &= \sum_{\{\nu_\alpha\}}\sum_{\{\nu_\beta\}}\left(\prod_{i=1}^{\alpha}(d^{\dagger}_{\lambda,\lambda'})_{\nu_i}\prod_{j=1}^{\beta}(d^{T}_{\lambda,\lambda'})_{\nu_j}\right)_{\mathbf{q},0} \\ &= \sum_{\{\nu_\alpha,\mathbf{q}'_\alpha\}}\sum_{\{\nu_\beta,\mathbf{q}'_\beta\}}\prod_{i=0}^{\alpha-1}(d^{\dagger}_{\lambda,\lambda'})_{\nu_i,\mathbf{q}'_i}\prod_{j=\alpha}^{\alpha+\beta-1}(d^{T}_{\lambda,\lambda'})_{\nu_j,\mathbf{q}'_j} \end{aligned} \tag{3.77}$$

where:

$$\sum_{\{\nu_\alpha,\mathbf{q}'_\alpha\}} \equiv \sum_{\nu_0,\mathbf{q}'_0}\sum_{\nu_1,\mathbf{q}'_1}\cdots\sum_{\nu_{\alpha-1},\mathbf{q}'_{\alpha-1}},\ \mathbf{q}' \equiv \mathbf{q}_i - \mathbf{q}_{i+1}, \mathbf{q}_0 \equiv \mathbf{q},\ \mathbf{q}_{\alpha+\beta} = 0$$

For this general problem, we find it useful to shift these summations to the absorption spectrum (note that, in our simplified model, we grouped the phonon momenta into one operator; we will see shortly why we have split them for the general problem). The new correlation function is:

$$\Pi^{c,v}_{\alpha,\beta}(\mathbf{k},\mathbf{q}) \equiv BP^{c,v}_{\mathbf{k}-\mathbf{q},\mathbf{k}}\prod_{i=0}^{\alpha-1}(d^{\dagger}_{c,v})_{\nu_i,\mathbf{q}'_i}\prod_{j=\alpha}^{\alpha+\beta}(d^{T}_{c,v})_{\nu_j,\mathbf{q}'_j} \tag{3.78}$$

and the absorption spectrum becomes:

$$A(t) = \sum_{\varepsilon_\lambda > \varepsilon_{\lambda'}}\sum_{\mathbf{k},\mathbf{q}}F^{\lambda,\lambda'}\sum_{\alpha,\beta}C^{\alpha,\beta}_{\lambda,\lambda'}\sum_{\{\nu_\alpha,\mathbf{q}'_\alpha\}}\sum_{\{\nu_\beta,\mathbf{q}'_\beta\}}\Pi^{c,v}_{\alpha,\beta}(\mathbf{k},\mathbf{q})$$

There are only four terms in the EOM that must be re-calculated for this new correlation function: 1) Contributions from the lattice, 2) The coefficient from normal ordering the phonon operators, 3) The Polaron dispersion, and 4) The spectrum side-band amplitude.

We also note that the source term is modified to account for the new phonon contribution of the correlation function. We begin with the lattice contributions:

$$\begin{aligned}[\Pi^{c,v}_{\alpha,\beta}(\mathbf{k},\mathbf{q}),\bar{H}_{latt}] &= BP^{\lambda,\lambda'}_{\mathbf{k}-\mathbf{q},\mathbf{k}}\sum_{\nu,\mathbf{q}'}(\hbar\omega_{\nu,\mathbf{q}'})\prod_{i=0}^{\alpha-1}(d^{\dagger}_{\lambda,\lambda'})_{\nu_i,\mathbf{q}'_i}\Big[\prod_{j=\alpha}^{\alpha+\beta-1}(d^{T}_{\lambda,\lambda'})_{\nu_j,\mathbf{q}'_j},D^{\dagger}_{\nu,\mathbf{q}'}\Big]D_{\nu,\mathbf{q}'}\\ &+BP^{\lambda,\lambda'}_{\mathbf{k}-\mathbf{q},\mathbf{k}}\sum_{\nu,\mathbf{q}'}(\hbar\omega_{\nu,\mathbf{q}'})D^{\dagger}_{\nu,\mathbf{q}'}\Big[\prod_{i=0}^{\alpha-1}(d^{\dagger}_{\lambda,\lambda'})_{\nu_i,\mathbf{q}'_i},D_{\nu,\mathbf{q}'}\Big]\prod_{j=\alpha}^{\alpha+\beta-1}(d^{T}_{\lambda,\lambda'})_{\nu_j,\mathbf{q}'_j}\\ &=\sum_{j=\alpha}^{\alpha+\beta-1}(\hbar\omega_{\nu_j,-\mathbf{q}'_j})\Pi^{c,v}_{\alpha,\beta}(\mathbf{k},\mathbf{q})-\sum_{i=0}^{\alpha-1}(\hbar\omega_{\nu_i,\mathbf{q}'_i})\Pi^{c,v}_{\alpha,\beta}(\mathbf{k},\mathbf{q})\end{aligned}\tag{3.79}$$

We now see why extracting the momenta is and phonon branch summations from the correlation function for the most general problem is useful. The commutator would not have been proportional to the correlation function had we not done so, since each mode contributes a different factor of $\hbar\omega_{\nu,\mathbf{q}}$ (of course, in the event that each mode has the same, flat dispersion, we can reduce our correlation function back to the one in the simplified problem). Phonon operator correlations, such as the normal ordering coefficient and the side-band amplitudes, are derived in the appendix, sec. A.1. We are now ready to rewrite the absorption spectrum in the form of Eq.(3.63):

$$\alpha(\omega)=\sum_{\varepsilon_c>\varepsilon_v}\sum_{\alpha,\beta}\sum_{\mathbf{q}}|F^{c,v}|^2\sum_{\{\alpha,\beta\}}\sum_{n}\frac{D^{c,v}_{\{\alpha,\beta\}}(\mathbf{q},T)|\Psi^{c,v}_{n,\{\alpha,\beta\}}(0)|^2\Gamma^{c,v}_{\{\alpha,\beta\}}}{\left(\tilde{E}^{\{\alpha,\beta\}}_{g,\mathbf{q}}+\Delta E^{\{\alpha,\beta\}}_{ph}-\hbar\omega-E^{\{\alpha,\beta\}}_{n}\right)^2+\left(\Gamma^{c,v}_{\{\alpha,\beta\}}\right)^2}\tag{3.80}$$

Where we have introduced the notation $\{\alpha,\beta\}$ to represent a configuration of the phonon branch and momentum of the absorbed and emitted phonons. The modified gap energy $\tilde{E}^{\{\alpha,\beta\}}_{g,\mathbf{q}}$ accounts for both the modified band gap of the polaron band structure as well as an

associated kinetic energy from the exciton center of mass, and $\Delta E_{ph}^{\{\alpha,\beta\}}$ represents the net energy gained (lost) from net absorption (emission) of phonons, and n denotes the Wannier energy states. The normal ordering factor $C_{\alpha,\beta}^{c,v}$ has been absorbed into the amplitude piece.

3.5.1 Approximated Fitting Expression

While Eq.(3.80) gives a full description of the relevant physics, it is not practical for fitting experimental data. In the presence of vibrational modes with arbitrary, momentum dependent dispersion and matrix elements, the simultaneous requirement of energy and momentum conservation prevents an accurate fitting. However, for the device in question, the phonon bandwidth is very small, and we may approximate the phonons as belonging to a flat band. In this limit, the phonon dispersion and matrix elements are constant (up to some cutoff momentum $\mathbf{q}_0$), and the net phonon energy of $\sum_\nu m_\nu \hbar\Omega_\nu$ characterizes the side-bands, where m_ν is the net number of phonons emitted from branch ν. In this case, we define the polarization functions:

$$\Pi_{\nu,m_\nu}^{c,v}(\mathbf{k}) \equiv (d_{c,v}^\dagger)_\nu^{m_\nu} \sum_{\beta=0}^{\infty} C_{m_\nu+\beta,\beta}^{c,v} (d_{c,v}^\dagger)_\nu^\beta (d_{c,v}^T)_\nu^\beta,\ m_\nu \geq 0 \tag{3.81}$$

$$\Pi_{\nu,m_\nu}^{c,v}(\mathbf{k}) \equiv \sum_{\alpha=0}^{\infty} C_{\alpha,m_\nu+\alpha}^{c,v} (d_{c,v}^\dagger)_\nu^\alpha (d_{c,v}^T)_\nu^\alpha (d_{c,v}^T)_\nu^{m_\nu},\ m_\nu < 0 \tag{3.82}$$

whose EOM would now have the form:

$$\sum_{\{m_\nu\}} \Big[f(\omega) + \sum_\nu m_\nu \hbar\Omega_\nu \Big] \Pi_{\{m_\nu\}}^{c,v}(\mathbf{k}) = \sum_{\{m_\nu\}} S_{\{m_\nu\}}(\mathbf{k}) \tag{3.83}$$

where:

$$\Pi^{c,v}_{\{m_\nu\}}(\mathbf{k}) \equiv \prod_{\nu} \Pi^{c,v}_{\nu,m_\nu}(\mathbf{k}) \tag{3.84}$$

Following the procedure outlined in the Appendix, sec. A.1.3, we find that the contribution to the amplitude of the phonon-side band from emitting m_ν phonons from branch ν is given by:

$$D^{c,v}_{\nu} = e^{-|g^{c,v}_{\nu}|^2(1+2n_\nu)} e^{\frac{1}{2}m_\nu \beta\Omega_\nu} I_{m_\nu}\left(\frac{|g^{c,v}_{\nu}|^2}{sinh(\beta\hbar\Omega_\nu/2)}\right) \tag{3.85}$$

Which comes from re-writing the exponential function in Eq.(A.16) in terms of the modified Bessel Functions of the first kind using the identity:

$$e^{\frac{1}{2}z(t+t^{-1})} = \sum_{m=-\infty}^{\infty} t^m I_m(z)$$

and the absorption coefficient becomes:

$$\alpha(\omega) = \sum_{\varepsilon_c > \varepsilon_v} |F^{c,v}|^2 \sum_{\{m_\nu \epsilon \mathbb{Z}\}} \sum_{n} \frac{\prod_\nu D^{c,v}_{\nu} \Gamma^{c,v}_{\nu}}{(\tilde{E}^{\nu}_{g} + \sum_\nu m_\nu \hbar\Omega_\nu - \hbar\omega - E_{n,\nu})^2 + (\Gamma^{c,v}_{m_\nu})^2} \tag{3.86}$$

Bibliography

[1] N. W. Ashcroft and N. D. Mermin, *Solid state physics*. New York, NY: Holt, Rinehart and Winston, 1976. [Online]. Available: https://cds.cern.ch/record/102652.

[2] J. Bardeen, L. N. Cooper, and J. R. Schrieffer, "Theory of superconductivity," *Phys. Rev.*, vol. 108, pp. 1175–1204, 5 Dec. 1957. DOI: 10.1103/PhysRev.108.1175. [Online]. Available: https://link.aps.org/doi/10.1103/PhysRev.108.1175.

[3] B. A. Bernevig, *Topological Insulators and Topological Superconductors*. Princeton: Princeton University Press, 2013, ISBN: 9781400846733. DOI: doi:10.1515/9781400846733. [Online]. Available: https://doi.org/10.1515/9781400846733.

[4] M. Sato and Y. Ando, "Topological superconductors: A review," *Reports on Progress in Physics*, vol. 80, no. 7, p. 076 501, May 2017, ISSN: 1361-6633. DOI: 10.1088/1361-6633/aa6ac7. [Online]. Available: http://dx.doi.org/10.1088/1361-6633/aa6ac7.

[5] J. C. Budich and B. Trauzettel, "From the adiabatic theorem of quantum mechanics to topological states of matter," *physica status solidi (RRL) – Rapid Research Letters*, vol. 7, no. 1–2, pp. 109–129, Jan. 2013, ISSN: 1862-6270. DOI: 10.1002/pssr.201206416. [Online]. Available: http://dx.doi.org/10.1002/pssr.201206416.

[6] M. Born and V. FOck, "Beweis des adiabatensatzes," *Zeitschrift für Physik*, vol. 51, pp. 165–180, 1928.

[7] S. Ryu and Y. Hatsugai, "Topological origin of zero-energy edge states in particle-hole symmetric systems," *Phys. Rev. Lett.*, vol. 89, p. 077 002, 7 Jul. 2002. DOI: 10.1103/PhysRevLett.89.077002. [Online]. Available: https://link.aps.org/doi/10.1103/PhysRevLett.89.077002.

[8] N. P. Armitage, E. J. Mele, and A. Vishwanath, "Weyl and dirac semimetals in three-dimensional solids," *Rev. Mod. Phys.*, vol. 90, p. 015 001, 1 Jan. 2018. DOI: 10.1103/RevModPhys.90.015001. [Online]. Available: https://link.aps.org/doi/10.1103/RevModPhys.90.015001.

[9] B. Q. Lv, T. Qian, and H. Ding, "Experimental perspective on three-dimensional topological semimetals," *Rev. Mod. Phys.*, vol. 93, p. 025 002, 2 Apr. 2021. DOI: 10.1103/RevModPhys.93.025002. [Online]. Available: https://link.aps.org/doi/10.1103/RevModPhys.93.025002.

[10] B. Yan and C. Felser, "Topological materials: Weyl semimetals," *Annual Review of Condensed Matter Physics*, vol. 8, no. Volume 8, 2017, pp. 337–354, 2017, ISSN: 1947-5462. DOI: https://doi.org/10.1146/annurev-conmatphys-031016-025458. [Online]. Available: https://www.annualreviews.org/content/journals/10.1146/annurev-conmatphys-031016-025458.

[11] I. Jang and K.-S. Kim, "Chiral pair of fermi arcs, anomaly cancellation, and spin or valley hall effects in weyl metals with broken inversion symmetry," *Physical Review B*, vol. 97, no. 16, Apr. 2018. DOI: 10.1103/physrevb.97.165201. [Online]. Available: https://doi.org/10.1103%2Fphysrevb.97.165201.

[12] J.-M. Hou and W. Chen, "Weyl semimetals in optical lattices: Moving and merging of weyl points, and hidden symmetry at weyl points," *Scientific Reports*, vol. 6, no. 1, Sep. 2016, ISSN: 2045-2322. DOI: 10.1038/srep33512. [Online]. Available: http://dx.doi.org/10.1038/srep33512.

[13] S. A. Oliaei Motlagh, V. Apalkov, and M. I. Stockman, "Transition metal dichalcogenide monolayers in an ultrashort optical pulse: Femtosecond currents and anisotropic electron dynamics," *Phys. Rev. B*, vol. 103, p. 155 416, 15 Apr. 2021. DOI: 10.1103/PhysRevB.103.155416. [Online]. Available: https://link.aps.org/doi/10.1103/PhysRevB.103.155416.

[14] L. Mouchliadis *et al.*, "Probing valley population imbalance in transition metal dichalcogenides via temperature-dependent second harmonic generation imaging," *npj 2D Materials and Applications*, vol. 5, 1 Jan. 2021. DOI: 10.1038/s41699-020-00183-z. [Online]. Available: https://doi.org/10.1038/s41699-020-00183-z.

[15] E. Sosenko, J. Zhang, and V. Aji, "Unconventional superconductivity and anomalous response in hole-doped transition metal dichalcogenides," *Physical Review B*, vol. 95, no. 14, Apr. 2017, ISSN: 2469-9969. DOI: 10.1103/physrevb.95.144508. [Online]. Available: http://dx.doi.org/10.1103/PhysRevB.95.144508.

[16] M. A. Rahimi, A. G. Moghaddam, C. Dykstra, M. Governale, and U. Zülicke, "Unconventional superconductivity from magnetism in transition-metal dichalcogenides," *Phys. Rev. B*, vol. 95, p. 104 515, 10 Mar. 2017. DOI: 10.1103/PhysRevB.95.104515. [Online]. Available: https://link.aps.org/doi/10.1103/PhysRevB.95.104515.

[17] R. Wakatsuki and K. T. Law, *Proximity effect and ising superconductivity in superconductor/transition metal dichalcogenide heterostructures*, 2016. arXiv: 1604.04898 [cond-mat.supr-con]. [Online]. Available: https://arxiv.org/abs/1604.04898.

[18] J. Clarke, "THE PROXIMITY EFFECT BETWEEN SUPERCONDUCTING AND NORMAL THIN FILMS IN ZERO FIELD," *Journal de Physique Colloques*, vol. 29, no. C2, pp. C2-3-C2–16, 1968. DOI: 10.1051/jphyscol:1968201. [Online]. Available: https://hal.science/jpa-00213516.

[19] P. G. DE GENNES, "Boundary effects in superconductors," *Rev. Mod. Phys.*, vol. 36, pp. 225–237, 1 Jan. 1964. DOI: 10.1103/RevModPhys.36.225. [Online]. Available: https://link.aps.org/doi/10.1103/RevModPhys.36.225.

[20] E. M. Lifshitz, L. P. Pitaevskii, J. B. Sykes, and M. J. Kearsley, *Statistical physics. Part 2, Theory of the condensed state* (Course of Theoretical Physics ; Volume 9), eng, 3rd ed. Oxford, [England: Butterworth-Heinemann, 1995 - 1980, ISBN: 9780080503509.

[21] R. M. Fernandes, *Lecture notes: Bcs theory of superconductivity.*

[22] D. Arovas, *Bcs theory of superconductivity*, Apr. 2023.

[23] D. Ivanov, *Bcs theory of superconductivity.*

[24] U. Khanna, A. Kundu, S. Pradhan, and S. Rao, "Proximity-induced superconductivity in weyl semimetals," *Phys. Rev. B*, vol. 90, p. 195 430, 19 Nov. 2014. DOI: 10.1103/PhysRevB.90.195430. [Online]. Available: https://link.aps.org/doi/10.1103/PhysRevB.90.195430.

[25] P. O. Sukhachov and E. V. Gorbar, "Superconductivity in weyl semimetals in a strong pseudomagnetic field," *Phys. Rev. B*, vol. 102, p. 014 513, 1 Jul. 2020. DOI: 10.1103/PhysRevB.102.014513. [Online]. Available: https://link.aps.org/doi/10.1103/PhysRevB.102.014513.

[26] Z. Faraei and S. A. Jafari, "Induced superconductivity in fermi arcs," *Phys. Rev. B*, vol. 100, p. 035 447, 3 Jul. 2019. DOI: 10.1103/PhysRevB.100.035447. [Online]. Available: https://link.aps.org/doi/10.1103/PhysRevB.100.035447.

[27] T. Meng and L. Balents, "Weyl superconductors," *Phys. Rev. B*, vol. 86, p. 054 504, 5 Aug. 2012. DOI: 10.1103/PhysRevB.86.054504. [Online]. Available: https://link.aps.org/doi/10.1103/PhysRevB.86.054504.

[28] G. Bednik, A. A. Zyuzin, and A. A. Burkov, "Anomalous hall effect in weyl superconductors," *New Journal of Physics*, vol. 18, no. 8, p. 085 002, Aug. 2016. DOI: 10.1088/1367-2630/18/8/085002. [Online]. Available: https://doi.org/10.1088%2F1367-2630%2F18%2F8%2F085002.

[29] G. Bednik, A. A. Zyuzin, and A. A. Burkov, "Superconductivity in weyl metals," *Phys. Rev. B*, vol. 92, p. 035 153, 3 Jul. 2015. DOI: 10.1103/PhysRevB.92.035153. [Online]. Available: https://link.aps.org/doi/10.1103/PhysRevB.92.035153.

[30] A. A. Burkov and L. Balents, "Weyl semimetal in a topological insulator multilayer," *Physical Review Letters*, vol. 107, no. 12, Sep. 2011. DOI: 10.1103/physrevlett.107.127205. [Online]. Available: https://doi.org/10.1103%2Fphysrevlett.107.127205.

[31] H. Wei, S.-P. Chao, and V. Aji, "Odd-parity superconductivity in weyl semimetals," *Phys. Rev. B*, vol. 89, p. 014 506, 1 Jan. 2014. DOI: 10.1103/PhysRevB.89.014506. [Online]. Available: https://link.aps.org/doi/10.1103/PhysRevB.89.014506.

[32] Y. Li and F. D. M. Haldane, "Topological nodal cooper pairing in doped weyl metals," *Phys. Rev. Lett.*, vol. 120, p. 067 003, 6 Feb. 2018. DOI: 10.1103/PhysRevLett.120.067003. [Online]. Available: https://link.aps.org/doi/10.1103/PhysRevLett.120.067003.

[33] L. Fu and C. L. Kane, "Superconducting proximity effect and majorana fermions at the surface of a topological insulator," *Phys. Rev. Lett.*, vol. 100, p. 096 407, 9 Mar. 2008. DOI: 10.1103/PhysRevLett.100.096407. [Online]. Available: https://link.aps.org/doi/10.1103/PhysRevLett.100.096407.

[34] L. Fu and C. L. Kane, "Josephson current and noise at a superconductor/quantum-spin-hall-insulator/superconductor junction," *Phys. Rev. B*, vol. 79, p. 161 408, 16 Apr. 2009. DOI: 10.1103/PhysRevB.79.161408. [Online]. Available: https://link.aps.org/doi/10.1103/PhysRevB.79.161408.

[35] G. Y. Cho, J. H. Bardarson, Y.-M. Lu, and J. E. Moore, "Superconductivity of doped weyl semimetals: Finite-momentum pairing and electronic analog of the ^{3}he-A phase," *Phys. Rev. B*, vol. 86, p. 214 514, 21 Dec. 2012. DOI: 10.1103/PhysRevB.86.214514. [Online]. Available: https://link.aps.org/doi/10.1103/PhysRevB.86.214514.

[36] B. Lu, K. Yada, M. Sato, and Y. Tanaka, "Crossed surface flat bands of weyl semimetal superconductors," *Phys. Rev. Lett.*, vol. 114, p. 096 804, 9 Mar. 2015. DOI: 10.1103/PhysRevLett.114.096804. [Online]. Available: https://link.aps.org/doi/10.1103/PhysRevLett.114.096804.

[37] S. A. Yang, H. Pan, and F. Zhang, "Dirac and weyl superconductors in three dimensions," *Phys. Rev. Lett.*, vol. 113, p. 046 401, 4 Jul. 2014. DOI: 10.1103/PhysRevLett.113.046401. [Online]. Available: https://link.aps.org/doi/10.1103/PhysRevLett.113.046401.

[38] R. Wang, L. Hao, B. Wang, and C. S. Ting, "Quantum anomalies in superconducting weyl metals," *Phys. Rev. B*, vol. 93, p. 184 511, 18 May 2016. DOI: 10.1103/PhysRevB.93.184511. [Online]. Available: https://link.aps.org/doi/10.1103/PhysRevB.93.184511.

[39] F. Setiawan, C.-T. Wu, and K. Levin, "Full proximity treatment of topological superconductors in josephson-junction architectures," *Phys. Rev. B*, vol. 99, p. 174 511, 17 May 2019. DOI: 10.1103/PhysRevB.99.174511. [Online]. Available: https://link.aps.org/doi/10.1103/PhysRevB.99.174511.

[40] A. Mourachkine, "Determination of the coherence length and the cooper-pair size in unconventional superconductors by tunneling spectroscopy," *Journal of Superconductivity*, vol. 17, no. 6, pp. 711–724, Dec. 2004, ISSN: 1572-9605. DOI: 10.1007/s10948-004-0831-7. [Online]. Available: http://dx.doi.org/10.1007/s10948-004-0831-7.

[41] R. Dawson and V. Aji, "Proximity effect of s-wave superconductor on an inversion-broken weyl semimetal," *Phys. Rev. B*, vol. 109, p. 094 517, 9 Mar. 2024. DOI: 10.1103/PhysRevB.109.094517. [Online]. Available: https://link.aps.org/doi/10.1103/PhysRevB.109.094517.

[42] E. Sosenko, J. Zhang, and V. Aji, "Unconventional superconductivity and anomalous response in hole-doped transition metal dichalcogenides," *Phys. Rev. B*, vol. 95, p. 144 508, 14 Apr. 2017. DOI: 10.1103/PhysRevB.95.144508. [Online]. Available: https://link.aps.org/doi/10.1103/PhysRevB.95.144508.

[43] W. L. McMillan, "Tunneling model of the superconducting proximity effect," *Phys. Rev.*, vol. 175, pp. 537–542, 2 Nov. 1968. DOI: 10.1103/PhysRev.175.537. [Online]. Available: https://link.aps.org/doi/10.1103/PhysRev.175.537.

[44] R. Landauer, "Spatial variation of currents and fields due to localized scatterers in metallic conduction," *IBM Journal of Research and Development*, vol. 32, no. 3, pp. 306–316, 1988. DOI: 10.1147/rd.323.0306.

[45] M. Büttiker, "Four-terminal phase-coherent conductance," *Phys. Rev. Lett.*, vol. 57, pp. 1761–1764, 14 Oct. 1986. DOI: 10.1103/PhysRevLett.57.1761. [Online]. Available: https://link.aps.org/doi/10.1103/PhysRevLett.57.1761.

[46] H. Haug and S. W. Koch, *Quantum Theory of the Optical and Electronic Properties of Semiconductors*, 5th. WORLD SCIENTIFIC, 2009, pp. 163–187. DOI: 10.1142/7184. eprint: https://www.worldscientific.com/doi/pdf/10.1142/7184. [Online]. Available: https://www.worldscientific.com/doi/abs/10.1142/7184.

[47] T. Feldtmann, M. Kira, and S. Koch, "Phonon sidebands in semiconductor luminescence," *physica status solidi (b)*, vol. 246, pp. 332–, Feb. 2009. DOI: 10.1002/pssb.200880322.

[48] F. Barati *et al.*, "Vibronic exciton–phonon states in stack-engineered van der waals heterojunction photodiodes," *Nano Letters*, vol. 22, no. 14, pp. 5751–5758, 2022.

[49] W. Shan *et al.*, "Nature of room-temperature photoluminescence in ZnO," *Applied Physics Letters*, vol. 86, no. 19, p. 191 911, May 2005, ISSN: 0003-6951. DOI: 10.1063/1.1923757. eprint: https://pubs.aip.org/aip/apl/article-pdf/doi/10.1063/1.1923757/14638687/191911_1_online.pdf. [Online]. Available: https://doi.org/10.1063/1.1923757.

[50] P. Han and G. Bester, "Determination of the phonon sidebands in the photoluminescence spectrum of semiconductor nanoclusters from ab initio calculations," *Phys. Rev. B*, vol. 106, p. 245 404, 24 Dec. 2022. DOI: 10.1103/PhysRevB.106.245404. [Online]. Available: https://link.aps.org/doi/10.1103/PhysRevB.106.245404.

[51] M. Kozhevnikov, B. Ashkinadze, E. Cohen, and A. Ron, "Lo-phonon sideband photoluminescence in pure gaas," *Solid State Communications*, vol. 106, no. 2, pp. 73–76, 1998, ISSN: 0038-1098. DOI: https://doi.org/10.1016/S0038-1098(97)10250-2. [Online]. Available: https://www.sciencedirect.com/science/article/pii/S0038109897102502.

[52] S. Brem *et al.*, "Phonon-assisted photoluminescence from indirect excitons in monolayers of transition-metal dichalcogenides," *Nano Letters*, vol. 20, no. 4, pp. 2849–2856, 2020, PMID: 32084315. DOI: 10.1021/acs.nanolett.0c00633. eprint: https://doi.org/10.1021/acs.nanolett.0c00633. [Online]. Available: https://doi.org/10.1021/acs.nanolett.0c00633.

[53] L. Zhou *et al.*, "Unconventional excitonic states with phonon sidebands in layered silicon diphosphide," *Nature Materials*, vol. 21, no. 7, pp. 773–778, Jun. 2022, ISSN: 1476-4660. DOI: 10.1038/s41563-022-01285-3. [Online]. Available: http://dx.doi.org/10.1038/s41563-022-01285-3.

[54] K. Hannewald and P. A. Bobbert, "Nonperturbative theory of exciton-phonon resonances in semiconductor absorption," *Phys. Rev. B*, vol. 72, p. 113 202, 11 Sep. 2005. DOI: 10.1103/PhysRevB.72.113202. [Online]. Available: https://link.aps.org/doi/10.1103/PhysRevB.72.113202.

[55] M. Kira and S. Koch, "Many-body correlations and excitonic effects in semiconductor spectroscopy," *Progress in Quantum Electronics*, vol. 30, no. 5, pp. 155–296, 2006, ISSN: 0079-6727. DOI: https://doi.org/10.1016/j.pquantelec.2006.12.002. [Online]. Available: https://www.sciencedirect.com/science/article/pii/S0079672706000280.

[56] O. Karni *et al.*, "Infrared interlayer exciton emission in MoS_2/WSe_2 heterostructures," *Phys. Rev. Lett.*, vol. 123, p. 247 402, 24 Dec. 2019. DOI: 10.1103/PhysRevLett.123.247402. [Online]. Available: https://link.aps.org/doi/10.1103/PhysRevLett.123.247402.

[57] K. L. Seyler *et al.*, "Signatures of moiré-trapped valley excitons in mose2/wse2 heterobilayers," *Nature*, vol. 567, no. 7746, pp. 66–70, Feb. 2019, ISSN: 1476-4687. DOI: 10.1038/s41586-019-0957-1. [Online]. Available: http://dx.doi.org/10.1038/s41586-019-0957-1.

[58] F. Barati, M. Grossnickle, S. Su, R. Lake, V. Aji, and N. Gabor, "Hot carrier-enhanced interlayer electron–hole pair multiplication in 2d semiconductor heterostructure photocells," *Nature Nanotechnology*, vol. 12, Dec. 2017. DOI: 10.1038/nnano.2017.203.

[59] R. W. Munn and R. Silbey, "Theory of electronic transport in molecular crystals. II. Zeroth order states incorporating nonlocal linear electron–phonon coupling," *The Journal of Chemical Physics*, vol. 83, no. 4, pp. 1843–1853, Aug. 1985, ISSN: 0021-9606. DOI: 10.1063/1.449372. eprint: https://pubs.aip.org/aip/jcp/article-pdf/83/4/1843/18954054/1843_1_online.pdf. [Online]. Available: https://doi.org/10.1063/1.449372.

Appendix A

Phonon Assisted Optical Absorption

A.1 Phonon Operator Correlations

To solve Eq.(3.63), we must obtain expressions for the polaron dispersion $\tilde{e}_{\lambda,\mathbf{k}}$, the phonon contribution to the absorption spectrum $D^{c,v}_{\alpha,\beta}(\mathbf{q})$, and the coefficients $C^{\alpha,\beta}_{c,v}$. We begin by normal ordering our phonon operators.

A.1.1 Phonon Operator Normal Ordering

We note a consequence of the Baker-Campbell-Hausdorff Lemma, under the assumption that operators A and B commute with their commutator $[A, B]$:

$$e^{A+B} = e^A e^B e^{-\frac{1}{2}[A,B]} \tag{A.1}$$

Applying this, we first re-order the operators that yield the coefficients $C^{\alpha,\beta}_{c,v}$:

$$\begin{aligned} C^{\lambda}_{\mathbf{k},\mathbf{k}'} - C^{\lambda'}_{\mathbf{k},\mathbf{k}'} &= g^{\lambda}_{\mathbf{k}-\mathbf{k}'}(D^{\dagger}_{\mathbf{k}-\mathbf{k}'} - D_{\mathbf{k}'-\mathbf{k}}) - g^{\lambda'}_{\mathbf{k}-\mathbf{k}'}(D^{\dagger}_{\mathbf{k}-\mathbf{k}'} - D_{\mathbf{k}'-\mathbf{k}}) \\ &= (g^{\lambda}_{\mathbf{k}-\mathbf{k}'} - g^{\lambda'}_{\mathbf{k}-\mathbf{k}'})D^{\dagger}_{\mathbf{k}-\mathbf{k}'} - (g^{\lambda}_{\mathbf{k}-\mathbf{k}'} - g^{\lambda'}_{\mathbf{k}-\mathbf{k}'})D_{\mathbf{k}'-\mathbf{k}} \\ &= (d^{\dagger}_{\lambda,\lambda'})_{\mathbf{k},\mathbf{k}'} - (d^{T}_{\lambda,\lambda'})_{\mathbf{k},\mathbf{k}'} \end{aligned}$$

we have:

$$\begin{aligned} [d^{\dagger}_{\lambda,\lambda'}, d^{T}_{\lambda,\lambda'}]_{\mathbf{k},\mathbf{k}'} &= \sum_{\mathbf{k}''}\{(d^{\dagger}_{\lambda,\lambda'})_{\mathbf{k},\mathbf{k}''}(d_{\lambda,\lambda'})_{\mathbf{k}',\mathbf{k}''} - (d_{\lambda,\lambda'})_{\mathbf{k}'',\mathbf{k}}(d^{\dagger}_{\lambda,\lambda'})_{\mathbf{k}'',\mathbf{k}'}\} \\ &= \sum_{\mathbf{k}''}(g^{\lambda}_{\mathbf{k}-\mathbf{k}''} - g^{\lambda'}_{\mathbf{k}-\mathbf{k}''})(g^{\lambda}_{\mathbf{k}'-\mathbf{k}''} - g^{\lambda'}_{\mathbf{k}'-\mathbf{k}''})^*[D^{\dagger}_{\mathbf{k}-\mathbf{k}''}, D_{\mathbf{k}'-\mathbf{k}''}] \\ &= -\sum_{\mathbf{q}}|g^{\lambda}_{\mathbf{q}} - g^{\lambda'}_{\mathbf{q}}|^2\delta_{\mathbf{k},\mathbf{k}'} \\ &\equiv -\tilde{G}_{\lambda,\lambda'}\delta_{\mathbf{k},\mathbf{k}'} \end{aligned}$$

This is an identity, allowing us to use Eq.(A.1) to re-write the exponential in Eq.(3.30):

$$\begin{aligned}[e^{C_\lambda - C_{\lambda'}}]_{\mathbf{q},0} &= \sum_{\mathbf{k}_1,\mathbf{k}_2} \left(e^{d^\dagger_{\lambda,\lambda'}}\right)_{\mathbf{q},\mathbf{k}_1} \left(e^{-d^T_{\lambda,\lambda'}}\right)_{\mathbf{k}_1,\mathbf{k}_2} \left(e^{\frac{1}{2}\left[d^\dagger_{\lambda,\lambda'}, d^T_{\lambda,\lambda'}\right]}\right)_{\mathbf{k}_2,0} \\ &= e^{-\frac{1}{2}\tilde{G}_{\lambda,\lambda'}} \sum_{\alpha,\beta} \frac{(-1)^\beta}{(\alpha!)(\beta!)} ([d^\dagger_{\lambda,\lambda'}]^\alpha [d^T_{\lambda,\lambda'}]^\beta)_{\mathbf{q},0}\end{aligned}$$

which yields the coefficients:

$$C^{\alpha,\beta}_{c,v} = e^{-\frac{1}{2}\tilde{G}_{c,v}} \frac{(-1)^\beta}{(\alpha!)(\beta!)} \tag{A.2}$$

Allowing for multiple phonon branches, we have:

$$\begin{aligned}[d^\dagger_{\lambda,\lambda'}, d^T_{\lambda,\lambda'}]_{\mathbf{k},\mathbf{k}'} &= \sum_{\nu,\nu'} \sum_{\mathbf{k}''} \{[(d^\dagger_{\lambda,\lambda'})_\nu]_{\mathbf{k},\mathbf{k}''} [(d)^{\nu'}_{\lambda,\lambda'}]_{\mathbf{k}',\mathbf{k}''} - [(d)^\nu_{\lambda,\lambda'}]_{\mathbf{k}'',\mathbf{k}} [(d^\dagger)^{\nu'}_{\lambda,\lambda'}]_{\mathbf{k}'',\mathbf{k}'}\} \\ &= \sum_{\nu,\nu'} \sum_{\mathbf{k}''} (g^{\lambda,\nu}_{\mathbf{k}-\mathbf{k}''} - g^{\lambda',\nu'}_{\mathbf{k}-\mathbf{k}''})(g^{\lambda,\nu}_{\mathbf{k}'-\mathbf{k}''} - g^{\lambda',\nu'}_{\mathbf{k}'-\mathbf{k}''})^* [D^\dagger_{\nu,\mathbf{k}-\mathbf{k}''}, D_{\nu',\mathbf{k}'-\mathbf{k}''}] \\ &= -\sum_{\nu,\mathbf{q}} |g^\lambda_{\nu,\mathbf{q}} - g^{\lambda'}_{\nu,\mathbf{q}}|^2 \delta_{\mathbf{k},\mathbf{k}'} \\ &\equiv -\tilde{G}_{\lambda,\lambda'} \delta_{\mathbf{k},\mathbf{k}'}\end{aligned}$$

where we have simply re-defined $\tilde{G}_{\lambda,\lambda'}$ to account for the phonon branches.

A.1.2 Polaron Dispersion

Applying the Baker-Campbell-Hausdorff Lemma, we have:

$$\begin{aligned}\bar{H}_{pol} &= \sum_{\lambda,\mathbf{k},\mathbf{q}} \left\{ \left(e^{-C_\lambda} \mathcal{E}_\lambda e^{C_\lambda}\right)_{\mathbf{k},\mathbf{k}-\mathbf{q}} P^{\lambda,\lambda}_{\mathbf{k}-\mathbf{q},\mathbf{k}} - \hbar\Omega |g^\lambda_{\mathbf{q}}|^2 P^{\lambda,\lambda}_{\mathbf{k},\mathbf{k}} \right\} \\ &= \sum_{\lambda,\mathbf{k},\mathbf{q}} \Big[\sum_{n=0}^{\infty} \frac{(-1)^n}{n!} \left\langle [(C_\lambda)^{(n)}, \mathcal{E}_\lambda]_{\mathbf{k},\mathbf{k}-\mathbf{q}} \right\rangle - \hbar\Omega \tilde{G}_\lambda \delta_{\mathbf{q},0} \Big] P^{\lambda,\lambda}_{\mathbf{k}-\mathbf{q},\mathbf{k}}\end{aligned}$$

The correlations are only nonzero for even powers of n, thus:

$$\sum_{n=0}^{\infty} \frac{(-1)^n}{n!} \left\langle [(C_\lambda)^{(n)}, \mathcal{E}_\lambda]_{\mathbf{k},\mathbf{k}-\mathbf{q}} \right\rangle = \sum_{n=0}^{\infty} \frac{1}{(2n)!} \left\langle [(C_\lambda)^{(2n)}, \mathcal{E}_\lambda]_{\mathbf{k},\mathbf{k}-\mathbf{q}} \right\rangle \tag{A.3}$$

Since the Q operators commute, so too do the C_λ operators, meaning the phonon operators in Eq.(A.3) are already normal ordered (with respect to C_λ, not $D_\mathbf{q}$). The correlations can thus be calculated by performing pairwise Wick's contractions between the C_λ operators. Furthermore, since the operators commute, each correlation must yield the same value.

This means we may write Eq.(A.3) as:

$$\sum_{n=0}^{\infty}\frac{1}{(2n)!}\left\langle[(C_\lambda)^{(2n)},\mathcal{E}_\lambda]_{\mathbf{k},\mathbf{k}-\mathbf{q}}\right\rangle=\sum_{n=0}^{\infty}\frac{1}{(2n)!}\frac{(2n)!}{(n!)(2^n)}\prod_{m=1}^{n}\left(\langle[C_\lambda,[C_\lambda,\mathcal{E}_\lambda]]_{\mathbf{k},\mathbf{k}-\mathbf{q}}\rangle\right)^m \tag{A.4}$$

From our initial work calculating how the electronic band structure transforms, we already know what the commutator evaluates to:

$$[C_\lambda,[C_\lambda,\mathcal{E}_\lambda]]_{\mathbf{k},\mathbf{k}-\mathbf{q}}=\sum_{\mathbf{q}'}(C_\lambda)_{\mathbf{k},\mathbf{q}'}(C_\lambda)_{\mathbf{q}',\mathbf{k}-\mathbf{q}}(\varepsilon_{\lambda,\mathbf{k}-\mathbf{q}}-2\varepsilon_{\lambda,\mathbf{q}'}+\varepsilon_{\lambda,\mathbf{k}}) \tag{A.5}$$

Finally, we note that the two operator Wick's contractions are given by:

$$\begin{aligned}\langle(C_\lambda)_{\mathbf{k}}(C_\lambda)_{\mathbf{q}}\rangle&=g^\lambda_{\mathbf{k}}g^\lambda_{\mathbf{q}}\left\langle(D^\dagger_{\mathbf{k}}-D_{-\mathbf{k}})(D^\dagger_{\mathbf{q}}-D_{-\mathbf{q}})\right\rangle\\&=-g^\lambda_{\mathbf{k}}g^\lambda_{\mathbf{q}}\left\langle D^\dagger_{\mathbf{k}}D_{-\mathbf{q}}+D_{-\mathbf{k}}D^\dagger_{\mathbf{q}}\right\rangle\\&=-|g^\lambda_{\mathbf{k}}|^2\delta_{\mathbf{k},-\mathbf{q}}(1+2n_{\mathbf{k}})\end{aligned} \tag{A.6}$$

where $n_{\mathbf{k}}=[exp(\beta\hbar\Omega_{\mathbf{k}})-1]^{-1}$ is the usual Planck distribution. Combining Eq.(A.5) and Eq.(A.6), we have:

$$\langle[C_\lambda,[C_\lambda,\mathcal{E}_\lambda]]_{\mathbf{k},\mathbf{k}-\mathbf{q}}\rangle=-2\sum_{\mathbf{q}'}|g^\lambda_{\mathbf{q}'}|^2(1+2n_{\mathbf{q}'})(\varepsilon_{\lambda,\mathbf{k}}-\varepsilon_{\mathbf{k}-\mathbf{q}'})\delta_{\mathbf{q},0} \tag{A.7}$$

Combining this with Eq.(A.4) yields:

$$\left\langle\left(e^{-C_\lambda}\mathcal{E}_\lambda e^{C_\lambda}\right)_{\mathbf{k},\mathbf{k}-\mathbf{q}}\right\rangle=\sum_{n=0}^{\infty}\sum_{m=0}^{n}\frac{(-1)^{n-m}}{n!}\frac{(n!)\delta_{\mathbf{q},0}}{(n-m)!(m!)}(\bar{G}_\lambda)^{n-m}\sum_{\mathbf{k}'}(G_\lambda)^m_{\mathbf{k},\mathbf{k}'}\varepsilon_{\lambda,\mathbf{k}'} \tag{A.8}$$

where we have used the binomial theorem while defining $\bar{G}_\lambda\equiv\sum_{\mathbf{q}}|g_{\lambda,\mathbf{q}}|^2(1+2n_{\mathbf{q}})$ and $(G_\lambda)_{\mathbf{k},\mathbf{k}'}\equiv|g^\lambda_{\mathbf{k}-\mathbf{k}'}|^2(1+2n_{\mathbf{k}-\mathbf{k}'})$. Thus:

$$\left\langle\left(e^{-C_\lambda}\mathcal{E}_\lambda e^{C_\lambda}\right)_{\mathbf{k},\mathbf{k}-\mathbf{q}}\right\rangle=\delta_{\mathbf{q},0}e^{-\bar{G}_\lambda}\sum_{\mathbf{k}'}\left(e^{G_\lambda}\right)_{\mathbf{k},\mathbf{k}'}\varepsilon_{\lambda,\mathbf{k}'} \tag{A.9}$$

Yielding the Polaron dispersion:

$$e_{\lambda,\mathbf{k}}=e^{-\bar{G}_\lambda}\sum_{\mathbf{k}'}\left(e^{G_\lambda}\right)_{\mathbf{k},\mathbf{k}'}\varepsilon_{\lambda,\mathbf{k}'}-\hbar\Omega\tilde{G}_\lambda \tag{A.10}$$

which is consistent with the zero temperature expression Feldtmann et. al derived[47]. If the model allows for multiple phonon branch, the Wick's contractions become:

$$\begin{aligned}\left\langle (C^{\lambda})_{\mathbf{k}}(C^{\lambda})_{\mathbf{q}}\right\rangle &= \sum_{\nu,\nu'} g^{\lambda,\nu}_{\mathbf{k}} g^{\lambda,\nu'}_{\mathbf{q}} \left\langle (D^{\dagger}_{\nu,\mathbf{k}} - D_{\nu,-\mathbf{k}})(D^{\dagger}_{\nu',\mathbf{q}} - D_{\nu',-\mathbf{q}})\right\rangle \\ &= -\sum_{\nu,\nu'} g^{\lambda,\nu}_{\mathbf{k}} g^{\lambda,\nu'}_{\mathbf{q}} \left\langle D^{\dagger}_{\nu,\mathbf{k}} D_{\nu',\mathbf{q}} + D_{\nu',-\mathbf{k}} D^{\dagger}_{\nu',\mathbf{q}}\right\rangle \\ &= -\sum_{\nu} |g^{\lambda,\nu}_{\mathbf{k}}|^2 \delta_{\mathbf{k},-\mathbf{q}}(1+2n_{\nu,\mathbf{k}})\end{aligned}$$

The momentum dependence of the contractions is unaffected by the presence of the phonon branch index, and each contraction simply acquires an additional summation over the index. We re-define:

$$\begin{aligned}\bar{G}_{\lambda} &\equiv \sum_{\nu,\mathbf{q}'} |g^{\lambda}_{\nu,\mathbf{q}'}|^2(1+2n_{\nu,\mathbf{q}'}) \\ (G_{\lambda})_{\mathbf{k},\mathbf{k}'} &\equiv \sum_{\nu} |g^{\lambda}_{\nu,\mathbf{k}-\mathbf{k}'}|^2(1+2n_{\nu,\mathbf{k}-\mathbf{k}'})\end{aligned}$$

to obtain the same expression for the Polaron dispersion.

A.1.3 Spectrum Side-band Amplitude

To obtain the general spectrum side-band amplitude (i.e. arbitrary phonon branches and momenta), we will make use of Eq.(3.58). In the general model, it reads:

$$[f_{c,v}(\omega) - E^{c,v}_{\{\alpha,\beta\}}]\bar{\Pi}^{c,v}_{\{\alpha,\beta\}}(\mathbf{k},\mathbf{q}) = S_{\{\alpha,\beta\}}(\mathbf{k},\mathbf{q}) \tag{A.11}$$

where $E^{c,v}_{\{\alpha,\beta\}}$ is the net phonon absorption/emission energy of a particular configuration of absorbed and emitted phonons, and for convenience we have simplified the remaining terms. Summing over all configurations, we have:

$$\sum_{\alpha,\beta} C^{\alpha,\beta}_{c,v} \sum_{\{\alpha,\beta\}} [f_{c,v}(\omega) - E^{c,v}_{\{\alpha,\beta\}}]\bar{\Pi}^{c,v}_{\{\alpha,\beta\}}(\mathbf{k},\mathbf{q}) = A^{v,c}_{\mathbf{k},\mathbf{q}} \left\langle (e^{C_v - C_c})_{-\mathbf{q},0}(e^{C_c - C_v})_{\mathbf{q},0}\right\rangle \tag{A.12}$$

where:

$$A^{v,c}_{\mathbf{k},\mathbf{q}} \equiv F^{v,c}\Big\{ f^{c}_{\mathbf{k}-\mathbf{q}}(1-f^{v}_{\mathbf{k}}) + \left\langle B^{\dagger}B\right\rangle (f^{c}_{\mathbf{k}-\mathbf{q}} - f^{v}_{\mathbf{k}})\Big\} \tag{A.13}$$

The R.H.S. of Eq.(A.12) comes from the original definition of $S_{\{\alpha,\beta\}}(\mathbf{k},\mathbf{q})$ and $C^{\alpha,\beta}_{c,v}$, and can be seen as the result of calculating contributions to the EOM from $\bar{H}_{pol-em}$ without splitting up the phonon operators into absorption and emission pieces. We now note an immediate implication of this expression: if the R.H.S. of Eq.(A.12) can be written as a sum over all configurations of the absorbed and emitted phonons, then we may equate both series element wise, and we will have obtained the side-band amplitudes. The R.H.S. is

given by [59]:

$$\left\langle (e^{C_v - C_c})_{-\mathbf{q},0} (e^{C_c - C_v})_{\mathbf{q},0} \right\rangle = \left\langle e^{-(d^\dagger_{c,v}\otimes\mathbb{1} - \mathbb{1}\otimes d^\dagger_{c,v}) + (d^T_{c,v}\otimes\mathbb{1} - \mathbb{1}\otimes d^T_{c,v})} \right\rangle_{-\mathbf{q},0;\mathbf{q},0}$$
$$= \left(e^{-\frac{1}{2}\left\langle \{d^\dagger_{c,v}, d^T_{c,v}\} \right\rangle} \right)_{-\mathbf{q},-\mathbf{q}} \left(e^{\left\langle d^T_{c,v}\otimes d^\dagger_{c,v} + d^\dagger_{c,v}\otimes d^T_{c,v} \right\rangle} \right)_{-\mathbf{q},0;\mathbf{q},0} \left(e^{-\frac{1}{2}\left\langle \{d^\dagger_{c,v}, d^T_{c,v}\} \right\rangle} \right)_{0,0} \tag{A.14}$$

The anti-commutator is:

$$\left(e^{-\frac{1}{2}\left\langle \{d^\dagger_{c,v}, d^T_{c,v}\} \right\rangle} \right)_{k,k'} = e^{-\frac{1}{2}\sum_{\nu,\mathbf{q}} |g^c_{\nu,\mathbf{q}} - g^v_{\nu,\mathbf{q}}|^2 (1+2n_{\nu,\mathbf{q}})}$$
$$= e^{-\frac{1}{2}(\tilde{G}_{c,v} + 2\bar{G}_{c,v})} \tag{A.15}$$

and the middle term is:

$$\left(e^{\left\langle d^T_{c,v}\otimes d^\dagger_{c,v} + d^\dagger_{c,v}\otimes d^T_{c,v} \right\rangle} \right)_{-\mathbf{q},0;\mathbf{q},0} = \left(e^{\bar{G}_{c,v}+\mathbb{1}} e^{\bar{G}_{c,v}} \right)_{\mathbf{q},0} \tag{A.16}$$

where $(\bar{G}_{c,v})_{\mathbf{k},\mathbf{k}'} \equiv \sum_\nu |g^c_{\nu\mathbf{k}-\mathbf{k}'} - g^v_{\nu\mathbf{k}-\mathbf{k}'}|^2 n_{\nu,\mathbf{k}-\mathbf{k}'}$ such that $\bar{G}_{c,v} = \sum_{\mathbf{q}} (\bar{G}_{c,v})_{\mathbf{q},0}$. Expanding the exponentials into their series form yields:

$$\left(e^{\bar{G}_{c,v}+\mathbb{1}} e^{\bar{G}_{c,v}} \right)_{\mathbf{q},0} = \sum_{\alpha,\beta} \frac{1}{\alpha!\beta!} [(\bar{G}_{c,v} + \mathbb{1})^\alpha (\bar{G}_{c,v})^\beta]_{\mathbf{q},0}$$
$$= \sum_{\alpha,\beta} \frac{1}{\alpha!\beta!} \sum_{\{\alpha,\beta\}} \prod_{i=0}^{\alpha-1} (\bar{G}_{c,v} + \mathbb{1})_{\nu_i,\mathbf{q}'_i} \prod_{j=\alpha}^{\alpha+\beta-1} (\bar{G}_{c,v})_{\nu_l,\mathbf{q}'_j} \tag{A.17}$$

which gives the expected side band amplitude:

$$D^{c,v}_{\{\alpha,\beta\}}(\mathbf{q},T) = \frac{1}{\alpha!\beta!} e^{-\bar{G}_{c,v} - \frac{1}{2}\tilde{G}_{c,v}} \prod_{i=0}^{\alpha-1} (\bar{G}_{c,v} + \mathbb{1})_{\nu_i,\mathbf{q}'_i} \prod_{j=\alpha}^{\alpha+\beta-1} (\bar{G}_{c,v})_{\nu_l,\mathbf{q}'_j} \tag{A.18}$$

with $\sum_i \mathbf{q}'_i + \sum_j \mathbf{q}'_j = \mathbf{q}$.

A.2 Exact Wannier Equation Solutions in 2-D

In the main text, we treat the Wannier function amplitudes and energies as fitting parameters. However, for certain systems, it is possible to solve the Wannier equation exactly. Here, we present exact solutions for a layered, two dimensional system with quadratic dispersion by following chapter 10 of Haugh and Koch [46]. We consider two cases: 1) the valence and conduction bands are within the same layer, and 2) the bands are separated by a distance d. We treat the Fröhlich term as a Darwin perturbation of the Coulomb interaction, and ignore it in this derivation. In polar coordinates, our Wannier equation is given by:

$$\{-\tilde{M}_{c,v}[\nabla_\rho^2 + \rho^{-2}\partial_\phi^2] - V^{v,c}(\rho)\}\Psi(\rho) = E\Psi(\rho)$$

where $\nabla_\rho^2 = \rho^{-1}\partial_\rho(\rho\partial_\rho)$, and the Coulomb interaction is left arbitrary. Following Haug and Koch, we apply separation of variables and obtain:

$$\frac{\rho^2}{R}\nabla_\rho^2 R + \tilde{M}_{c.v}^{-1}[\rho^2 V^{v,c}(\rho) + E\rho^2]R = -\frac{1}{\Phi}\partial_\phi^2\Phi \equiv \kappa^2 \tag{A.19}$$

For periodic $\Phi(\phi)$, we obtain the usual solution:

$$\Phi(\phi) \sim e^{im\phi}, m\epsilon\mathcal{Z}$$

with the constant κ replaced by the integer m, and for the radial equation:

$$-[\nabla_\rho^2 + \tilde{M}_{c,v}^{-1}V^{v,c}(\rho)]R(\rho) = \frac{E}{\tilde{M}_{c,v}}R(\rho) - \frac{m^2}{\rho^2}R(\rho)$$

The Coulomb interaction will be of the form $e^2 f(\rho)$. We define the parameters:

$$\lambda \equiv \frac{e^2}{\alpha\tilde{M}_{c,v}} = \frac{1}{\alpha a_0}, \quad \alpha^2 = -\frac{4E}{\tilde{M}_{c,v}} \implies \lambda^2 = -\frac{e^4}{4\tilde{M}_{c,v}E}$$

and make the substitution $r = \rho\alpha$:

$$\left[-\frac{1}{r}\partial_r(r\partial_r) - \frac{\lambda}{\alpha}f(r/\alpha)\right]R(r) = -\frac{1}{4}R(r) - \frac{m^2}{r^2}R(r) \tag{A.20}$$

A.2.1 Intra-Layer Coulomb Interaction

If the bands ε_v and ε_c are part of the same layer in the heterostructure, the Coulomb interaction is given by:

$$V_0^{v,c}(\rho) = \frac{e^2}{\rho}$$

which yields the radial equation:

$$\left[\frac{1}{r}\partial_r(r\partial_r) + \frac{\lambda}{r} - \frac{1}{4} - \frac{m^2}{r^2}\right]R(r) = 0$$

For large r, the radial function must obey:

$$\frac{\partial^2 R_\infty}{\partial r^2} - \frac{1}{4}R_\infty = 0 \implies R_\infty(r) \sim e^{-r/2}$$

At the origin, we must have:

$$-m^2 R_0(r) = 0 \implies R_0(r) \sim r^{|m|}$$

We make the Ansatz:

$$R_m(r) = r^\ell e^{-r/2}\gamma_m(r),\ \ell \equiv |m|$$

and obtain:

$$[r\partial_r^2 + (2\ell + 1 - r)\partial_r + \lambda - \ell - \tfrac{1}{2}]\gamma_m(r) = 0 \tag{A.21}$$

As derived in Haugh and Koch. We employ the Frobenius method and take $\gamma_m(r) \equiv \sum_k c_k r^k$. Plugging this into Eq.(A.21), we have:

$$\sum_{k=1}^{\infty}[k(k+1) + (2\ell+1)(k+1)]c_{k+1}r^k + \sum_{k=0}^{\infty}(\lambda + \ell - \tfrac{1}{2} - k)c_k r^k = 0$$

yielding the recursion relation:

$$c_{k+1} = c_k \frac{k - (\lambda - \ell - \frac{1}{2})}{(k+1)(k+2\ell+1)} \tag{A.22}$$

In order for the radial function to be normalizable, the polynomial $\gamma_m(r)$ must have finite order. Thus, there must be some a_ν such that, for all $k > \nu$, $a_k = 0$. We must have:

$$\lambda = \nu + \ell + \tfrac{1}{2} \equiv n + \tfrac{1}{2}$$

where n is the principle quantum number. The allowed energy levels are given by:

$$E_n = -\frac{4E_0}{(2n+1)^2},\ E_0 \equiv \frac{e^4}{4\tilde{M}_{c,v}} = \frac{\tilde{M}_{c,v}}{4a_0^2} \tag{A.23}$$

which gives us an expression for α:

$$\alpha = \frac{2}{a_0(2n+1)}$$

A.2.2 Inter-Layer Coulomb Interaction

If the bands ε_v and ε_c belong to layers separated by a distance d, Eq.(A.20) becomes:

$$\left[\frac{1}{r}\partial_r(r\partial_r) + \frac{\lambda}{\sqrt{r^2 + r_0^2}} - \frac{1}{4} - \frac{m^2}{r^2}\right]R(r) = 0 \tag{A.24}$$

where $r_0 = \alpha d$. We can manipulate this expression into a form more suitable for the Frobenius method by taking the transformation $y^2 = r^2 + r_0^2$. The differential term in

Eq.(A.24) is now:

$$\frac{1}{r}\partial_r(r\partial_r)f = \frac{1}{r}\left\{r\left(\frac{\partial y}{\partial r}\right)^2\frac{\partial^2 f}{\partial y^2} + \left[\frac{\partial y}{\partial r}\left(r\frac{\partial}{\partial y}\frac{\partial y}{\partial r}+1\right)\right]\frac{\partial f}{\partial y}\right\}$$

Noting:

$$\frac{\partial y}{\partial r} = \frac{r}{y} \implies \frac{\partial}{\partial y}\frac{\partial y}{\partial r} = \frac{r_0^2}{ry^2}$$

we obtain:

$$\frac{1}{r}\partial_r(r\partial_r)f = \left(\frac{y^2-r_0^2}{y^2}\right)\partial_y^2 f + \frac{1}{y^3}(y^2+r_0^2)\partial_y f$$

Thus:

$$\left[\left(\frac{y^2-r_0^2}{y^2}\right)\partial_y^2 + \frac{1}{y^3}(y^2+r_0^2)\partial_y + \frac{\lambda}{y} - \frac{1}{4} - \frac{m^2}{y^2-r_0^2}\right]R(y) = 0$$

For large y, we have:

$$\frac{\partial^2 R_\infty}{\partial y^2} - \frac{1}{4}R_\infty = 0 \implies R_\infty(y) \sim e^{-(y-r_0)/2}$$

And for $y = r_0$, we have:

$$-m^2 R_0(r) = 0 \implies R_0(y) \sim (y-r_0)^{|m|}$$

This gives the Ansatz:

$$R_m(y) = (y-r_0)^{|m|}e^{-(y-r_0)/2}\gamma_m(y)$$

which yields:

$$\left\{\frac{y^2-r_0^2}{y^2}\partial_y^2 + \left[\frac{y^2-r_0^2}{y^2}\left(\frac{2\ell}{y-r_0}-1\right) + \frac{y^2+r_0^2}{y^3}\right]\partial_y + \frac{y^2-r_0^2}{y^2}\left(\frac{\ell(\ell-1)}{(y-r_0)^2} - \frac{\ell}{y-r_0} + \frac{1}{4}\right)\right.$$
$$\left. + \frac{y^2+r_0^2}{y^3}\left(\frac{\ell}{y-r_0} - \frac{1}{2}\right) + \frac{\lambda}{y} - \frac{1}{4} - \frac{\ell^2}{y^2-r_0^2}\right\}\gamma_m = 0 \qquad \text{(A.25)}$$

We will find it useful to re-write Eq.(A.25) as a function of $(y-r_0)$. After applying an overall factor of $y^3(y^2-r_0^2)$ to remove singularities, we find:

$$x^2 A(x)\gamma_m'' + xB(x)\gamma_m' + C(x)\gamma_m = 0 \tag{A.26}$$

where $x = y - r_0$ and the polynomial factors are:

$$A(x) = x^3 + 5r_0x^2 + 8r_0^2x + 4r_0^3$$

$$\begin{aligned} B(x) = &-x^4 + [2\ell - 5r_0 + 1]x^3 + [10\ell r_0 - 8r_0^2 + 4r_0]x^2 \\ &+ [16\ell r_0^2 - 4r_0^3 + 6r_0^2]x + 4r_0^3(1 + 2\ell) \end{aligned}$$

$$\begin{aligned} C(x) = &[\lambda - \ell - \tfrac{1}{2}]x^4 + [-\tfrac{1}{4}r_0 + (4\lambda - 5\ell - 2)]r_0x^3 \\ &+ [-\tfrac{3}{4}r_0^2 + r_0(5\lambda - 8\ell - 3) + \ell(2\ell - 1)]r_0x^2 \\ &+ [-\tfrac{1}{2}r_0^2 + r_0(2\lambda - 4\ell - 2) + \ell(5\ell - 4)]r_0^2x + 3\ell^2 r_0^3 \end{aligned}$$

Eq. (A.25) is now in Frobenius normal form with a regular singular point at $x = 0$. This allows us to expand γ_m as:

$$\gamma_m(x) \equiv \sum_{k=0}^{\infty} c_k x^{k+p}$$

where p is chosen such that c_0 is nonzero for nonzero r_0. Matching powers of x, we obtain the recursion relation:

$$\begin{aligned} 0 = &\, c_{k-4}[\lambda - \ell - \tfrac{1}{2} - (k + p - 4)] \\ &+ c_{k-3}[(k + p - 3)(k + p - 3 + 2\ell - 5r_0) + r_0(-\tfrac{1}{4}r_0 + 4\lambda - 5\ell - 2)] \\ &+ c_{k-2}(r_0)[(k + p - 2)(5(k + p - 3) + 10\ell - 8r_0 + 4) - \tfrac{3}{4}r_0^2 + r_0(5\lambda - 8\ell - 3) + \ell(2\ell - 1)] \\ &+ c_{k-1}(r_0^2)[(k + p - 1)(8(k + p - 2) + 16\ell - 4r_0 + 6) - \tfrac{1}{2}r_0^2 + r_0(2\lambda - 4\ell - 2) + \ell(5\ell - 4)] \\ &+ c_k(r_0^3)[4(k + p)^2 + 8\ell(k + p) + 3\ell^2] \end{aligned} \tag{A.27}$$

At $k = 0$, we have:

$$c_0(r_0)^3[4p^2 + 8\ell p + 3\ell^2] = 0$$

For $r_0 = 0$, this is trivially true for all p and we may take $p = 0$, which recovers the original recursion relation given by Eq.(A.22). For nonzero r_0, we must have:

$$p = \ell(-1 \pm \tfrac{1}{2})$$

The wave function should be non-singular at the origin, thus $p = -\ell/2$, and the wave functions are now given by:

$$R(x) = x^{\ell/2}e^{-x/2}f(x)$$

where $f(x)$ is the polynomial:

$$f(x) = \sum_{k=0}^{\nu} c_k x^k$$

The order ν of $f(x)$ is determined by the c_{k-4} coefficient in Eq.(A.27):

$$\begin{aligned} c_v(\lambda - \tfrac{\ell}{2} - \tfrac{1}{2} - \nu) &= 0 \\ \implies \lambda &= \tfrac{1}{2}(2\nu + \ell + 1) \end{aligned}$$

Defining the principle quantum number $2n = 2\nu + \ell$, the energies are now:

$$E_n = \frac{-4E_0}{(2n+1)^2},\ \alpha = \frac{2}{a_0(2n+1)}$$

which are the energies of the Intra-layer problem, but with ℓ restricted to an even integer. The coefficients satisfy:

$$\begin{aligned} 0 = {} & c_{k-4}[\tfrac{1}{2}(n-3\ell) - (k-4)] \\ & + c_{k-3}[(k + \tfrac{\ell}{2} - 3)(k + \tfrac{3\ell}{2} - 3 - 5r_0) + r_0(-\tfrac{1}{4}r_0 + 2n - 5\ell)] \\ & + c_{k-2}(r_0)[(k - \tfrac{\ell}{2} - 2)(5(k-3) + \tfrac{15\ell}{2} - 8r_0 + 4) - \tfrac{3}{4}r_0^2 + r_0(\tfrac{1}{2}(5n-1) - 8\ell - 3) + \ell(2\ell - 1)] \\ & + c_{k-1}(r_0^2)[(k - \tfrac{\ell}{2} - 1)(8(k-2) + 12\ell - 4r_0 + 6) - \tfrac{1}{2}r_0^2 + r_0(n - 4\ell - 1) + \ell(5\ell - 4)] \\ & + c_k(r_0^3)[4(k - \tfrac{\ell}{2})^2 + 8\ell(k - \tfrac{\ell}{2}) + 3\ell^2] \end{aligned} \tag{A.28}$$